

DISSERTATION

WILDFIRE IMPACTS ON WESTERN UNITED STATES SNOWPACK

Submitted by

Jeremy Giovando

Department of Civil and Environmental Engineering

In partial fulfillment of the requirements

For the degree of Doctor of Philosophy

Colorado State University

Fort Collins, Colorado

Spring 2022

Doctoral Committee:

Advisor: Jeffrey Niemann

Mazdak Arabi

Steven Fassnacht

Camille Stevens-Rumann

Copyright by Jeremy Giovando 2022

All Rights Reserved

ABSTRACT

WILDFIRE IMPACTS ON WESTERN UNITED STATES SNOWPACK

Snowpack in the western U.S. is critical for water supply and is threatened by wildfires, which are becoming larger and more common. Numerous studies have examined impacts of wildfire on snow water equivalent (SWE), but many of these studies are limited in the number of observation locations, and they have sometimes produced conflicting results. The objective of this study is to distinguish the net effects of wildfires on snowpack from those of climate. Data from 45 burned sites from the SNOTEL network are used to perform an empirical analysis to determine SWE impacts from wildfire. For each burned site, unburned control sites are identified from the same level III ecoregion. Impacts of climate changes on snowpack are analyzed first by comparing pre-wildfire and post-wildfire snow water equivalent at the unburned sites. Combined climate and wildfire effects are considered by comparing pre-wildfire and post-wildfire SWE at the burned sites. Wildfire impacts are then isolated by taking the difference between the burned and unburned sites. Four separate snow measures are considered in this analysis and include annual maximum SWE, normalized annual maximum SWE, peak SWE date, and melt-out date. Wildfires have on average advanced melt-out (9 days) and maximum SWE dates (6 days) and reduced annual maximum SWE (10%) across all the sites considered in the analysis. The combined effects of climate and wildfire have advanced melt-out and maximum SWE dates approximately 14 days and 10 days, respectively, while decreasing maximum SWE for the combined effects was approximately 10%. The wildfire-induced

changes in SWE were compared to several possible controlling variables including burn severity, leaf-area index change, dominant pre-wildfire tree genus, years since the fire, and site elevation.

Due to increasing wildfire magnitude, the potential vulnerability of snowpack is an important consideration for water managers. An analysis to quantify the spatial variability of wildfire impacts on snowpack within the western U.S. ecoregions and vulnerabilities of annual maximum SWE was performed. Random forest models were developed for each measure using topographic, climatic, and land cover predictor variables along with snowpack data from wildfire impacted SNOTEL sites. The results indicate terrain slope is an important variable for maximum SWE, while incoming shortwave radiation and aridity are important for peak SWE date and melt-out date changes, respectively. The largest spatial variability amongst all snow measures is maximum SWE with a range of 5% increase to over 10% decrease due to wildfire impacts. Spatial variability for peak SWE and melt-out dates varied between ecoregions with the largest range in the northern and mid-latitude ecoregions. Peak SWE and melt-out dates are expected to be earlier with the exception of the Arizona-New Mexico Mountains where later melt-out dates are possible. South-facing gentle slopes were identified as the most vulnerable for maximum SWE changes. The total snow water volume difference due to wildfires occurring between 2015 through 2020 ranged from a 1% increase in the North Cascades to a 6% reduction in the Arizona-New Mexico Mountains.

A consequence of increased wildfire activity in the western U.S. has resulted in increasing post-wildfire risk assessments by federal, state, and local governments. Locations of these assessments include watersheds which have snowmelt as part of the hydrologic regime. The current gap in generalized recommendations for water managers related to parameter adjustments in snow models presents challenges for water managers performing these risk

assessments. Data from wildfire impacted SNOTEL sites were again used to estimate changes in two key parameters (the melt-rate function and the snowfall threshold temperature). The observed changes from pre- and post-wildfire periods at each SNOTEL site were used to develop a suite of general linear models to adjust the melt-rate function and threshold temperature. The model inputs include readily available topographic, climatic, and land cover information. The results indicate melt-rates typically increase after a wildfire, especially for periods later in ablation season. The snowfall threshold temperatures were more variable and site dependent, although the statistically significant changes suggest increases in the threshold temperature will occur post-wildfire. The coefficients from the models suggest that changes to the vegetation canopy are most important for estimating melt-rate and threshold temperature differences beginning immediately after the fire event though approximately 10 years post-wildfire. After vegetation canopy, other important input variables include the air temperature and topographic characteristics (i.e., elevation, northness, and eastness).

ACKNOWLEDGEMENTS

I would like to acknowledge my advisor, Jeff Niemann, and my committee members for all of their time and effort. In addition, I would like to acknowledge my family, friends and colleagues that help me through this enormous effort. Their constant encouragement was needed and very much appreciated. Finally, I would like to acknowledge Dr. Jorge Ramirez for his inspiration and knowledge that led to my research.

DEDICATION

This dissertation is dedicated to my wife, Renee, for her unwavering support and for her foundational presences in our family as I completed this venture. I also dedicate this effort to my children, Isabella and Ava. You are amazing people and I am so very proud to be your father. And to my parents who have always given me immeasurable support and encouragement throughout my life.

TABLE OF CONTENTS

ABSTRACT.....	ii
ACKNOWLEDGEMENTS.....	v
DEDICATION.....	vi
CHAPTER 1 - INTRODUCTION.....	1
1.1 CLIMATE CHANGE IMPACTS ON SNOWPACK	2
1.2 WILDFIRE TRENDS.....	4
1.3 CLIMATE AND WILDFIRE CONNECTION.....	4
1.4 WILDFIRE IMPACTS ON ENERGY BALANCE.....	5
1.5 WILDFIRE IMPACTS ON SNOWPACK.....	6
1.6 SNOWPACK VULNERABILITY.....	7
1.7 POST-WILDFIRE SNOW AND SNOWMELT RESPONSE MODELING.....	9
1.8 RESEARCH MOTIVATION	10
1.9 STUDY OBJECTIVES.....	11
1.10 REFERENCES	13
CHAPTER 2 - WILDFIRE IMPACTS ON SNOWPACK PHENOLOGY IN A CHANGING CLIMATE WITHIN THE WESTERN U.S.	24
2.1 OVERVIEW	24
2.2 INTRODUCTION	25
2.3 DATA AND METHODS	28
2.3.1 SNOTEL Data	28
2.3.2 Site Characteristics	31
2.3.3 Summary Methods.....	33
2.4 RESULTS	34
2.4.1 Changes in Snow Phenology Measures.....	34
2.4.2 Potential Controls on SWE Changes	44
2.5 DISCUSSION.....	53
2.6 CONCLUSIONS	57
2.7 REFERENCES	61
CHAPTER 3 - REGIONAL SNOWPACK VULNERABILITY TO WILDFIRE AND CHANGING CLIMATE WITHIN THE WESTERN U.S.	70
3.1 OVERVIEW	70
3.2 INTRODUCTION	71
3.3 DATA	76
3.3.1 SNOTEL Data	76
3.3.2 Snowpack Measures	78
3.3.3 Topographic and Land Cover Data	79
3.3.4 Forest Inventory and Analysis Data	80
3.3.5 Incoming Shortwave Radiation	81
3.3.6 Climate Data.....	81
3.3.7 Potential Evaporation	82
3.3.8 Snowpack Data.....	82
3.3.9 Predictor variables	83

3.4 METHODS	89
3.4.1 Random Forest Models.....	89
3.4.2 Model Development	91
3.4.3 Model Training and Variable Importance	92
3.4.4 Model Application.....	93
3.4.5 Model Evaluation	94
3.5 RESULTS	95
3.5.1 RF Model Training and Evaluation.....	95
3.5.2 Input Variable Importance.....	98
3.5.3 Spatial Variability.....	100
3.5.4 Identification and evaluation of snow vulnerable areas	102
3.5.6 Snow Water volume changes due to fires from 2015-2020	108
3.6 DISCUSSION	109
3.7 CONCLUSIONS	112
3.8 REFERENCES	116
CHAPTER 4 - WILDFIRE IMPACTS FOR TEMPERATURE INDEX SNOWPACK MODEL	
PARAMETERS	131
4.1 OVERVIEW	131
4.2 INTRODUCTION	132
4.3 DATA	138
4.3.1 SNOTEL Data	138
4.3.2 Land Cover Data.....	140
4.3.3 Burn Severity.....	142
4.3.4 Topographic Data.....	142
4.3.5 Climatic Data.....	144
4.4 METHODS	147
4.4.1 Melt-rate Function	147
4.4.2 Px Temperature	153
4.4.3 Model evaluation	155
4.5 RESULTS	156
4.5.1 Variable Correlation	156
4.5.2 Melt-rate function component changes	159
4.5.3 Px Temperature Differences.....	161
4.5.4 Models for Estimating Melt-rate changes post-wildfire.....	162
4.5.5 Models for Estimating Px Temperature changes post-wildfire.....	164
4.5.6 Model Evaluation	166
4.6 DISCUSSION.....	168
4.7 CONCLUSIONS	172
4.7 REFERENCES	175
CHAPTER 5 – CONCLUSIONS	188
5.1 SUMMARY OF RESULTS	188
5.2 FUTURE RESEARCH.....	191
5.3 REFERENCES	194
APPENDIX A.....	195

CHAPTER 1 - INTRODUCTION

There are continued concerns regarding freshwater supply for the United States. Fennell (2014) reports that water managers in 40 states expected water shortages by 2023. Within the eleven western U.S. states, water managers from 10 of the 11 states anticipate water shortages ranging from local to statewide scales. The consequences for water shortages could affect approximately one fourth of the country's population (U.S. Census Bureau, 2019). An example of where water supply cannot meet current demands is the Colorado River Basin. For the first time since the development of major water storage projects in the Colorado River Basin, there has been a Federally declared water shortage (<https://www.usbr.gov/newsroom/#/news-release/3950>), which results in the states of Arizona and Nevada receiving only 18% and 7% of their annual allotments for 2022, respectively. The streamflow that feeds reservoir storage systems and other water supply infrastructure in the western U.S. is principally derived from snowmelt runoff (Doesken & Judson, 1996; Hammond et al., 2018; D. Li et al., 2017; Sexstone et al., 2020; Stewart et al., 2004). Snowmelt has been estimated to account for 75% of the total runoff in the western U.S. (Doesken & Judson, 1996) although estimates range from 53% (Li et al., 2017) to 80% (Stewart et al., 2004). The timing and magnitude of peak snow water equivalent (SWE) are key variables in predicting peak streamflow (Clow, 2010; Curry & Zwiers, 2018). The melt rate of the snowpack is a key driver of the summer baseflow conditions (Barnhart et al., 2016) as well as streamflow temperatures (Du et al., 2020), which are both important for aquatic ecology.

1.1 CLIMATE CHANGE IMPACTS ON SNOWPACK

The primary forcing variables for snowpack accumulation and ablation are air temperature and precipitation during the winter and spring seasons in the western U.S. Therefore, changes in air temperature or precipitation will have direct impacts on the seasonal snowpack. Climate change has resulted in a global temperature increase of 0.63 °C based on comparing the 1850-1900 period to 1986-2005 largely due to anthropogenic activities (IPCC, 2019). Based on estimates presented in the 4th National Climate Assessment report (<https://nca2018.globalchange.gov/>), the annual air temperature in the western U.S. has increased 0.8°C between the 1986-2016 period and the baseline period of 1901-1960 (Vose et al., 2017). Bonfils et al. (2008) used daily maximum and minimum temperature data in mountainous areas of the western U.S. to evaluate trends for the western U.S. They found statistically significant trends for daily minimum and maximum temperatures in the region for January through March. The estimated temperature changes were 1.83 °C and 1.54 °C for minimum and maximum air temperature, respectively, for the period of 1950 through 1999. Bonfils et al. (2008) concluded that the increases in temperature are from anthropogenic climate change. Using daily precipitation records, Zhang et al. (2021) reported a decrease in annual total precipitation for the western U.S. of 2.3 mm per decade for the period 1976-2019. A statistically significant decreasing trend of approximately 11 mm per decade was reported for the areas in southern Colorado, northern New Mexico, and northern Arizona (Zhang et al., 2021). Other areas of the western U.S. did not have statistically significant changes in annual precipitation (Zhang et al., 2021). The ratio of snowfall to total winter precipitation is also decreasing across the western U.S. (Knowles et al., 2006). During 1949-2004, Knowles et al. (2006) found the amount of snowfall decreased by 50% relative to similar precipitation totals. Feng & Hu (2007) found

similar decreases in the snowfall to precipitation ratio. They reported large decreases for the months of January and March, averaging 3.6% and 2.9% per decade for sites in the Northwest. Their study did not quantify changes in the snowfall ratio for other parts of the western U.S.

Water vapor gradients between the snow surface and atmosphere are a key driver for sublimation from the snowpack (Sexstone et al., 2018). Therefore observed trends in the vapor pressure deficit are also important for understanding climate change impacts on snowpack. Ficklin & Novick (2017) found trends for increasing vapor pressure deficit over the western U.S for 1979 through 2013 as a result of air temperature increases. However, the increases in vapor pressure deficit from December through March were less than 0.005 kPa per year and were not statistically significant.

Declines in peak snow water equivalent (SWE) across the western U.S. have been reported in several studies (Grundstein & Mote, 2010; Mote et al., 2018; Pierce et al., 2008; Zeng et al., 2018). They reported decreases range from 15% to 31% for 1 April SWE (Mote et al., 2018). While meteorological drought and inter-annual wintertime temperature variability contribute to episodic decreases, the observed trends can be attributed to climate change that has already occurred (Pierce et al., 2008). Areas that will be most sensitive to future warming are in transitional snow zones where the mean winter temperatures are near freezing (Luce et al., 2014; Nolin & Daly, 2006). For areas in the Northwest, almost 9,200 km² of seasonally snow covered area are “at risk”(Nolin & Daly, 2006). Mote (2003) found that lower elevation sites had the largest decrease in April 1 SWE (40% decreasing trend) which is consistent with Grundstein and Mote (2010) who reported 80% of sites below 1000 m had statistically significant declines in snowpack compared to 62% of sites above this elevation. Musselman et al. (2021) used cumulative snowmelt prior to 1 April to assess climate impacts on snowpack. They found that

34% to 42% of 634 snow monitoring sites in western North America had statistically significant increases in cumulative melt before 1 April.

1.2 WILDFIRE TRENDS

Along with climate change, wildfires are another potential change to snowpack. Wildfires are part of the western United States ecology and have been throughout history. Large wildfires have been documented through analyzing lake sediments in mountainous regions (Calder et al., 2015). An increase in the number of large wildfires (>400 ha) has occurred in recent decades for the western United States. Westerling et al. (2006) found that approximately four times the number of large wildfires occurred from 1987 through 2003 compared to 1970 through 1986. In addition, they found the total burned area was over six times greater for the period after 1987. These findings were reinforced by Dennison et al. (2014) who reported statistically significant increases in the number of large wildfires in several ecoregions of the western U.S. from 1984 through 2011. As an example, the Arizona-New Mexico Mountains experienced increases of 462% and 1266% in the number of fires and total area burned, respectively, for the 2003-2012 period (Westerling, 2016).

1.3 CLIMATE AND WILDFIRE CONNECTION

Climate change and wildfire occurrence are connected through changes in temperature and precipitation. Increased temperatures result in increased vapor pressure deficits (even with similar annual precipitation amounts), which produce great stress on vegetation (Barron-Gafford et al., 2007; Eamus et al., 2013). This stress results in lower moisture in vegetation which increases the flammability of the vegetation (Littell et al., 2016; Swetnam & Betancourt, 1998). Anthropogenic climate change between 1979 and 2015 doubled fuel aridity beyond what would be expected from natural climate variability (Abatzoglou & Williams, 2016). Heidari et al.,

(2021) reports the number of fires in portions of the western U.S. could increase 400% relative to the historical period of 1986-2015 with climate change. The coupling between changes in climate and subsequent responses in wildfire probability suggest increased fire occurrences and severity in the future (Cannon & DeGraff, 2009; Flannigan et al., 2006; Stavros et al., 2014).

Recovery of forests after wildfires depends on subsequent weather patterns and distance to nearest seed producing trees (Haffey et al., 2018; Rodman et al., 2020; Stevens-Rumann & Morgan, 2019). Harvey et al. (2016) found drought severity following a wildfire was a statistically significant predictor of tree seedling establishment and resulted in a 62 % reduction in seed establishment rates for each unit increase of drought severity. Locations that have experienced multiple fires may have up to 31% lower tree seedling density even if post-wildfire drought isn't a factor (Stevens-Rumann & Morgan, 2016).

1.4 WILDFIRE IMPACTS ON ENERGY BALANCE

Wildfire has been shown to alter radiative fluxes (shortwave and longwave) and turbulent fluxes (sensible and latent) through changes in the vegetation canopy and surface albedo (Amiro et al., 2006; Burles & Boon, 2011, Gleason et al., 2013; Gleason et al., 2019; Liu et al., 2005; Prater & Delucia, 2006). One of the most consistent changes to the annual surface energy balance after a wildfire is increased ground surface temperature, which is associated with decreased sensible heat and net energy fluxes from the ground surface (Li et al., 2017; Liu et al., 2019). It was found that fires increased ground surface temperatures approximately 0.15 °C the first year after the fire (Liu et al. 2019). Liu et al. (2005) compared sites in Alaska of varying burn age (i.e., sites burned 3-years, 15-years, and 80-years prior to the study) and sensible heat flux from the ground were reduced by over 50% at the 3-year and 15-year sites compared to the 80-year site. While the annual net energy flux is decreased, it has been shown net shortwave

flux increases for burned areas relative to unburned areas during the winter and spring seasons (Burles & Boon, 2011; Gleason et al., 2013). Burles and Boon (2011) found increased net shortwave radiation for the months of April and May when comparing burned plots relative to unburned plots six years after a wildfire occurred. The ratio of the net shortwave radiation between burned and unburned locations was 2-3.5 times. Gleason et al. (2013) reported a 60% increase in net shortwave radiation during the accumulation period and a 200% increase during the ablation period for areas of the Cascade Mountains in Oregon. The net shortwave radiation increases are due to increased incoming shortwave radiation reaching the snow surface once the canopy is removed (Gleason et al., 2013). The post-wildfire response for net longwave radiation is different compared to the net shortwave. When a wildfire removes the vegetation canopy, the absorption of incoming shortwave radiation by the vegetation canopy and tree trunks decreases, which results in reduced downwelling longwave radiation to the snow surface (Burles & Boon, 2011). The reduced downwelling longwave radiation is not sufficient to offset the outgoing longwave radiation from the snowpack, so the net longwave radiation shifts from positive for unburned sites to negative for burned locations. The reduction in canopy coverage due to wildfires also reduces surface roughness and therefore increases near surface wind speeds and turbulent fluxes. Burles & Boon (2011) reported an increase of over two orders of magnitude for sensible heat flux during the April through May period post-wildfire. In contrast, they reported decreases of approximately 150% in latent heat flux during the same months post-wildfire due to the strong control transpiration has on latent heat flux (Williams & Torn, 2015).

1.5 WILDFIRE IMPACTS ON SNOWPACK

The impact of wildfires on seasonal snowpack accumulation and ablation has less consensus within the literature. Numerous studies have examined impacts of wildfire on

snowpack, but many of these studies are limited in the number of observation locations, and they have sometimes produced conflicting results. Goeking and Tarboton (2020) summarized the impacts of land surface disturbances (including wildfire, harvest, drought and insect mortality) on snowpack. Overall, 34 of 42 studies that they summarize found increases in annual maximum SWE following forest disturbances while 10 studies found decreases in annual maximum SWE (some studies reported both increases and decreases). Furthermore, 9 of 13 studies in Canada and the northern U.S. reported consistent increases in annual maximum SWE in response to disturbances. In contrast, only 5 of 13 studies conducted in lower latitudes of the U.S. reported consistent increases (Goeking & Tarboton, 2020). Maxwell & St. Clair (2019) investigated whether peak SWE varies with burn severity or percent overstory tree mortality in a mid-latitude, subalpine forest in Utah. They found that peak SWE increased 15% and peak depth 17% for every 20% increase in overstory tree mortality. Slope, basal area, and canopy height did not have a significant influence on the SWE increase. During a two-year study of the Twitchell Canyon fire in south-central Utah, Maxwell et al. (2019) found that snowpack disappeared earlier in burned areas compared to unburned areas, especially on south-facing slopes. However, peak SWE did not vary between burned and unburned areas. Stevens (2017) examined wildfire impacts on snow accumulation at the stand and tree scales in the Sierra Nevada mountains of California. The unburned forest had the highest overall snowpack depth, and snowpack depth decreased 78% for high severity burn areas.

1.6 SNOWPACK VULNERABILITY

Snowpack vulnerability can be defined by the sensitivity and susceptibility of regional snowpack to changes when a wildfire occurs. Snowpack vulnerability can be evaluated for peak SWE, date of peak SWE, or melt-out date due to climatic change or land cover disturbance

caused by wildfire. The quantification of snowpack vulnerability within the context of climate change has been presented in regional watershed planning and water supply risk assessments (Nolin & Daly, 2006). They estimate over 9000 km² of the areas in the northwest U.S. are at risk of reduced snow cover. However, there are limited studies considering SWE vulnerability to wildfire at regional scales that can be used for planning and risk assessments. Based on the summary of previous studies presented by Goeking & Tarboton (2020), the vast majority of studies were performed over relatively small domains. This means their results would apply mostly to plot scales or to small stream catchments. In contrast, Stevens (2017) collected snow depth measurements in the Sierra Nevada Mountains and found fire severity had a negative effect on snow depth. In conjunction with the data collection, they developed statistical models to predict changes in snow depth using burn severity, canopy gaps, and topographic aspect in the Sierra Nevada Mountains. Based on the linear model parameter estimates, they found inverse relationships between burn severity and snow depth. The parameter estimates for canopy gap and northeast aspect indicate a positive relationship with snow depth while southwest aspect was negative. These results would have predictive power for the area from which the training data was derived but limited applicability in other regions. Micheletty et al. (2014) used remote sensing data to evaluate the spatial variability of melt-out after fires in California. They found melt-out occurred on average 9 days earlier in burn areas based on snow cover data from 11 years (6 years pre-wildfire and 5 years post-wildfire). Again, their results are most relevant for estimating post-wildfire changes in snowpack for areas of the Sierra Nevada Mountains. Other studies not in burned areas have evaluated tree canopy influence for snowpack variability over regional scales. Tennant et al. (2017) reported canopy height explained the most snow depth variation relative to other physiographic variables for areas in southern Idaho and the central

Sierra Nevada Mountains. Fassnacht et al. (2012) found canopy density was the least important variable (out of a total of 27 topographic and physiographic) explaining snowpack distribution within Arizona, Colorado, New Mexico, Utah, and Wyoming.

1.7 POST-WILDFIRE SNOW AND SNOWMELT RESPONSE MODELING

Following a wildfire event, hydrologic monitoring and modeling are often performed to assess the impacts on streamflow (Ebel, 2013; Hallema et al., 2017; Rengers et al., 2016). It has been documented that streamflow from a watershed often increases immediately following a fire (Ebel et al., 2012; Moody & Martin, 2001; Neary et al., 2003; Stoof et al., 2012). Many studies report hydraulic conductivity parameters used for streamflow simulation of pre and post-wildfire conditions (Ebel et al., 2016; Ebel & Moody, 2017; Moody et al., 2016; Rengers et al., 2016; Wieting et al., 2017). For example, Ebel & Moody (2020) suggest a typical post-wildfire field saturated hydraulic conductivity of 20 mm hr^{-1} and sorptivity of $6 \text{ mm hr}^{-0.5}$ within one year of the fire. However, most recommendations for model parameters are focused on modeling post-wildfire rainfall events.

Complete evaluations of both flood risk and long-term water supply estimates can include snow modeling (Hock, 2003; USACE 2021). A range of models have been developed to estimate changes in peak SWE and snowmelt following a wildfire. Moeser et al. (2020) used the SnowPALM model to estimate post-wildfire changes in peak SWE and melt-out dates for areas in northern New Mexico. Their model generally predicted increases for peak SWE, although over 30% of the area was predicted to have decreased peak SWE. The model also predicted later melt-out dates for the study area. While they do not directly report melt-rates, increased peak SWE and later melt-out dates could result in lower overall melt-rates. The authors indicate that their results are likely not transferable to other regions and do not specifically provide any

suggestions for model parameterization. Another detailed energy balance snow model was developed by Burles and Boon (2011) for southwestern Alberta. The spatial extents for their study were two 2500 m² plots in burned and unburned forest stands. They used hourly meteorological data collected at both plots to simulate snow accumulation and ablation. Both the modeled and measured melt-rates were increased when compared to the unburned study plot. Because Burles & Boon (2011) were predicting melt using a full energy balance approach, they do not offer estimates of parameter values for temperature index snow models, which remain widely used in practice (Follum et al., 2015; Hock, 2003). Seibert et al. (2010) used a temperature index snow model to determine parameter changes between burned and unburned watersheds in western Washington. Due to the equifinality of the model parameterization process, they used a Monte Carlo technique to calibrate observed streamflows and quantify parameter changes for the burned watersheds. Through the Monte Carlo parameter evaluation, they reported higher melt-rates (50% increase) in the burned watersheds and decreased rain-snow threshold (50% increase) values. Given the variety of models used in post-wildfire snow modeling, there is very limited information on how snow model parameters should be adjusted post-wildfire.

1.8 RESEARCH MOTIVATION

Research related to wildfire impacts on snowpack has been completed using a variety of measurement and analysis methods in various ecoregions. Due to variability between studies, it is difficult to determine generalized impacts beyond very specific locations. Moreover, the transferability of prior findings to other locations is often explicitly stated by the authors as not being possible due to their methods. Consequently, previous research efforts have limited applicability in determining where snowpack, and thus potential snowmelt runoff for water

supply, are most sensitive to wildfire disturbances before these catastrophic events occur. Additionally, information provided by previous research efforts provides few suggestions on how to translate observed changes in snowpack in burned areas into generalized recommendations for temperature index model parameter adjustments. Often during the initial months following a wildfire, several federal, state, and local organizations perform risk assessments for life, property, and infrastructure. These risk assessments generally include hydrologic modeling because flooding can have direct impacts both within the wildfire affected areas and to areas far outside the actual burn perimeter. Due to the urgent need to identify areas of high risk, water and emergency managers need straightforward recommendations for estimating changes in flood risk due to snowmelt. The motivation for this research is centered on providing quantitative information about snowpack changes post-wildfire for water managers.

1.9 STUDY OBJECTIVES

The research presented in this study focuses on quantifying snowpack changes following wildfire, which is necessary for planning purposes, along with generalized recommendations on how to adjust hydrologic models used for risk assessments. Based on the potential range of impacts that both wildfire and climate change have on the land surface energy balance, this research targets three key objectives that progress the scientific understanding of how wildfires, within the context of climate change, impact snowpack. These objectives include:

- 1) Quantification of wildfire impacts on snow phenology using data from the NRCS SNOTEL network, which are consistent across ecoregions.
- 2) Quantification of snowpack vulnerability across ecoregions in the western U.S. based on a consistent set of input variables that are available for large domains.

- 3) Quantification of post-wildfire modeling parameters adjustments for temperature index snow models.

1.10 REFERENCES

- Abatzoglou, J. T., & Williams, A. P. (2016). Impact of anthropogenic climate change on wildfire across western US forests. *Proceedings of the National Academy of Sciences of the United States of America*, *113*(42), 11770–11775. <https://doi.org/10.1073/pnas.1607171113>
- Amiro, B. D., Orchansky, A. L., Barr, A. G., Black, T. A., Chambers, S. D., Chapin, F. S., Goulden, M. L., Litvak, M., Liu, H. P., McCaughey, J. H., McMillan, A., & Randerson, J. T. (2006). The effect of post-fire stand age on the boreal forest energy balance. *Agricultural and Forest Meteorology*, *140*(1–4), 41–50. <https://doi.org/10.1016/j.agrformet.2006.02.014>
- Barnhart, T. B., Molotch, N. P., Livneh, B., Harpold, A. A., Knowles, J. F., & Schneider, D. (2016). Snowmelt rate dictates streamflow. *Geophysical Research Letters*, *43*(15), 8006–8016. <https://doi.org/10.1002/2016GL069690>
- Barron-Gafford, G. A., Grieve, K. A., & Murthy, R. (2007). Leaf- and stand-level responses of a forested mesocosm to independent manipulations of temperature and vapor pressure deficit. *New Phytologist*, *174*, 614–625.
- Bonfils, C., Santer, B. D., Pierce, D. W., Hidalgo, H. G., Bala, G., Das, T., Barnett, T. P., Cayan, D. R., Doutriaux, C., Wood, A. W., Mirin, A., & Nozawa, T. (2008). Detection and attribution of temperature changes in the mountainous Western United States. *Journal of Climate*, *21*(23), 6404–6424. <https://doi.org/10.1175/2008JCLI2397.1>
- Boon, S. (2009). Snow ablation energy balance in a dead forest stand. *Hydrological Processes*, *23*(November 2008), 2600–2610. <https://doi.org/10.1002/hyp>
- Burles, K., & Boon, S. (2011). Snowmelt energy balance in a burned forest plot , Crowsnest Pass, Alberta, Canada. *Hydrological Processes*, *25*, 3012–3029. <https://doi.org/10.1002/hyp.8067>

- Calder, W. J., Parker, D., Stopka, C. J., Jiménez-Moreno, G., & Shuman, B. N. (2015). Medieval warming initiated exceptionally large wildfire outbreaks in the Rocky Mountains. *Proceedings of the National Academy of Sciences of the United States of America*, *112*(43), 13261–13266. <https://doi.org/10.1073/pnas.1500796112>
- Cannon, S. H., & DeGraff, J. (2009). The increasing wildfire and post-fire debris-flow threat in western USA, and implications for consequences of climate change. *Landslides - Disaster Risk Reduction*, 177–190. https://doi.org/10.1007/978-3-540-69970-5_9
- Clow, D. W. (2010). Changes in the timing of snowmelt and streamflow in Colorado: A response to recent warming. *Journal of Climate*, *23*(9), 2293–2306. <https://doi.org/10.1175/2009JCLI2951.1>
- Curry, C. L., & Zwiers, F. W. (2018). Examining controls on peak annual streamflow and floods in the Fraser River Basin of British Columbia. *Hydrology and Earth System Sciences*, *22*(4), 2285–2309. <https://doi.org/10.5194/hess-22-2285-2018>
- Dennison, P. E., Brewer, S. C., Arnold, J. D., & Moritz, M. A. (2014). Large wildfire trends in the western United States, 1984-2011. *Geophys. Res. Lett.*, *41*, 2928–2933.
- Doesken, N., & Judson, A. (1996). *The Snow Booklet: A guide to the Science, Climatology, and Measurement of Snow in the United States*.
- Du, X., Goss, G., & Faramarzi, M. (2020). Impacts of hydrological processes on stream temperature in a cold region watershed based on the SWAT equilibrium temperature model. *Water (Switzerland)*, *12*(4). <https://doi.org/10.3390/W12041112>
- Eamus, D., Boulain, N., Cleverly, J., & Breshears, D. D. (2013). Global change-type drought-induced tree mortality : vapor pressure deficit is more important than temperature per se in

- causing decline in tree health. *Ecology and Evolution*, 3(8), 2711–2729.
<https://doi.org/10.1002/ece3.664>
- Ebel, B. A. (2013). Wildfire and Aspect Effects on Hydrologic States after the 2010 Fourmile Canyon Fire. *Vadose Zone Journal*, 12(1), vzj2012.0089.
<https://doi.org/10.2136/vzj2012.0089>
- Ebel, B. A., & Moody, J. A. (2017). Synthesis of soil-hydraulic properties and infiltration timescales in wildfire-affected soils. *Hydrological Processes*, 31(2), 324–340.
<https://doi.org/10.1002/hyp.10998>
- Ebel, B. A., & Moody, J. A. (2020). *Parameter estimation for multiple post-wildfire hydrologic models*. July, 4049–4066. <https://doi.org/10.1002/hyp.13865>
- Ebel, B. A., Moody, J. A., & Martin, D. A. (2012). Hydrologic conditions controlling runoff generation immediately after wildfire. *Water Resources Research*, 48(3), 1–13.
<https://doi.org/10.1029/2011WR011470>
- Ebel, B. A., Rengers, F. K., & Tucker, G. E. (2016). Observed and simulated hydrologic response for a first-order catchment during extreme rainfall 3 years after wildfire disturbance. *Water Resources Research*, 52, 9367–9389. <https://doi.org/10.1111/j.1752-1688.1969.tb04897.x>
- Fassnacht, S. R., Dressler, K. A., Hultstrand, D. M., Bales, R. C., & Patterson, G. (2012). Temporal inconsistencies in coarse-scale snow water equivalent patterns: Colorado river basin snow telemetry-topography regressions. *Pirineos*, 167(167), 165–185.
<https://doi.org/10.3989/Pirineos.2012.167008>
- Feng, S., & Hu, Q. (2007). Changes in winter snowfall/precipitation ratio in the contiguous United States. *Journal of Geophysical Research Atmospheres*, 112(15), 1–12.
<https://doi.org/10.1029/2007JD008397>

- Fennell, A.-M. (2014). Freshwater Supply Concerns Continue, and Uncertainties Complicate Planning. *GAO Reports, May*, 1–105.
<http://search.ebscohost.com/login.aspx?direct=true&db=buh&AN=96167804&site=ehost-live>
- Ficklin, D. L., & Novick, K. A. (2017). Historic and projected changes in vapor pressure deficit suggest a continental-scale drying of the United States atmosphere. *Journal of Geophysical Research Atmospheres*, *122*, 2061–2079.
- Flannigan, M. D., Amiro, B. D., Logan, K. A., Stocks, B. J., & Wotton, B. M. (2006). Forest fires and climate change in the 21ST century. *Mitigation and Adaptation Strategies for Global Change*, *11*(4), 847–859. <https://doi.org/10.1007/s11027-005-9020-7>
- Follum, M. L., Downer, C. W., Niemann, J. D., Roylance, S. M., & Vuyovich, C. M. (2015). A radiation-derived temperature-index snow routine for the GSSHA hydrologic model. *Journal of Hydrology*, *529*(P3), 723–736. <https://doi.org/10.1016/j.jhydrol.2015.08.044>
- Gleason, K. E., McConnell, J. R., Arienzo, M. M., Chellman, N., & Calvin, W. M. (2018). Four-fold increase in solar forcing on snow in western U.S. burned forests since 1999. *Nature Communications*, *2019*, 1–8. <https://doi.org/10.1038/s41467-019-09935-y>
- Gleason, K. E., Nolin, A. W., & Roth, T. R. (2013). Charred forests increase snowmelt : Effects of burned woody debris and incoming solar radiation on snow ablation. *Geophysical Research Letters*, *40*, 4654–4661. <https://doi.org/10.1002/grl.50896>
- Goeking, S. A., & Tarboton, D. G. (2020). Forests and Water Yield : A Synthesis of Disturbance Effects on Streamflow and Snowpack in Western Coniferous Forests. *Journal of Forestry*, 172–192. <https://doi.org/10.1093/jofore/fvz069>

- Grundstein, A., & Mote, T. (2010). Trends in average snow depth across the Western United States. *Physical Geography*, 31(2), 172–185. <https://doi.org/10.2747/0272-3646.31.2.172>
- Haffey, C., Sisk, T. D., Allen, C. D., Thode, A. E., & Margolis, E. Q. (2018). Limits to Ponderosa Pine Regeneration Following Large High-severity Forest Fires in the United States Southwest. *Fire Ecology*, 14(1), 143–163. <https://doi.org/10.4996/fireecology.140114316>
- Hallema, D. W., Sun, G., Bladon, K. D., Norman, S. P., Caldwell, P. V., Liu, Y., & McNulty, S. G. (2017). Regional patterns of postwildfire streamflow response in the Western United States: The importance of scale-specific connectivity. *Hydrological Processes*, 31(14), 2582–2598. <https://doi.org/10.1002/hyp.11208>
- Hammond, J. C., Saavedra, F. A., & Kampf, S. K. (2018). How Does Snow Persistence Relate to Annual Streamflow in Mountain Watersheds of the Western U.S. With Wet Maritime and Dry Continental Climates? *Water Resources Research*, 54(4), 2605–2623. <https://doi.org/10.1002/2017WR021899>
- Harvey, B. J., Donato, D. C., & Turner, M. G. (2016). High and dry: Post-fire tree seedling establishment in subalpine forests decreases with post-fire drought and large stand-replacing burn patches. *Global Ecology and Biogeography*, 25(6), 655–669. <https://doi.org/10.1111/geb.12443>
- Heidari, H., Arabi, M., & Warziniack, T. (2021). Effects of climate change on natural-caused fire activity in western U.S. national forests. *Atmosphere*, 12(8), 1–16. <https://doi.org/10.3390/atmos12080981>
- Hock, R. (2003). Temperature index melt modelling in mountain areas. *Journal of Hydrology*, 282(1–4), 104–115. [https://doi.org/10.1016/S0022-1694\(03\)00257-9](https://doi.org/10.1016/S0022-1694(03)00257-9)

- Knowles, N., Dettinger, M., & Cayan, D. R. (2006). Trends in Snowfall Versus Rainfall for the Western United States, 1949-2001. *Journal of Climate*, *19*(April 2007), 4545–4559.
- Li, D., Wrzesien, M. L., Durand, M., Adam, J., & Lettenmaier, D. P. (2017). How much runoff originates as snow in the western United States, and how will that change in the future? *Geophysical Research Letters*, *44*(12), 6163–6172. <https://doi.org/10.1002/2017GL073551>
- Li, F., Lawrence, D. M., & Bond-Lamberty, B. (2017). Impact of fire on global land surface air temperature and energy budget for the 20th century due to changes within ecosystems. *Environmental Research Letters*, *12*(4). <https://doi.org/10.1088/1748-9326/aa6685>
- Littell, J. S., Mckenzie, D., Peterson, D. L., & Westerling, A. L. (2009). Climate and wildfire area burned in western U.S. ecoprovinces, 1916-2003. *Ecological Applications*, *19*(4), 1003–1021. <https://doi.org/10.1890/07-1183.1>
- Littell, J. S., Peterson, D. L., Riley, K. L., Liu, Y., & Luce, C. H. (2016). A review of the relationships between drought and forest fire in the United States. *Global Change Biology*, *22*(7), 2353–2369. <https://doi.org/10.1111/gcb.13275>
- Liu, H., Randerson, J. T., Lindfors, J., & Iii, F. S. C. (2005). *Changes in the surface energy budget after fire in boreal ecosystems of interior Alaska : An annual perspective*. *110*(January), 1–12. <https://doi.org/10.1029/2004JD005158>
- Liu, Z., Ballantyne, A. P., & Cooper, L. A. (2019). Biophysical feedback of global forest fires on surface temperature. *Nature Communications*, *10*(1), 214. <https://doi.org/10.1038/s41467-018-08237-z>
- Luce, C. H., Lopez-Burgos, V., & Holden, Z. A. (2014). Sensitivity of snowpack storage to precipitation and temperature using spatial and temporal analog models. *Water Resources Research*, *50*, 9447–9462. <https://doi.org/10.1002/2013WR014979>.Reply

- Maxwell, J. D., Call, A., & St. Clair, S. B. (2019). Wildfire and topography impacts on snow accumulation and retention in montane forests. *Forest Ecology and Management*, 432(July 2018), 256–263. <https://doi.org/10.1016/j.foreco.2018.09.021>
- Maxwell, J., & St. Clair, S. B. (2019). Snowpack properties vary in response to burn severity gradients in montane forests. *Environmental Research Letters*, 14, 124094. <https://doi.org/10.1088/1748-9326/ab5de8>
- Micheletty, P. D., Kinoshita, A. M., & Hogue, T. S. (2014). Application of MODIS snow cover products : wildfire impacts on snow and melt in the Sierra Nevada. *Hydrology and Earth System Sciences Discussions*, 18, 4601–4615. <https://doi.org/10.5194/hess-18-4601-2014>
- Moeser, C. D., Broxton, P. D., Harpold, A., & Robertson, A. (2020). Estimating the Effects of Forest Structure Changes From Wild fire on Snow Water Resources Under Varying Meteorological Conditions. *Water Resources Research*, 56, 1–23. <https://doi.org/10.1029/2020WR027071>
- Moody, J. A., Ebel, B. A., Nyman, P., Martin, D. A., Stoof, C., & Mckinley, R. (2016). Relations between soil hydraulic properties and burn severity. *International Journal of Wildland Fire*, 25(3), 279–293. <https://doi.org/10.1071/WF14062>
- Moody, J. A., & Martin, D. A. (2001). Post-fire, rainfall intensity-peak discharge relations for three mountainous watersheds in the Western USA. *Hydrological Processes*, 15(15), 2981–2993. <https://doi.org/10.1002/hyp.386>
- Mote, P. W. (2003). Trends in snow water equivalent in the Pacific Northwest and their climatic causes. *Geophysical Research Letters*, 30(12). <https://doi.org/10.1029/2003GL017258>

- Mote, P. W., Li, S., Lettenmaier, D. P., Xiao, M., & Engel, R. (2018). Dramatic declines in snowpack in the western US. *Npj Climate and Atmospheric Science*, 1(1).
<https://doi.org/10.1038/s41612-018-0012-1>
- Musselman, K. N., Addor, N., Vano, J. A., & Molotch, N. P. (2021). Winter melt trends portend widespread declines in snow water resources. *Nature Climate Change*, 11(5), 418–424.
<https://doi.org/10.1038/s41558-021-01014-9>
- Neary, D. G., Gottfried, G. J., & Ffolliott, P. F. (2003). Post-Wildfire Watershed Flood Responses. *Second International Fire Ecology and Fire Management Congress, Orlando, Florida, 16-20 November 2003, Paper 1B7*, 1–8.
- Nolin, A. W., & Daly, C. (2006). Mapping “at risk” snow in the Pacific Northwest. *Journal of Hydrometeorology*, 7(5), 1164–1171. <https://doi.org/10.1175/JHM543.1>
- Pierce, D. W., Barnett, T. P., Hidalgo, H. G., Das, T., Bonfils, C., Santer, B. D., Bala, G., Dettinger, M. D., Cayan, D. R., Mirin, A., Wood, A. W., & Nozawa, T. (2008). Attribution of declining Western U.S. Snowpack to human effects. *Journal of Climate*, 21(23), 6425–6444. <https://doi.org/10.1175/2008JCLI2405.1>
- Prater, M. R., & Delucia, E. H. (2006). Non-native grasses alter evapotranspiration and energy balance in Great Basin sagebrush communities. *Agricultural and Forest Meteorology*, 139, 154–163. <https://doi.org/10.1016/j.agrformet.2006.08.014>
- Rengers, F. K., McGuire, L. A., Kean, J. W., Staley, D. M., & Hobbey, D. E. J. (2016). Model simulations fo flood and debris flow timing in steep catchments after wildfire. *Water Resources Research*, 52, 6041–6061. <https://doi.org/10.1111/j.1752-1688.1969.tb04897.x>
- Rodman, K. C., Veblen, T. T., Chapman, T. B., Rother, M. T., Wion, A. P., & Redmond, M. D. (2020). Limitations to recovery following wildfire in dry forests of southern Colorado and

northern New Mexico, USA. *Ecological Applications*, 30(1), 1–20.

<https://doi.org/10.1002/eap.2001>

Seibert, J., McDonnell, J. J., & Woodsmith, R. D. (2010). Effects of wildfire on catchment runoff response: A modelling approach to detect changes in snow-dominated forested catchments.

Hydrology Research, 41(5), 378–390. <https://doi.org/10.2166/nh.2010.036>

Sexstone, G. A., Clow, D. W., Fassnacht, S. R., Liston, G. E., Hiemstra, C. A., Knowles, J. F., & Penn, C. A. (2018). Snow Sublimation in Mountain Environments and Its Sensitivity to

Forest Disturbance and Climate Warming. *Water Resources Research*, 54(2), 1191–1211.

<https://doi.org/10.1002/2017WR021172>

Sexstone, G. A., Driscoll, J. M., Hay, L. E., Hammond, J. C., & Barnhart, T. B. (2020). Runoff sensitivity to snow depletion curve representation within a continental scale hydrologic

model. *Hydrological Processes*, 34(11), 2365–2380. <https://doi.org/10.1002/hyp.13735>

Stavros, E. N., Abatzoglou, J. T., McKenzie, D., & Larkin, N. K. (2014). Regional projections of the likelihood of very large wildland fires under a changing climate in the contiguous

Western United States. *Climatic Change*, 126(3–4), 455–468.

<https://doi.org/10.1007/s10584-014-1229-6>

Stevens-Rumann, C., & Morgan, P. (2016). Repeated wildfires alter forest recovery of mixed-

-conifer ecosystems. *Ecological Applications*, 26(6), 1842–1853.

Stevens-Rumann, C. S., & Morgan, P. (2019). Tree regeneration following wildfires in the

western US: a review. *Fire Ecology*, 15(1), 1–17. [https://doi.org/10.1186/s42408-019-0032-](https://doi.org/10.1186/s42408-019-0032-1)

1

Stevens, J. T. (2017). Scale-dependent effects of post- fire canopy cover on snowpack depth in

montane coniferous forests. *ECOLOGICAL APPLICATIONS*, 27(6), 1888–1900.

- Stewart, I. T., Cayan, D. R., & Dettinger, M. D. (2004). Changes in Snowmelt Runoff Timing in Western North America under a 'Business as Usual' Climate Change Scenario. *Climatic Change*, 62(1), 217–232. <https://doi.org/10.1023/B:CLIM.0000013702.22656.e8>
- Stoof, C. R., Vervoort, R. W., Iwema, J., Elsen, E. van den, Ferreira, A. J. D., & Ritsema, C. J. (2012). Hydrological response of a small catchment burned by experimental fire. *Hydrology and Earth System Sciences*, 16, 267–285. <https://doi.org/10.5194/hess-16-267-2012>
- Swetnam, T. W., & Betancourt, J. L. (1998). Mesoscale Disturbance and Ecological Response to Decadal Climatic Variability in the American Southwest. *Journal of Climate*, 41, 329–359. https://doi.org/10.1007/978-90-481-8736-2_32
- Tennant, C. J., Harpold, A. A., Lohse, K. A., Godsey, S. E., Crosby, B. T., Larsen, L. G., Brooks, P. D., Van Kirk, R. W., & Glenn, N. F. (2017). Regional sensitivities of seasonal snowpack to elevation, aspect, and vegetation cover in western North America. *Water Resources Research*, 53(8), 6908–6926. <https://doi.org/10.1002/2016WR019374>
- Vose, R. S., Easterling, D. R., Kunkel, K. E., LeGrande, A. N., & Wehner, M. F. (2017). Temperature changes in the United States. *Climate Science Special Report: Fourth National Climate Assessment, I*, 185–206. <https://doi.org/10.7930/J0N29V45.U.S.>
- Westerling, A. L. (2016). Increasing western US forest wildfire activity : sensitivity to changes in the timing of spring. *Phil. Trans. R. Soc. B*, 371.
- Westerling, A. L., Hidalgo, H. G., Cayan, D. R., & Swetnam, T. W. (2006). Warming and earlier spring increase western US forest wildfire activity. *Science*, 313(5789), 940–943. <https://doi.org/10.1126/science.1128834>
- Wieting, C., Ebel, B. A., & Singha, K. (2017). Quantifying the effects of wildfire on changes in soil properties by surface burning of soils from the Boulder Creek Critical Zone

Observatory. *Journal of Hydrology: Regional Studies*, 13(April), 43–57.

<https://doi.org/10.1016/j.ejrh.2017.07.006>

Williams, I. N., & Torn, M. S. (2015). Vegetation controls on surface heat flux partitioning, and land-atmosphere coupling. *Geophysical Research Letters*, 42(21), 9416–9424.

<https://doi.org/10.1002/2015gl066305>

Zeng, X., Broxton, P., & Dawson, N. (2018). Snowpack Change From 1982 to 2016 Over Conterminous United States. *Geophysical Research Letters*, 45, 12,940–12,947.

<https://doi.org/10.1029/2018GL079621>

Zhang, F., Biederman, J. A., Dannenberg, M. P., Yan, D., Reed, S. C., & Smith, W. K. (2021). Five Decades of Observed Daily Precipitation Reveal Longer and More Variable Drought Events Across Much of the Western United States. *Geophysical Research Letters*, 48(7), 1–

11. <https://doi.org/10.1029/2020GL092293>

CHAPTER 2 - WILDFIRE IMPACTS ON SNOWPACK PHENOLOGY IN A CHANGING CLIMATE WITHIN THE WESTERN U.S.

2.1 OVERVIEW

Snowpack in the western U.S. is critical for water supply and is threatened by wildfires, which are becoming larger and more common. Numerous studies have examined impacts of wildfire on snow water equivalent (SWE), but many of these studies are limited in the number of observation locations, and they have sometimes produced conflicting results. The objective of this study is to distinguish the net effects of wildfires on snowpack from those of climate. To quantify impacts, 45 burned sites from the SNOTEL network were used. For each burned site, unburned control sites are identified from the same level III ecoregion. Impacts of climate changes on snowpack are analyzed first by comparing pre-wildfire and post-wildfire snow water equivalent at the unburned sites. Combined climate and wildfire effects are considered by comparing pre-wildfire and post-wildfire SWE at the burned sites. Wildfire impacts are then isolated by taking the difference between the burned and unburned sites. Wildfires have on average advanced melt-out (9 days) and maximum SWE dates (6 days) and reduced annual maximum SWE (10%) across all the sites we considered. The combined effects of climate and wildfire have advanced melt-out and maximum SWE dates approximately 14 days and 10 days, respectively, while decreasing maximum SWE for the combined effects was approximately 10%. The wildfire-induced changes in SWE were compared to several possible controlling variables including burn severity, leaf-area index change, dominant pre-wildfire tree genus, years since the fire, and site elevation.

2.2 INTRODUCTION

Snowpack is extremely important for agricultural production and domestic water supply in numerous regions of the world. In 2000, approximately one sixth of the world's population lived in snow-dominated, low-reservoir-storage regions (Barnett et al., 2005), and snowmelt contributes a large percentage of the total annual runoff in several major river systems (Barnett et al., 2005; Li et al., 2017; Mankin et al., 2015; Viviroli et al., 2007). The eleven western states within the contiguous U.S. include approximately one fourth of the country's population (U.S. Census Bureau, 2019) and greatly depend on snowmelt for their water supply. Snowmelt has been estimated to account for 75% of the total runoff in the western U.S. (Doesken & Judson, 1996) although estimates range from 53% (Li et al., 2017) to 80% (Stewart et al., 2004).

Changes in the magnitude and timing of snow accumulation and melt (i.e., snowpack phenology) could have trillions of dollars of economic impact in the western U.S. (Sturm et al., 2017). Impacts range from abbreviated winter sports seasons to changes in streamflow timing downstream. The timing and magnitude of peak snow water equivalent (SWE) are key variables in predicting peak streamflow (Clow, 2010; Curry & Zwiers, 2018). The melt rate of the snowpack is a key driver of the summer baseflow conditions (Barnhart et al., 2016) as well as streamflow temperatures (Du et al., 2020), which are important for aquatic ecology.

The snowpack phenology depends on the energy balance of the snowpack, and the snowpack energy balance is highly influenced by the forest canopy (Marks & Winstral, 2001; Musselman et al., 2012; Revuelto et al. 2015; Varhola et al., 2010). Several studies have considered the net relationship between the canopy and snowpack, but the conclusions about this relationship vary substantially with location. For example, Veatch et al. (2009) found that forest edges strongly influence patterns of snow depth in New Mexico and have greater snow depths

than either open or densely forested areas. In contrast, Hubbart et al. (2015) found greater accumulation and later melt-out dates for clear cut areas than forested areas in northern Idaho.

Changes in the canopy can occur for several reasons including tree mortality, drought, and land surface disturbance. The most abrupt of these causes is land surface disturbance, which can include blowdown events, avalanches, and wildfires. A recent review by Goeking and Tarboton (2020) summarizes the impacts of land surface disturbances on several aspects of the water balance. Overall, 34 of 42 studies that they summarize found increases in annual maximum SWE following forest disturbances while 10 studies found decreases in annual maximum SWE (some studies reported both increases and decreases). Furthermore, 9 of 13 studies in Canada and the northern U.S. reported consistent increases in annual maximum SWE in response to disturbances. In contrast, only 5 of 13 studies conducted in lower latitudes of the U.S. reported consistent increases (Goeking & Tarboton, 2020).

Among the land surface disturbances, wildfire is of particular concern because it can impact large land areas and because the canopy changes can occur quickly. The occurrence and magnitude of wildfires are increasing in the western U.S. (Dennison et al., 2014; Littell et al., 2009; Westerling et al., 2006). Warmer and drier conditions in the western U.S. in part due to climate change have been found to be an important factor in the increased fire activity (Dennison et al., 2014; Yang et al., 2015). Nearly all studies of wildfire impacts on snowpack have focused on specific regions, and their results vary. Gleason et al. (2018) reported a four-fold increase in solar energy absorbed by the snowpack after wildfires, which caused earlier melt-out dates at locations in Colorado, Utah, and Wyoming. Maxwell and St. Clair (2019) investigated whether peak snowpack varies with burn severity or percent overstory tree mortality in a mid-latitude, subalpine forest. They found that peak SWE increased 15% and peak depth 17% for every 20%

increase in overstory tree mortality. They also found that slope, basal area, and canopy height did not have a significant influence on the SWE increase. During a two-year study of the Twitchell Canyon fire in south-central Utah, Maxwell et al. (2018) found that snowpack disappeared earlier in burned areas compared to unburned areas, especially on south-facing slopes. However, peak SWE did not vary between burned and unburned areas. Stevens (2017) examined wildfire impacts on snow accumulation at the stand and tree scales in the Sierra Nevada mountains of California. The unburned forest had the highest overall snowpack depth, and snowpack depth decreased 78% for high severity burn areas. However, within the unburned areas, the depths were greatest in canopy openings. Stevens (2017) also found that open areas had greater average snow depth at the tree scale while unburned areas had a greater average depth at the stand scale. Harpold et al. (2014) evaluated snowpack changes in New Mexico following the Las Conchas Fire. Based on several hundred measurements of snowpack, the burned area had approximately 10% less average SWE than unburned areas. They concluded that a lack of strong vegetation controls in burned areas led to topographically controlled variability at peak snowpack. Overall, it is difficult to get a general picture of wildfire impacts on snowpack because each study focused on different aspects of snowpack, had different quantities and qualities of available data, and performed the comparisons in different ways. Specifically, studies that report pre- vs. post-wildfire comparisons for the same location avoid the confounding effects of spatial heterogeneity of snowpack (Broxton et al., 2016; Sexstone & Fassnacht, 2014). However, that approach combines the effects of wildfire occurrence with any climate changes (i.e., interannual precipitation or temperature changes) during the study period. Anthropogenic climate change is impacting all regions within the western U.S. including

observed increases in average annual temperatures (Vose et al., 2017) and decreasing trends in snowpack (Mote et al., 2018; Zeng et al., 2018).

The objective of this study is to distinguish the net effects of wildfires on snowpack from those of climate change using a consistent methodology for different ecoregions in the western U.S. The study uses Snow Telemetry (SNOTEL) data, which is consistently collected and reported for numerous sites across the western U.S. and Alaska. We identified burned SNOTEL sites along with comparable unburned sites within the same level 3 ecoregion. The SWE records for the burned and unburned sites are divided into pre- and post-wildfire periods based on the date of the wildfire at the burned site. The difference between the post-wildfire and pre-wildfire SWE at the unburned sites is used to analyze the impacts of climate changes (climate signal). The difference between the post-wildfire and pre-wildfire snowpack at the burned sites is used to determine the combined impacts of climate change and wildfires (combined signal). Finally, the difference between the combined and climate signals is used to isolate the effects of the wildfires. The results are analyzed first by ecoregion. Then, they are divided by burn severity and other site characteristics to identify potential controls on the impacts of wildfires.

2.3 DATA AND METHODS

2.3.1 SNOTEL Data

SNOTEL sites are operated by the Natural Resources Conservation Service (NRCS, 2021) and range from southern New Mexico (latitude 33.4° N) to central Alaska (latitude 65.1° N) (Figure 1). From SNOTEL, we use the daily SWE and precipitation values along with the site elevations. Quality control was performed through visual inspection of the SWE and precipitation time series. Any apparent reporting errors were discussed with local NRCS Snow Survey offices and removed from the analysis if confirmed. Any years with more than 10% of

daily precipitation or SWE values missing were removed from the dataset. Of the 1576 station-years available for the burned sites, 24 were removed.

Burned locations and dates were determined based on information provided by each NRCS Snow Survey Data Collection Office. Through 2019, 45 sites were identified as being directly impacted by wildfires across the entire network. Figure 2 shows the periods when both SWE and precipitation data are available for each burned site. The date each site burned is also shown on the timeline. The average pre-wildfire period is approximately 23 years with over 87% of the burned sites having at least 10 years. The average post-wildfire period is approximately 12 years with 44% of the sites having at least 10 years.

For each burned site, at least two similar SNOTEL sites were identified that were not burned. The unburned sites were selected to be in the same level 3 ecoregion. A level 3 ecoregion represents a region that is similar in geology, physiography, vegetation, climate, and soils (Omernik & Griffith, 2014). For approximately 80% of the burned locations, there were at least two unburned sites identified within a distance of 50 km and an elevation difference of ± 300 m. The remaining unburned sites required expansion of the search radius or elevation range. The sites that did not meet the initial search criteria are noted in the supporting data. The time series for each of the 110 unburned sites was divided based on the fire date of the associated burned site. For example, if a site was burned in 2007 and has a period of record from 1985 to 2019, the pre-wildfire period would be 1985 through 2007 and the post-wildfire period would be 2008 through 2019. Subsequently, all unburned sites associated with this location would also split the period of record in 2007 with the pre-wildfire period spanning the first year of the unburned site's period of record until 2007. Validation of unburned site selection process was performed using the daily SWE time series for pre-wildfire periods for each burned SNOTEL

site and the associated unburned locations using the Kling-Gupta efficiency scores (KGE) (Gupta et al., 2009). The associated unburned sites used for comparison with each burned site had an overall average $KGE = 0.82$ determined by using functions in the *hydroGOF* R package (Zambrano- Bigiarini, 2020).

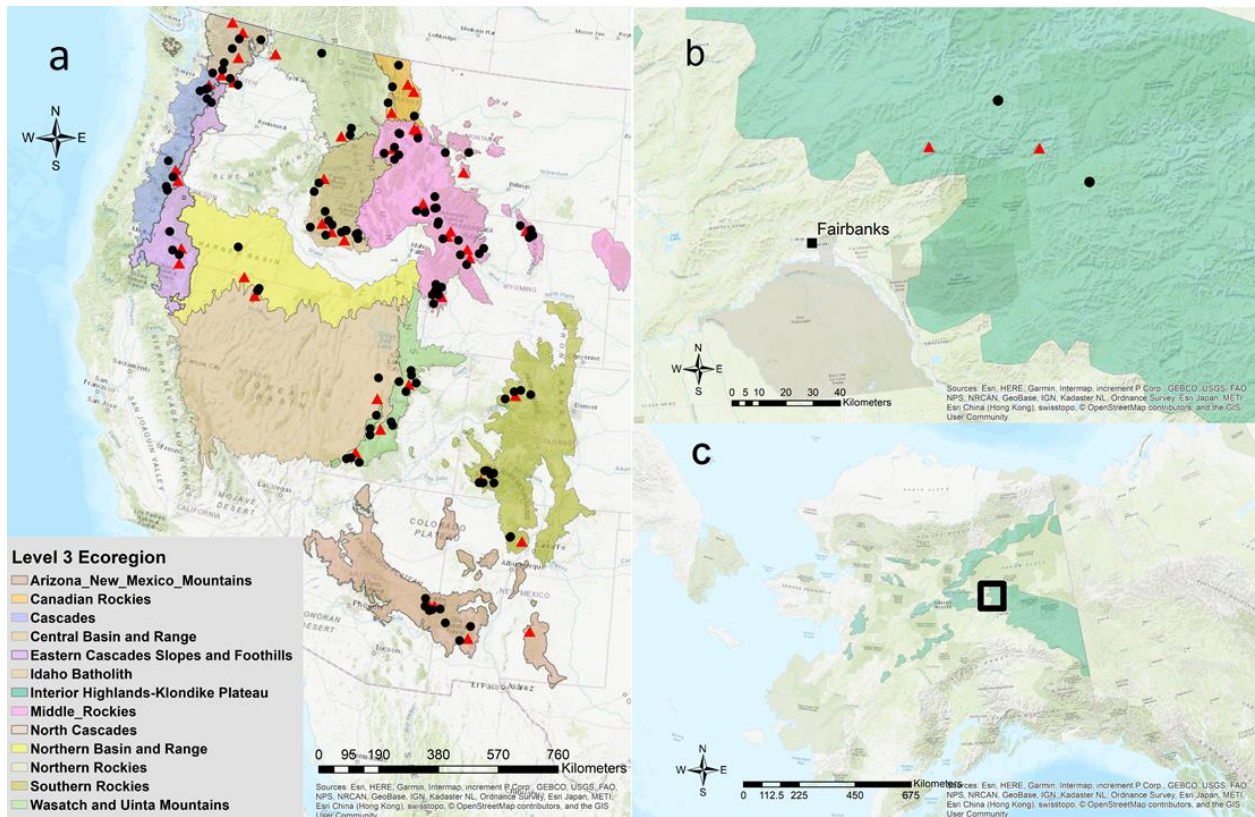


Figure 1. Map of burned (red triangles) and unburned (black circles) SNOTEL sites in (a) western coterminous United States and (b) Alaska. The Alaska sites are located northeast of Fairbanks in the central part of the state (c).

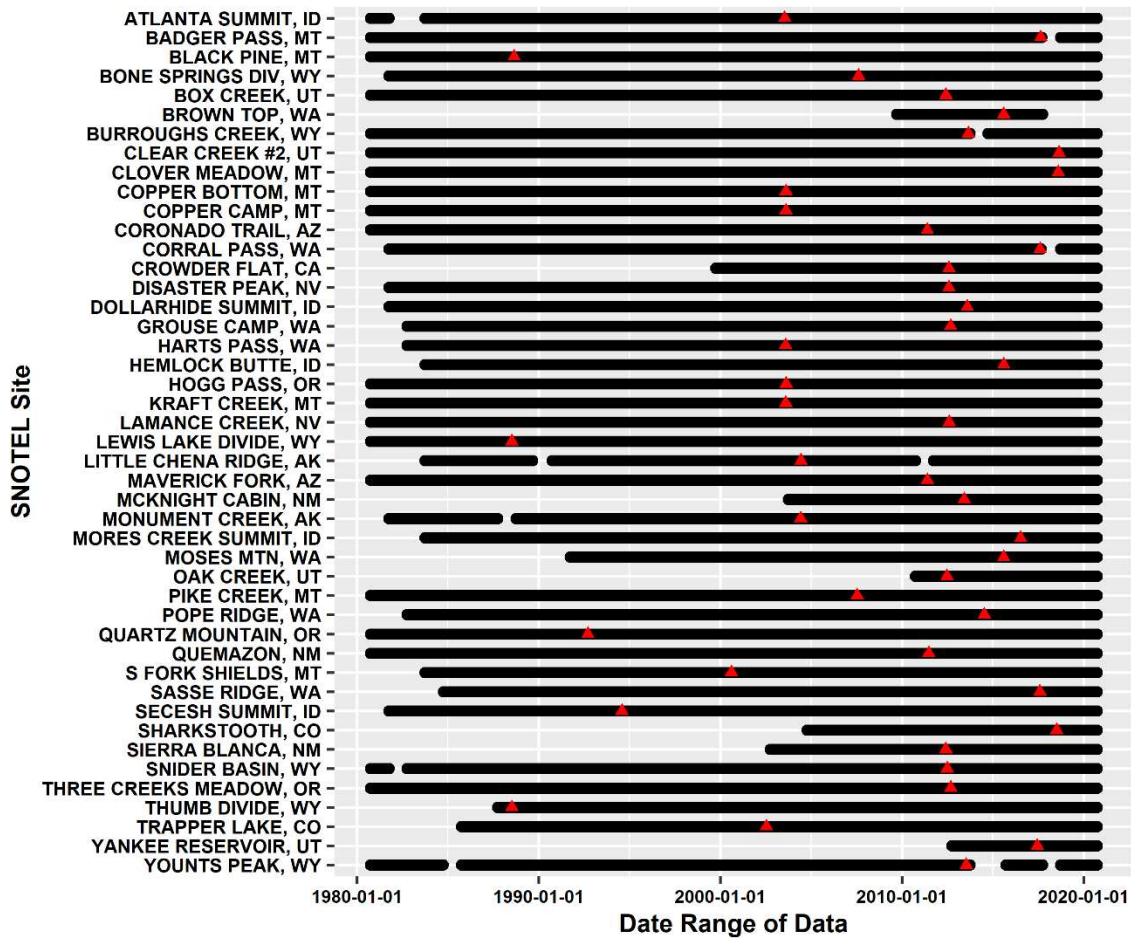


Figure 2. Period of record used for each burned SNOTEL site. The red triangles identify the wildfire dates.

2.3.2 Site Characteristics

Pre-wildfire tree genus and canopy density were considered as potential mediators of wildfire's impact on SWE. U.S. Department of Agriculture Forest Service (USDA-FS) Forest Inventory and Analysis (FIA) data from 2017 were used to obtain the dominant tree genus for the area around each burned SNOTEL location (FIA data were not available for all pre-wildfire periods). The date of the dataset may reduce the data's explanatory power if the dominant tree genus changed after the fire. However, the FIA dataset provides consistent forest stand level information on the extent, distribution, and forest composition (Burrill et al., 2018). The

dominant tree genus was determined as the most common genus in a 1 km² box centered on the burned SNOTEL site. Frequently occurring genera were pine (*Pinus*), fir (includes both *Abies* and *Pseudotsuga*), and spruce (*Picea*). Only three sites were hemlock (*Tsuga*), and three sites were other genera. For analysis purposes, those six sites are grouped as “hemlock/other.”

Canopy density was quantified using leaf-area index (LAI), which for coniferous canopies is defined as one-half the total needle surface area per unit ground area (Jonckheere et al., 2004). The MODIS 8-day 500 m (MCD15A2H) LAI product (Myneni et al., 2015) was used, which has good agreement when compared with ground-based measurements of LAI (Jensen et al., 2011). The phenology of the canopy can cause LAI to vary seasonally. Because winter LAI is most relevant to snowpack (Xiao et al., 2019), LAI values from the beginning of October were used for all locations (LAI from summer dates were also used in the analysis and produced similar results). The October LAI represents the beginning of the snow accumulation season and the lowest LAI prior to snow cover (Yang et al., 2006). The average pre-wildfire and post-wildfire LAI values at the burned SNOTEL sites are 5.0 and 3.1, respectively. The change in LAI was calculated by subtracting the October LAI that immediately followed the fire from the October LAI that immediately preceded the fire. Due to the limited period of MODIS observations, LAI was not available for fires that occurred prior to 2003. Therefore only 37 of the 45 burned sites are used in analyses that consider LAI.

Burn severity was obtained from the Monitoring Trends in Burn Severity program (MTBS) (<https://www.mtbs.gov/project-overview>). This program is an inter-agency effort led by the USDA-FS and the U.S. Geological Survey with the goal of providing consistent categorized burn severity information for all fires since 1984 (Eidenshink et al., 2007). In the western U.S., the MTBS information is available through 2019 for fires greater than 1000 acres.

Burn severity from MTBS has been used in other studies that examined patterns and impacts of burn severity on the landscape (Arkle et al., 2012; Baker, 2015; Bradley et al., 2016). In this study, the categorical burn severity (i.e., low, moderate, and high) was used, which is based on threshold values of the differenced Normalized Burn Ratio (dNBR) (Eidenshink et al., 2007). Burn severity is defined as the loss of above ground organic matter and organic matter in the soil (Keeley, 2009). The near infrared and shortwave infrared wavelengths are used to quantify NBR, and the difference between pre-wildfire and post-wildfire values is the final dNBR estimate. The consistency of these categories between fires has been questioned (Kolden et al., 2015), but Meigs et al. (2011) showed that the MTBS burn severity categorization is related to tree mortality, so it might indicate the change in canopy condition during the snow season. Picotte et al. (2020) also noted that the MTBS program uses various measures to promote consistency between analysts. Due to the temporal and spatial extents of the SNOTEL dataset and associated fires, the MTBS data burn severity categories provide the most consistent data available.

2.3.3 Summary Methods

Four measures are used to quantify the snow phenology: (1) annual maximum SWE, (2) annual maximum normalized SWE (nSWE), (3) date of annual maximum SWE, and (4) annual melt-out date. The annual maximum SWE was determined using a 01 October through 30 September water year. If the maximum value occurred over multiple dates, the first date was selected. nSWE normalizes the SWE to account for interannual variations in precipitation. The annual maximum nSWE was calculated as the maximum SWE divided by the total October through April precipitation. The melt-out date is identified as the first day when SWE equaled zero. For each measure of snow phenology, median values were calculated for the pre- and post-

wildfire periods. Then, the difference between the post-wildfire and pre-wildfire medians was calculated. At unburned sites, this change is expected to reflect changes in climate between the two periods. At burned sites, this change reflects the combined changes in climate and the effects of the wildfire. To isolate the effect of the fire, the difference between the change at the burned sites and the unburned sites was calculated as the fire signal.

To assess the significance of the changes, the non-parametric Wilcoxon Rank Sum Test was applied to evaluate the hypothesis that the snow phenology measures from the pre- and post-wildfire periods are drawn from the same populations (Helsel et al., 2020). The test was applied to both the burned and unburned sites and significance was determined using a p-value of 0.05.

2.4 RESULTS

2.4.1 *Changes in Snow Phenology Measures*

The changes in median melt-out dates between the pre-wildfire and post-wildfire periods are shown in Figure 3. The sites are also grouped by level 3 ecoregions (Omernik & Griffith, 2014) to examine the behavior for regions that are similar in geology, physiography, vegetation, climate, and soil. Overall, 78% of the unburned locations had earlier melt-out dates for their post-wildfire periods than their pre-wildfire periods (Figure 3a). The sites in the Arizona-New Mexico Mountains ecoregion in particular had much earlier melt-out dates for the post-wildfire periods. Some site-to-site variability is observed within ecoregions (e.g., 5 of the 12 ecoregions contain sites with later post-wildfire melt-out dates), but the changes tend to be similar within ecoregions. Overall, the results suggest that the climate during the post-wildfire periods was less favorable to late season snowpack than the pre-wildfire period for most ecoregions.

In contrast, the burned SNOTEL sites almost uniformly (42 of 45 sites and all ecoregions) had earlier melt-out dates for their post-wildfire periods (Figure 3b). About half of

the ecoregions contain one or more burned sites where the change in melt-out date is statistically significant according to the test described earlier. The change in the melt-out date is also more negative at the burned sites than the unburned sites. Overall, 84% (38 out of 45) burned sites had larger changes in melt-out date than the unburned comparison sites. The earlier melt-out dates likely occur in part because the wildfires reduce the canopy coverage and decrease the snowpack albedo (due to pyrogenic carbon particles and burned wood debris), both of which increase the available energy and promote snowmelt (Gleason et al., 2013). The shift to earlier melt-out dates averaged approximately 20 days for the 11 statistically significant sites.

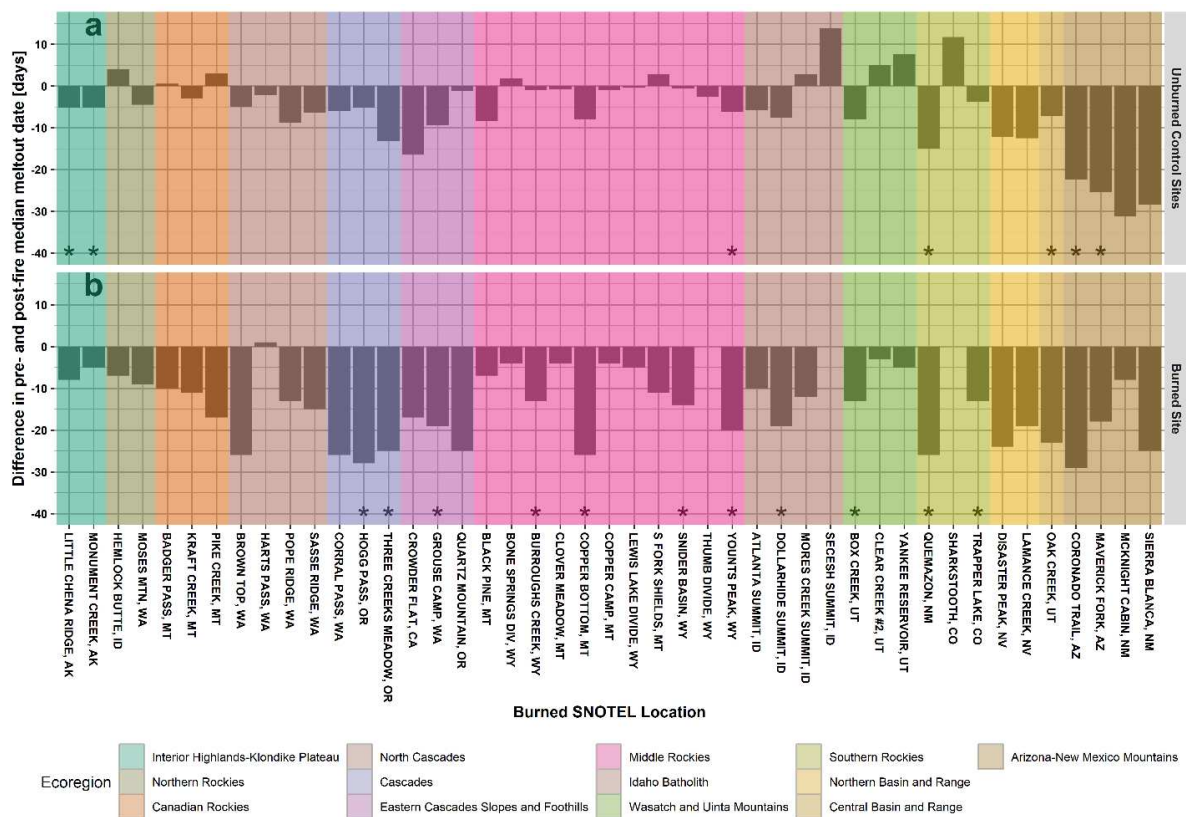


Figure 3. Difference in pre- and post-wildfire melt-out dates at (a) unburned control sites and (b) associated burned sites. For each unburned site, the difference is calculate using the wildfire date at the associated burned site. A negative value indicates an earlier melt-out date post-wildfire than pre-wildfire. An asterisk indicates a statistically significant (p -value < 0.05) difference between pre- and post-wildfire periods at a burned site. Ecoregions are listed from approximately northwest to southeast (see Figure 1).

The changes in the median date of maximum SWE between the post-wildfire and pre-wildfire periods are presented in Figure 4 for both the unburned and burned sites. A weak majority of unburned sites (56%) had earlier maximum SWE dates for the post-wildfire period than the pre-wildfire period (Figure 4a). Clear differences are observed in the behavior of different ecoregions. The northernmost ecoregions (left side of figure) typically had later maximum SWE dates for the post-wildfire period while the southern ecoregions (right side of figure) typically had earlier maximum SWE dates. Sites that had earlier post-wildfire melt-out dates (Figure 3a) also tended to have earlier maximum SWE dates (Figure 4a), and the average magnitude of change is often similar. This similarity suggests that the factors producing the changes at the unburned sites (likely precipitation and temperature changes) are similarly impacting both the accumulation and ablation periods for the snowpack.

Most burned sites (78% or 35 out of 45) had earlier maximum SWE dates post-wildfire than pre-wildfire (Figure 4b). About half the ecoregions contain one or more sites where the change in maximum SWE date is statistically significant. Overall, the values are more negative for the burned sites than the unburned sites. The burned sites also exhibit more variability within ecoregions than the unburned sites. Within a given ecoregion, the unburned canopy may promote similarity between sites because the dominant vegetation type is one criterion for defining ecoregions. When the canopy is reduced and altered by a wildfire, site-specific factors such as slope and aspect may play larger relative roles as discussed by Harpold et al. (2014) and promote variability within ecoregions. The average shift in maximum SWE at the 11 statistically significant sites was approximately 13 day earlier.

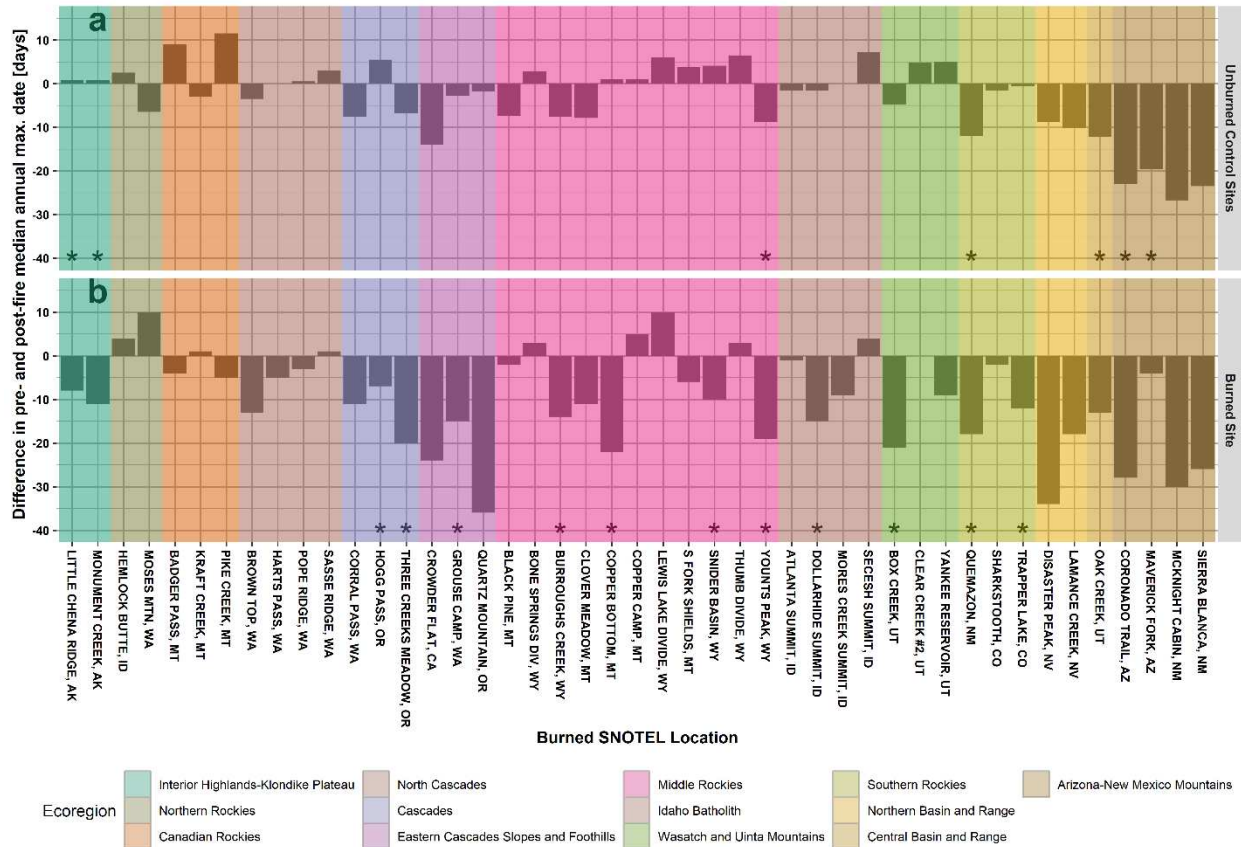


Figure 4. Difference in median dates of maximum SWE for pre- and post-wildfire periods and (a) unburned control sites and (b) associated burned sites. For each unburned site, the difference is calculate using the wildfire date at the associated burned site. A negative value indicates an earlier date of maximum SWE post-wildfire than pre-wildfire. An asterisk indicates a statistically significant (p -value < 0.05) difference between pre- and post-wildfire periods at the burned site. Ecoregions are listed from approximately northwest to southeast (see Figure 1).

The changes in the maximum depth of SWE between the pre-wildfire and post-wildfire periods are shown in Figure 5. Overall, 62% of unburned sites (28 out of 45) had an increase in maximum SWE for the post-wildfire period (Figure 5a). Thus, the earlier melt-out and maximum SWE dates are not necessarily associated with lower maximum SWE values. For the unburned sites, the direction and magnitude of change tends to be similar within a given ecoregion, but it varies notably between ecoregions. The largest changes are observed in the southern ecoregions (Northern Basin and Range, Southern Basin and Range, and Arizona-New

Mexico Mountains). The large differences in these ecoregions suggests that precipitation and/or temperature differed substantially between the pre- and post-wildfire periods.

In contrast to the unburned sites, 60% of burned sites (27 out of 45) had reductions in maximum SWE in the post-wildfire periods (Figure 5b), and 8 of 13 ecoregions contain one or more sites where the change was statistically significant. More site-to-site variability is observed within ecoregions for the burned sites than the unburned sites with some locations having very large changes in the maximum SWE. These results suggest that the change in maximum SWE from a single burned location may not be representative of other burned parts of an ecoregion. The average maximum SWE decrease for the 11 statistically significant sites was approximately 26%.

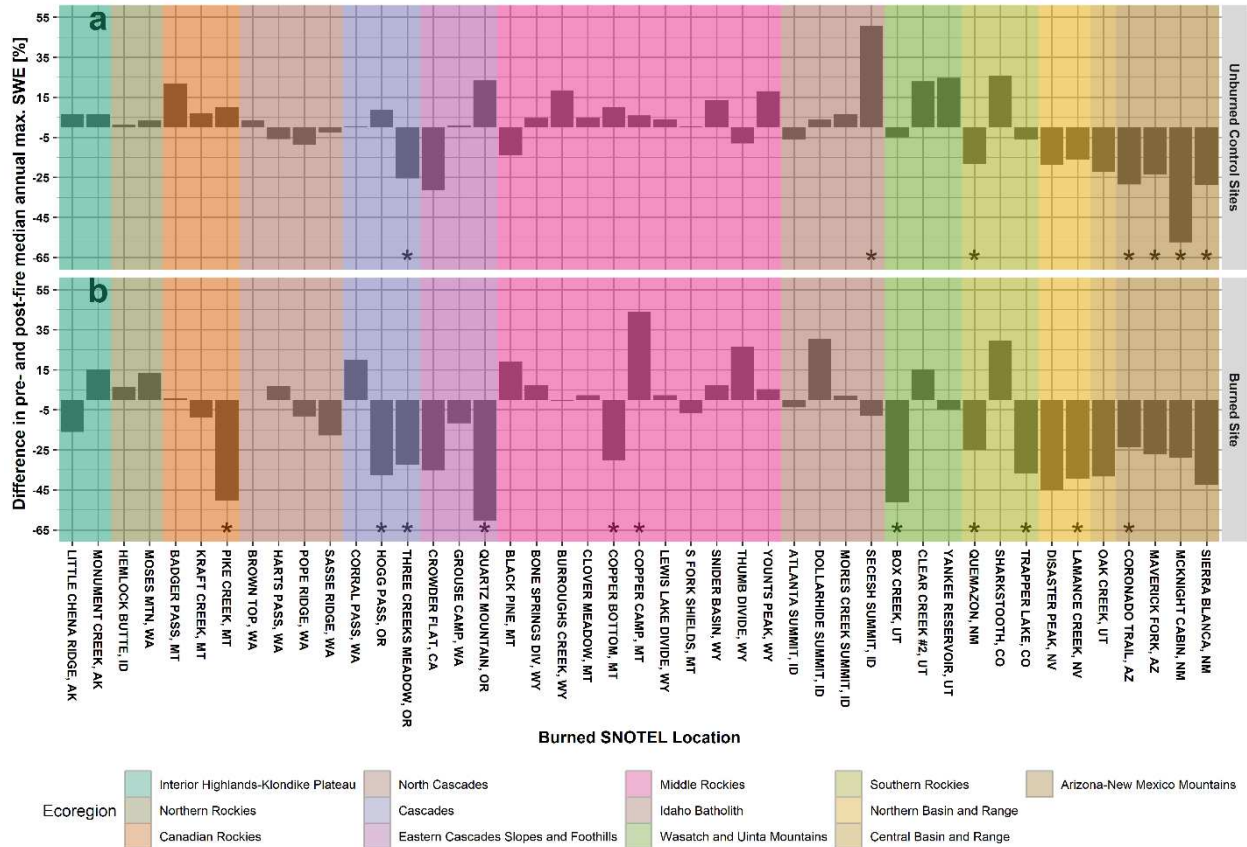


Figure 5. Percent difference in median annual maximum SWE for pre- and post-wildfire periods for burned and unburned sites. The average percent difference for unburned sites is based on similar pre- and post-wildfire periods for the associated with the burned SNOTEL listed. Negative value indicates lower SWE post-wildfire. An asterisk indicates statistically significant (p -value < 0.05) between pre- and post-wildfire periods at burned sites. Ecoregions are listed from approximately northwest to southeast (see Figure 1)

The change in annual maximum nSWE between the post-wildfire and pre-wildfire periods is shown in Figure 6. Inter-annual precipitation variations are reduced when using nSWE in the analysis, so remaining differences at the unburned sites reflect changes in other climatic factors. Slightly less than half (49% or 22 out of 45) of the unburned sites had decreases in maximum nSWE between the pre- and post-wildfire periods, and in most ecoregions, the changes in nSWE are small. Thus, differences in precipitation between the two periods primarily caused changes in the maximum SWE at the unburned sites. However, for the Arizona-New Mexico Mountains, large changes are still observed in nSWE between the pre- and post-wildfire

periods. This persistence suggests other climate factors (such as wintertime temperature) are the main sources of change in maximum SWE for this ecoregion.

Maximum nSWE decreased in the post-wildfire periods for approximately 67% (30 out of 45) of the burned sites, and 10 of 13 ecoregions contain at least one site where the difference is statistically significant. While most burned sites had decreases in maximum nSWE, most ecoregions also include sites where the maximum nSWE increased. The exceptions are the most northern and southern ecoregions considered. The Interior Highlands-Klondike Plateau in Alaska had consistent increases in nSWE while the Arizona-New Mexico Mountains had consistent decreases in nSWE. For the 16 statistically significant burned sites, the average nSWE decrease was approximately 16% between fire periods.

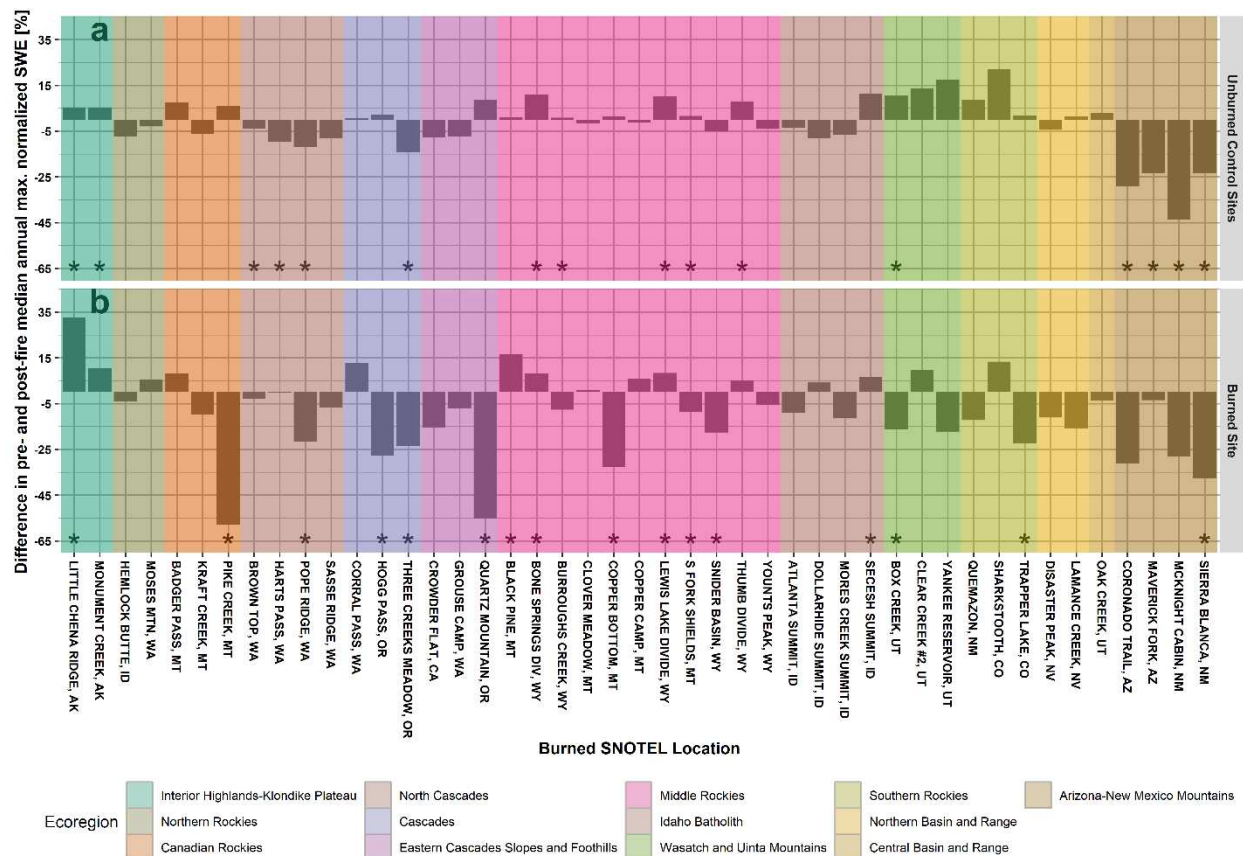


Figure 6. Percent difference in annual maximum nSWE between pre- and post-wildfire periods. The average percent difference for unburned sites is based on similar pre- and post-wildfire periods for the associated with the burned SNOTEL listed. Negative value indicates lower nSWE post-wildfire. An asterisk indicates statistically significant (p -value < 0.05) between pre- and post-wildfire periods at burned sites. Ecoregions are listed from approximately northwest to southeast (see Figure 1)

Table 1 summarizes the average change between the pre- and post-wildfire periods for the unburned and burned sites by ecoregion. The climate signal results consider the unburned sites. They show that the melt-out and maximum SWE dates advanced by averages of 6 and 5 days, respectively, for the post-wildfire period when all ecoregions are combined. The climate signal also reduced maximum SWE values for the post-wildfire period by an average of about 2%. For regions within the Cold Desert level 2 ecoregion (10.1), climate-related reductions in maximum SWE are largely explained by reductions in precipitation. This is apparent because the reductions in nSWE are much smaller than the reductions in SWE. The efficiency of

snowpack production changed little between the two periods. In the Upper Gila Mountains level 2 ecoregion (13.1), the change in maximum SWE is mostly unrelated to precipitation changes. In the Boreal Cordillera level 2 ecoregion (6.2), SWE changes are due to a combination of precipitation and other factors. The largest changes in SWE properties occurred in southern part of the Boreal Cordillera (6.2) ecoregion and the Cold Desert (10.1) and Upper Gila Mountain (13.1) ecoregions.

The combined signal results in Table 1 considers the burned sites. Overall, the largest changes in the snow phenology measures occurred in the Cascades, Eastern Cascades Slopes and Foothills, and Southern Rockies level 3 ecoregions. For the Cascades and Southern Rockies, a majority of sites exhibited statistically significant changes for the phenological measures.

The wildfire signal results are derived by taking the difference between the combined signal (burned sites) and climate signal (unburned sites). Overall, wildfires advanced melt-out and peak SWE dates in the ecoregions by averages of 9 and 7 days, respectively. In addition, wildfires reduced peak SWE values in the ecoregions by an average of about 13%. While these reductions varied by ecoregion, nearly all ecoregions experienced an average reduction. The changes in melt-out and maximum SWE dates are more consistent across ecoregions than the changes in maximum SWE. The maximum SWE changes ranged from -35% to 7% between the ecoregions. Overall, the wildfires had stronger impacts on SWE properties than climate changes during the period of study.

Table 1. Average changes in the melt-out date, date of maximum SWE, maximum SWE, and normalized maximum SWE within ecoregions. The climate signal section calculates the changes using the unburned sites, and the combined signal section uses the burned sites. The wildfire signal section takes the difference of the combined and climate signals. An asterisk indicates that most burned sites within the ecoregion had statistically significant changes (p-value < 0.05).

Ecoregion		Climate Signal				Combined Signal				Wildfire Signal			
		Post-Fire Minus Pre-wildfire at Unburned Sites				Post-Fire Minus Pre-wildfire at Burned Sites				Burned Diff. Minus Unburned Diff.			
Number	Name	Melt-out Date [days]	Max. SWE Date [days]	Max. SWE [%]	Max. nSWE [%]	Melt-out Date [days]	Max. SWE Date [days]	Max. SWE [%]	Max. nSWE [%]	Melt-out Date [days]	Max. SWE Date [days]	Max. SWE [%]	Max. nSWE [%]
6.1.1	Interior Highlands-Klondike Plateau	-5	1	7.3	6.0	-6	-9	-4.3	22.9	-1	-10	-11.5	16.9
6.2.3	Northern Rockies	0	-2	2.8	-4.7	-8	7	9.8	0.7	-8	9	7.0	5.4
6.2.4	Canadian Rockies	0	6	13.3	2.6	-13	-3	-19.4	-19.8	-13	-9	-32.7	-22.4
6.2.5	North Cascades	-6	0	-4.1	-8.5	-13	-5	-4.8	-7.8	-8	-5	-0.8	0.6
6.2.7	Cascades	-8	-3	-4.1	-2.7	-26*	-13*	-16.7*	-12.8*	-18	-9	-12.6	-10.1
6.2.8	Eastern Cascades Slopes and Foothills	-9	-6	-1.1	-0.9	-20	-25	-35.9	-25.9	-11	-19	-34.8	-24.9
6.2.10	Middle Rockies	-2	0	7.6	3.2	-10	-6	6.9	-2.4*	-8	-5	-0.7	-5.7
6.2.15	Idaho Batholith	1	1	13.6	-1.6	-10	-5	5.1	-2.4	-11	-6	-8.5	-0.8
6.2.13	Wasatch and Uinta Mountains	2	2	15.4	14.9	-7	-10	-13.7	-8.0	-9	-12	-29.1	-22.9
6.2.14	Southern Rockies	-2	-5	0.8	11.1	-13*	-11*	-10.9*	-7.1	-11	-6	-11.7	-18.2
10.1.3	Northern Basin and Range	-12	-10	-13.5	-1.2	-21	-26	-42.4	-13.4	-9	-16	-28.9	-12.2
10.1.5	Central Basin and Range	-7	-12	-25.0	3.3	-23	-13	-38.3	-3.7	-16	0	-13.4	-7.1
13.1.1	Arizona-New Mexico Mountains	-27	-23	-37.6	-30.2	-20	-22	-30.6	-25.1	7	1	7.0	5.1
Average		-5.9	-4.0	-1.9	-0.7	-14.7	-10.7	-15.0	-8.1	-8.8	-6.7	-13.1	-7.4
Median		-5.3	-2.0	0.8	-0.9	-13.2	-10.0	-13.7	-7.8	-8.9	-6.1	-11.7	-7.1

2.4.2 Potential Controls on SWE Changes

In this section, examination of other variables and their effects of wildfire on SWE phenology is explored. Similar to Table 1, the change in the snow phenology measures between the pre-wildfire and post-wildfire periods is calculated first. At the unburned sites, this difference is considered a climate signal, and at the burned sites, this difference is a combined wildfire and climate signal. The wildfire signal is then obtained by comparing the changes at the unburned and burned sites. The readily available information includes the burn severity, change in leaf-area index, dominant pre-wildfire tree genus, time since the fire, and land surface elevation.

2.4.2.1 Burn Severity

Figure 7 compares the changes in the snow phenology measures at the unburned and burned sites when the sites are grouped according to the burn severity (at the burned site). The effect of the wildfire is seen for all three burn severity categories and does not appear to depend on the burn severity (i.e., the differences of the average values for the unburned and burned sites does not exhibit a clear trend with changing burn severity). Similarly, Figures 7c and 7d show that the wildfires typically reduced SWE and nSWE for all burn severity categories with no clear dependence on burn severity.

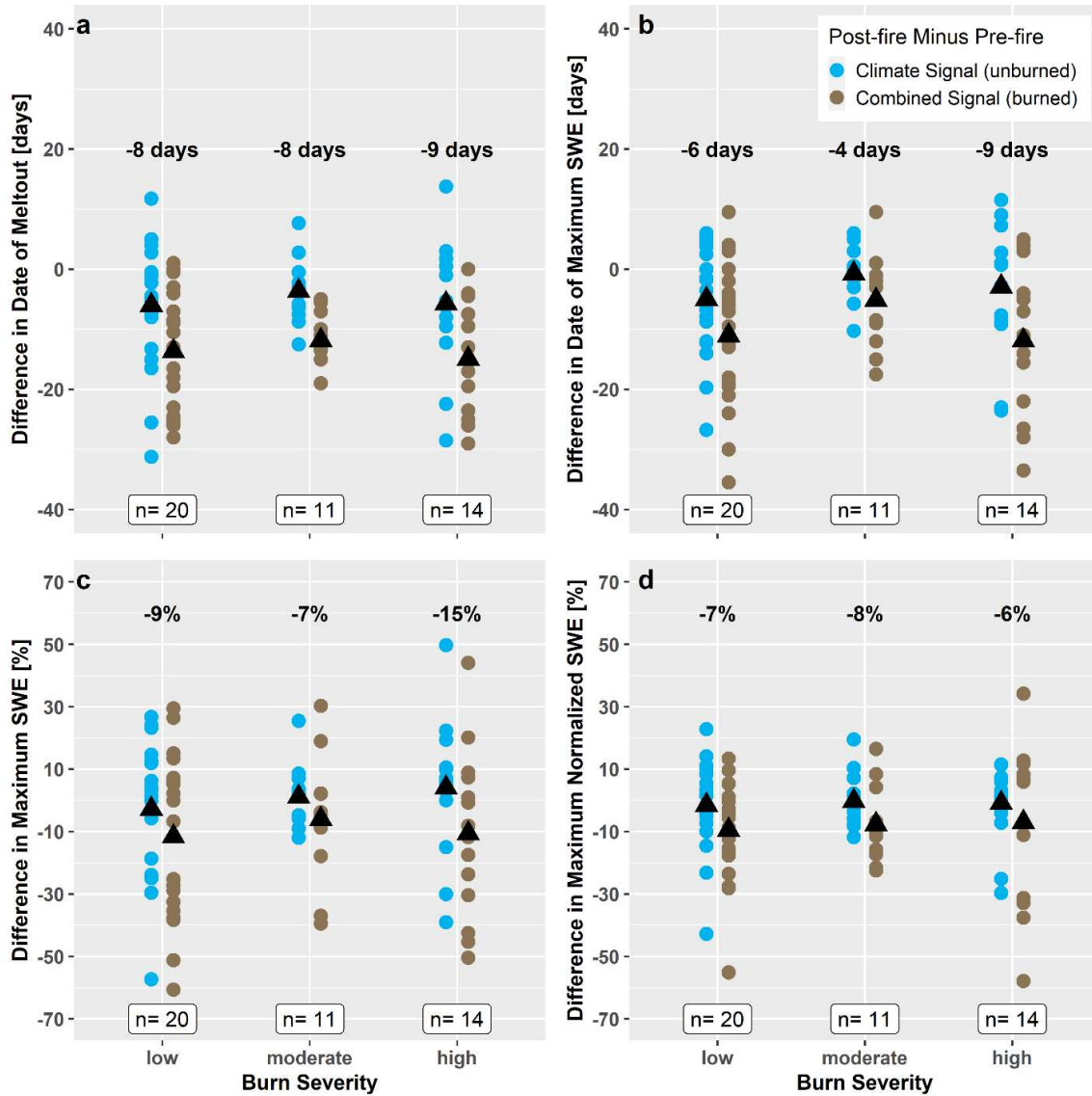


Figure 7. Differences in snow phenology measures between post-wildfire and pre-wildfire periods for the unburned sites (climate signal) and burned sites (combined signal) when the sites are grouped by burn severity (at the burned sites). The sample size n for each grouping is shown at the bottom of each panel. Black triangles show the average values. The differences in the average values (i.e., the fire signal) are shown at the top of each panel.

2.4.2.2 Leaf-area Index

Figure 8 compares the changes in snow phenology measures at the unburned and burned sites when the sites are grouped by the change in burned site LAI. The difference between the unburned and burned sites suggests that wildfires typically promoted earlier melt-out and

maximum SWE dates when LAI decreased (Figure 8a and 8b). Earlier dates are potentially a result of increased shortwave radiation on the snow surface during both the accumulation and ablation periods due to reduced canopy cover and increased snowpack albedo. However, the burned sites typically had earlier melt-out and peak SWE dates than the unburned sites even if LAI increased at the burned site. All three sites in this LAI category (Mores Creek Summit, Bone Springs Divide, and Brown Top) had below normal annual precipitation immediately preceding the fire and above normal annual precipitation immediately post-wildfire. Therefore, the apparent dependence on LAI for these sites is partially due to local precipitation variations. Figure 8c and 8d suggest that more substantial LAI decreases at the burned sites tended to produce more substantial reductions in maximum SWE and nSWE. In particular, when LAI decreased by more than 1.5, the average difference between the unburned and burned sites was 13% and 9% for maximum SWE and nSWE, respectively. Smaller reductions in LAI are associated with much smaller average differences between the unburned and burned sites (2-4%).

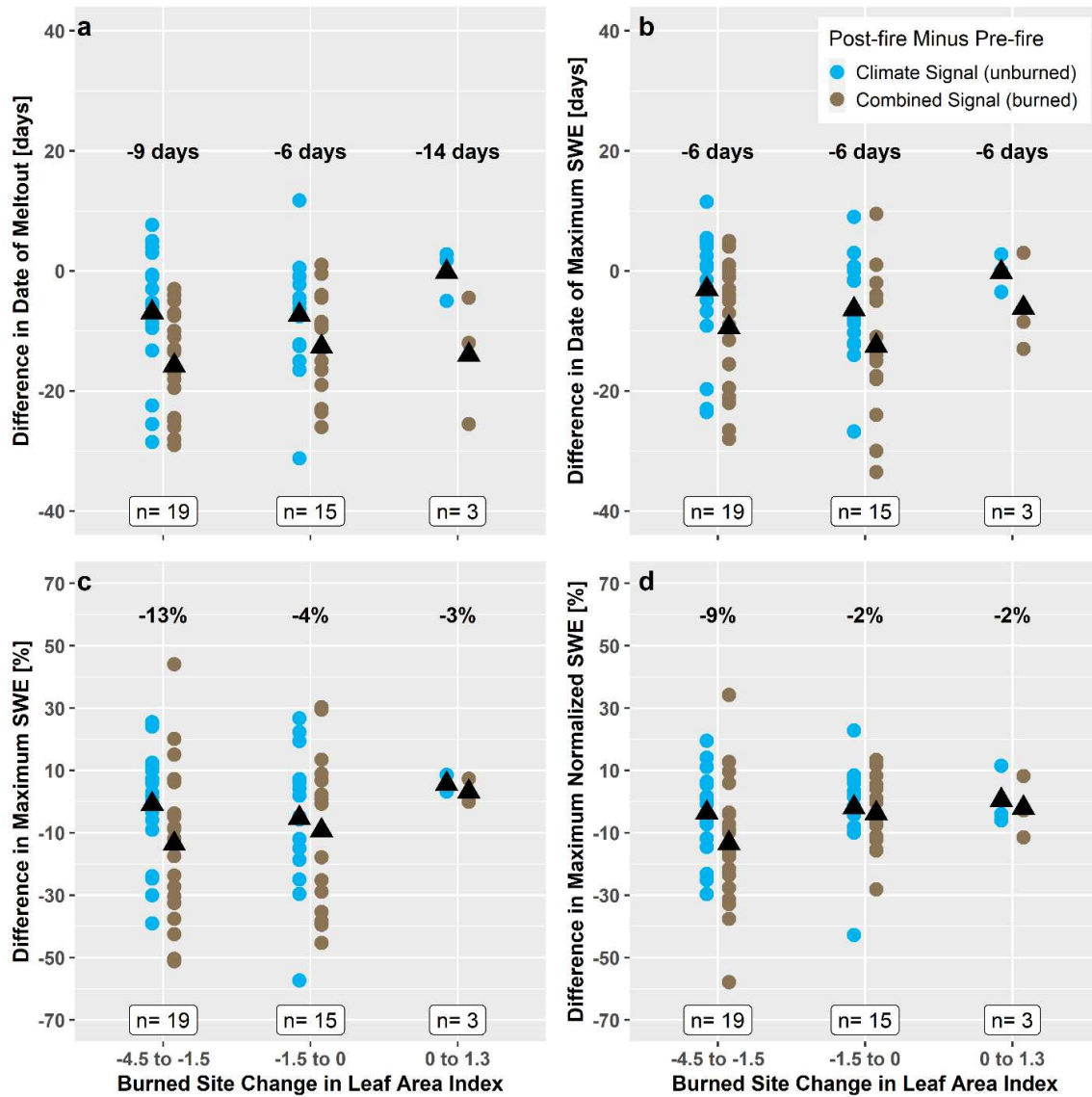


Figure 8. Differences in snow phenology measures between post-wildfire and pre-wildfire periods for the unburned sites (climate signal) and burned sites (combined signal) when the sites are grouped by change in leaf area index (LAI). A negative change indicates a post-fire reduction in LAI. The sample size n for each grouping is shown at the bottom of each panel. Black triangles show the average values. The differences in the average values (i.e., the fire signal) are shown at the top of each panel.

2.4.2.3 Tree Genera

Figure 9 compares the change in the snow phenology measures for the unburned and burned sites when the sites are grouped by dominant pre-wildfire trees genus. For melt-out dates (Figure 9a), substantial differences in behavior are observed between the different genera. The

largest differences in melt-out dates between the unburned and burned sites occurred for the hemlock/other sites while the smallest differences occurred for the pine and spruce sites. The differences in the date of maximum SWE have less variability between the different vegetation types (Figure 9b). Wildfires typically advanced the dates of maximum SWE for all genera categories, but the largest average change occurred again for the hemlock/other category. In Figure 9c, the change in maximum SWE is typically more negative for the burned sites than the unburned sites for all genera categories. The largest difference between the unburned and burned sites (i.e., wildfire signal) occurs for the hemlock/other category (Figure 9c). However, the nSWE results (Figure 9d) show less variability in wildfire signal between the genera categories.

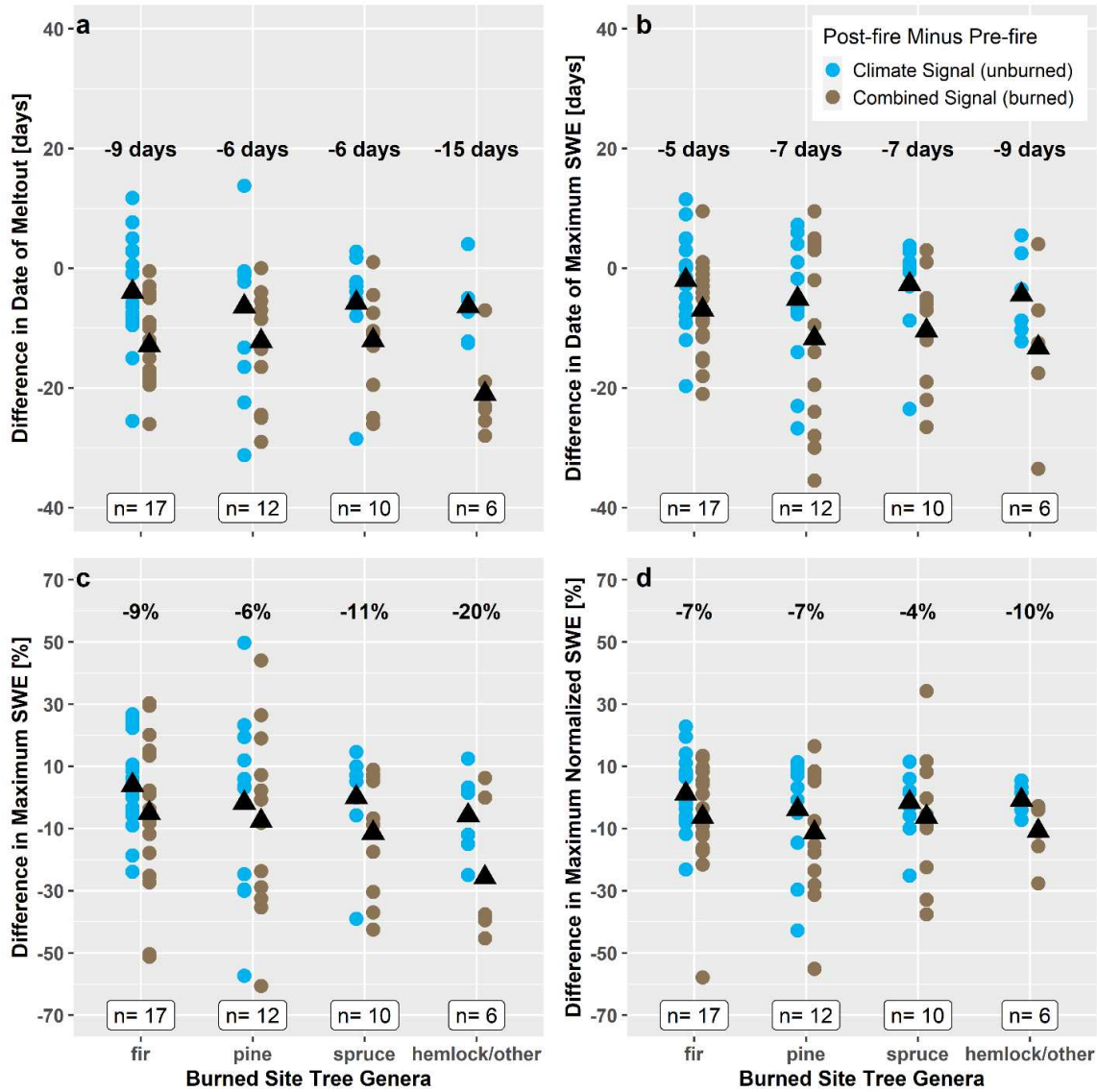


Figure 9. Differences in snow phenology measures between post-wildfire and pre-wildfire periods for the unburned sites (climate signal) and burned sites (combined signal) when the sites are grouped by tree species. The sample size n for each grouping is shown at the bottom of each panel. Black triangles show the average values. The differences in the average values (i.e., the fire signal) are shown at the top of each panel.

2.4.2.4 Time Since Fire

Figure 10 compares the changes in the snow phenology measures between the unburned and burned sites when the sites are grouped according to the time since fire occurrence. For both the unburned and burned sites, the changes in all four measures are typically most severe for the

5-to-10-year category while the 10-to-32-year category shows the greatest variability in the changes. Comparing the unburned and burned sites suggests that the effect of the wildfires on melt-out and maximum SWE dates typically persists beyond 10 years. For SWE and nSWE, the largest average impact of the wildfires occurs beyond 10 years. Overall, the results suggest that most sites have not recovered to pre-wildfire conditions within their available periods of record. Based on the studies summarized in Stevens-Rumann & Morgan (2019), it is not uncommon for little or no tree regeneration to occur after wildfires in parts of the western U.S. Several variables that can influence recovery include genera, distance to seed source, water stress, precipitation, elevation, slope, aspect, and plant competition.

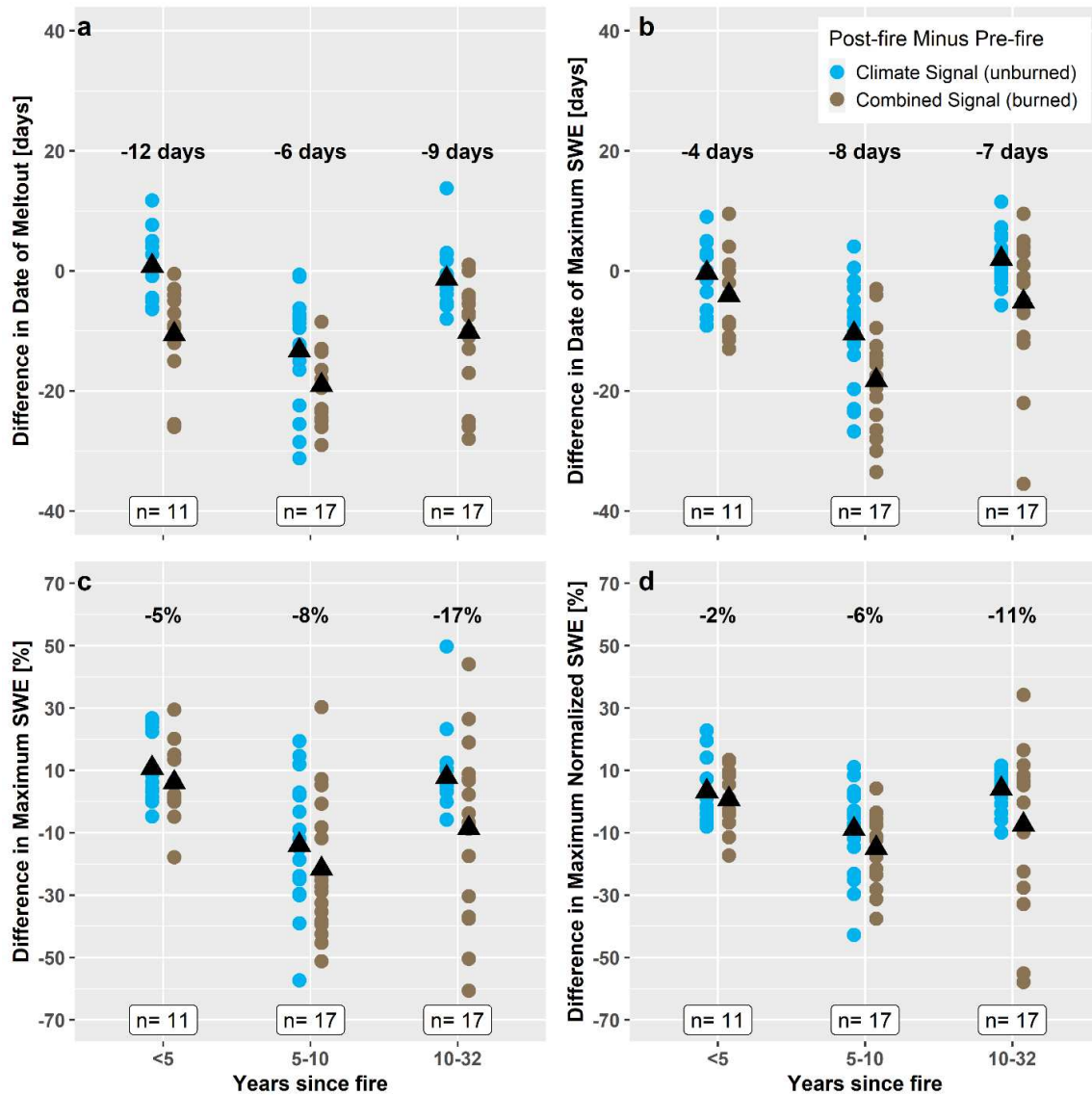


Figure 10. Differences in snow phenology measures between post-wildfire and pre-wildfire periods for the unburned sites (climate signal) and burned sites (combined signal) when the sites are grouped by years since the fire. The sample size n for each grouping is shown at the bottom of each panel. Black triangles show the average values. The differences in the average values (i.e., the fire signal) are shown at the top of each panel.

2.4.2.5 Elevation

Figure 11 compares the change in the snow phenology measures for the burned and unburned sites when the sites are grouped by elevation. The changes in melt-out and peak SWE dates are typically more severe at burned sites than unburned sites irrespective of the elevation

category, but the greatest advances in these dates typically occur at the lowest elevations (Figure 11a and 11b). Similarly, the burned sites usually exhibit greater reductions in SWE than the unburned sites (Figure 11c) for all elevation categories. Wildfires produced the greatest average effect on SWE and nSWE for sites in the lowest elevation category (below 1960 m). Above 1960 m, the wildfire's impact on SWE and nSWE does not exhibit a consistent dependence on elevation. The lack of dependence of nSWE on elevation may occur due to varied geographic location, climate and vegetation for sites within each elevation category.

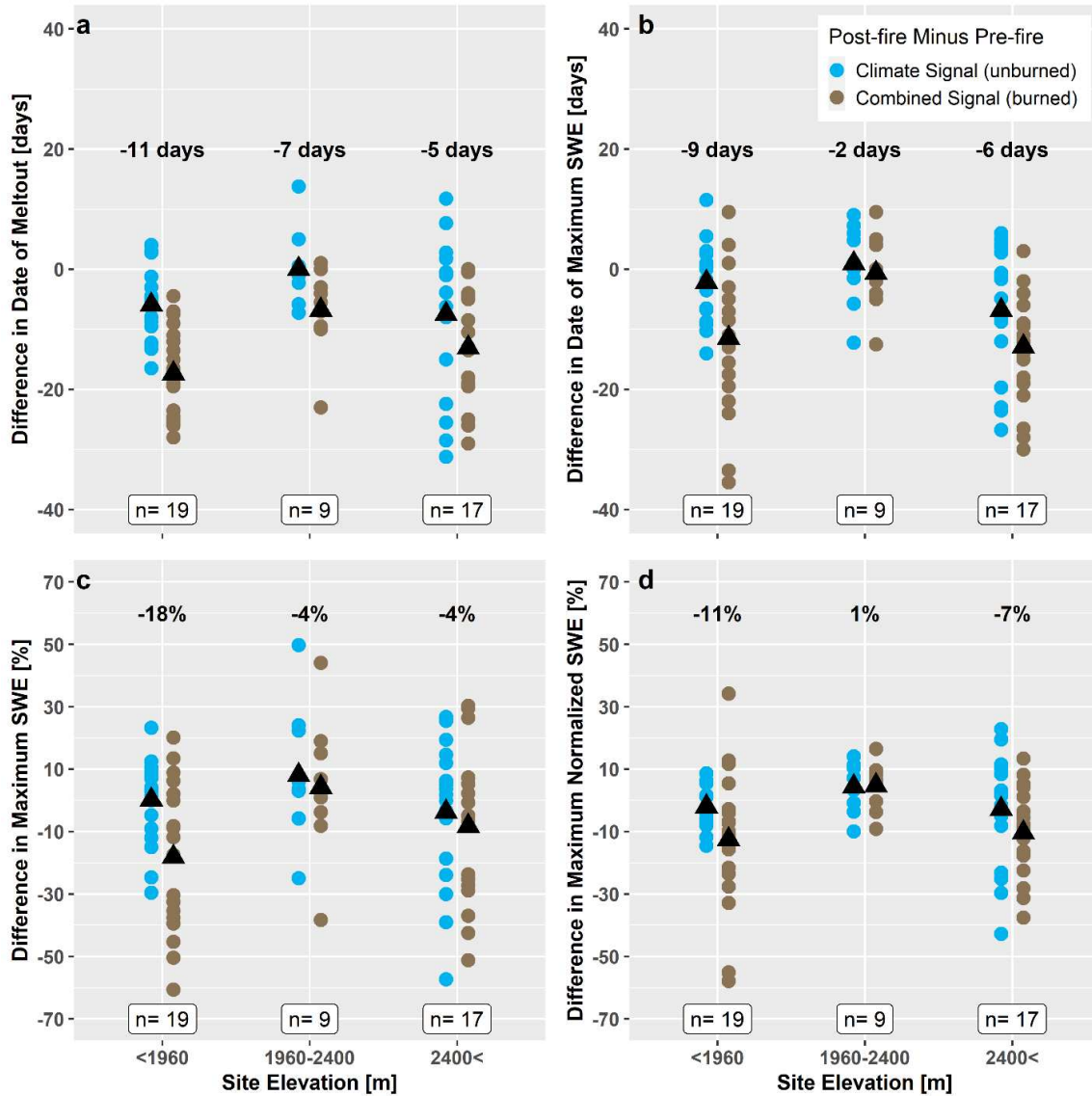


Figure 11. Differences in snow phenology measures between post-wildfire and pre-wildfire periods for the unburned sites (climate signal) and burned sites (combined signal) when the sites are grouped by burned site elevation. The sample size n for each grouping is shown at the bottom of each panel. Black triangles show the average values. The differences in the average values (i.e., the fire signal) are shown at the top of each panel.

2.5 DISCUSSION

Overall, the results suggest that wildfires typically produce lower annual maximum SWE values compared to pre-wildfire or nearby unburned conditions. The reductions are likely related to increased shortwave radiation and albedo changes for the snow surface (Burles & Boon, 2011;

Gleason et al., 2018; Gleason & Nolin, 2016). In addition to the increased shortwave radiation reaching the snow surface, turbulent fluxes can also effect the total energy available for melt following a wildfire. Burles & Boon (2011) found both net shortwave radiation and sensible heat flux were important drivers of snowmelt in burned areas. In New Mexico, increased latent heat flux through sublimation of the snowpack was suggested as a cause for reduced SWE (Harpold et al., 2014). The wildfire-induced changes to maximum SWE vary by ecoregion, and more northern ecoregions have some sites that show increases in maximum SWE due to wildfire (Figure 5). The results generally support the summary by Goeking & Tarboton (2020), who found that studies in the higher latitude regions of the U.S. and southern Canada observed increases in SWE while studies in lower latitudes observed reductions in SWE due to wildfire. The results for sites in Alaska indicate increases in nSWE even as the unburned sites in the region have minimal change in nSWE. The results also agree with Hubbart et al. (2015), who observed increases in SWE in the Northern Rockies. However, the results differ somewhat in other northern ecoregions because the majority of burned sites still indicate decreases in annual maximum SWE or nSWE. Furthermore, the results support the findings from Stevens (2017), who found that SWE decreased substantially in burned areas of the Sierra Nevada Mountains.

The tendency of wildfires to produce earlier melt-out dates has also been documented in previous research (Gleason et al., 2018). The magnitude of change seen in the climate signal results is also similar to Harpold et al. (2012), who found changes from 2 to 5 days per decade for watersheds in the southwestern U.S. In addition, the results typically show earlier dates regardless of ecoregion, burn severity, change in LAI, tree genus, years since the fire occurred, and elevation. This result initially appears to conflict with Hubbart et al. (2015), who observed later melt-out dates in clear cut areas compared to undisturbed locations. However, the change

in snow albedo due to pyrogenic carbon particles is significant in burn areas and can last for several years (Gleason et al., 2013; Gleason et al., 2018; Gleason & Nolin, 2016). Furthermore, the snow surface energy balance after a fire can still include absorption of shortwave radiation and emission of longwave radiation by standing timber. Such absorption and emission do not occur if the canopy has been completely removed.

The relationship between post-wildfire changes in snow phenology measures and readily available fire, watershed or land surface variables is complex. None of the phenology measures were strongly controlled by a single explanatory variable, but certain measures indicated more substantial responses for certain variable classifications (e.g., larger reductions in LAI and sites with lower elevations). The complexities likely arise because reduced canopy density, and therefore interception, has been shown to generally increase snow accumulation (Veatch et al., 2009; Varhola et al. 2010). Yet the changes in snow albedo and energy fluxes in a burned landscape present unique conditions that may overwhelm any canopy interception changes. The apparent insensitivity to burn severity could be due to errors in the categorization of burn severity. Shadows from snags and standing dead trees with remaining crown structure can influence the dNBR values and can result in misclassifications (Fassnacht et al., 2021). These results are seemingly inconsistent with previous research, which found that canopy removal through logging can significantly influence snow accumulation (Storck et al., 2002; Varhola et al., 2010). Therefore high burn severity would be classified in areas with complete canopy removal. The present results suggest that changes in snow accumulation and ablation in burned forests may not be directly comparable to measurements from areas with complete tree removal (i.e., clear cut areas). In Figures 7a and 7b, the relationship with burn severity indicates unburned sites typically exhibit negative values, which suggests that those sites typically had

earlier melt-out and maximum SWE dates in the post-wildfire period (due to changes in the climate). However, the burned sites are typically more negative, which suggests that the wildfires typically advanced the dates further.

Using SNOTEL to represent snowpack processes in surrounding landscape does have limitations. Based on the equipment at these sites, small openings in the canopy are required to allow snowfall to accumulate on the snow measurement sensor (<https://www.nrcs.usda.gov/wps/portal/wcc/home/aboutUs/monitoringPrograms/automatedSnowMonitoring/>). The sites are not directly influenced by snowfall interception or ablation due to opening of the canopy near the sensor. They can be influenced by radiation and shading from the surrounding canopy. Therefore, SNOTEL sites impacted by wildfire may not capture changes in accumulation due to decreased canopy interception following a wildfire. However, these sites can represent energy balance changes due to increased incoming shortwave radiation and snow surface albedo changes. The removal of the canopy following a fire can also impact turbulent fluxes which are not directly measured by SNOTEL sites. Even with these limitations, SNOTEL data provides systematic records with consistent measurement methods and temporal resolution, which is important for separating wildfire and climate effects on snow phenology.

Pairing unburned SNOTEL sites as a reference for pre-wildfire conditions at burned sites does introduce additional uncertainty in the analysis based on the spatial variability of snowpack (Sexstone & Fassnacht, 2014). Even pairing sites within the same ecoregion can be challenging depending on the snow phenology measure being considered. The actual SWE accumulation and ablation will vary based on local site conditions, which control energy balance fluxes (Tennant et al., 2017). The unburned site selection based on distance and elevation differences relative to the burned site, provides a reasonable pairing of sites based on the KGE values. By using paired

SNOTEL sites there is still uncertainty in the analysis which requires further investigation to fully quantify. Controlling for regional climate trends was done using unburned SNOTEL sites, there are other factors that could not be controlled using this data. These factors include local orographic precipitation patterns, the inter-annual variability of cloudy days which impacts the net shortwave radiation input to the snowpack and wind redistribution which may be occurring once the canopy is removed.

2.6 CONCLUSIONS

This study used SWE data from 45 SNOTEL sites that have been impacted by wildfire and 110 comparison SNOTEL sites that have not been impacted by wildfire. The dataset at the burned sites was divided into pre- and post-wildfire periods, and the dataset at the comparison sites was divided using the same points in time. Several measures of snow phenology were derived from the SWE data at each site including annual melt-out date, date of maximum SWE, maximum SWE, and maximum normalized SWE (maximum SWE divided by October through April total precipitation). Data were grouped by ecoregion, burn severity, change in LAI, dominant pre-wildfire trees genus, years since fire, and elevation. The following conclusions can be drawn from the study:

- Overall, climate has a strong influence on SWE and should be considered when quantifying the wildfire signal. In most ecoregions, normalizing the peak SWE by the total winter precipitation reduced the changes in the snow phenology measures at the unburned sites between the pre- and post-wildfire periods to small values. Thus, much of the climate signal is due to variations in precipitation. However, for the southernmost ecoregion (Arizona-New Mexico Mountains), substantial differences persisted at the

unburned sites even after this normalization. In that case, the difference between the pre- and post-wildfire periods was due to another factor, perhaps wintertime temperatures.

- Wildfires produced earlier melt-out dates for all ecoregions except the Arizona-New Mexico Mountains. On average, the wildfires advanced the melt-out date by 9 days for the ecoregions considered.
- Wildfires produced earlier peak SWE dates for all ecoregions except the Northern Rockies and the Arizona-New Mexico Mountains. On average, the wildfires advanced the peak SWE date by 7 days for the ecoregions considered.
- Wildfires produced lower maximum SWE values for most ecoregions. On average, wildfires reduced peak SWE by approximately 13% for the ecoregions considered. However, part of the reduction was likely due to localized precipitation occurring over some of the unburned sites. On average, wildfires reduced peak nSWE by 7% for the ecoregions considered. Nonetheless, increases in peak nSWE were observed for several of the northern ecoregions.
- When the climate and wildfire signals are combined, the largest changes in SWE timing and depth occurred in the Cascades, Eastern Cascades Slopes and Foothills, and Southern Rockies. For the Cascades and Southern Rockies, many of the changes were significant using a p-value of 0.05.
- The impact of wildfire on the snow phenology measures does not exhibit a clear dependence on burn severity but is more sensitive to the change in LAI. In particular, larger reductions in LAI typically produced larger changes in the peak SWE and nSWE values.

- The effect of the wildfire depends on the dominant pre-wildfire tree genus. The smallest changes in the snow phenology measures typically occurred for spruce and pine forests, while the largest changes usually occurred for the hemlock/other category.
- The effects of the wildfires on the snow phenology measures persist more than 10 years after the fires. The changes to the melt-out and peak SWE dates exhibit no clear dependence on the time since fire (for the periods of record available in this study), while changes to maximum SWE and nSWE were largest for times greater than 10 years.
- The effects of wildfires on the snow phenology measures are strongest at low elevations (below 1960 m). For higher elevations, the wildfire effects exhibit no clear dependence on elevation.

The analyzed dataset represents a range of climates and ecosystems, but it has important limitations. The sample size is not evenly distributed between ecoregions, so aggregated measures tend to emphasize ecoregions with more data. Similarly, the pre- and post-wildfire time periods are not the same across all sites, which emphasize individual years from sites with shorter records. We also have assumed the burned SNOTEL sites provide reasonable representations of the snow accumulation and ablation processes for the area near the site. The spatial representativeness may be limited depending on the exact site location. Finally, the unburned comparison sites were selected based on two key geographic factors. A in-depth analysis on pairing burned sites with the burned locations could refine the estimated changes due to wildfire.

This study helps address some limitations of previous efforts while still prompting several opportunities for future research. Future efforts may include assembling additional pre-

and post-wildfire snow measurements into a comprehensive dataset that can be compared with the SNOTEL sites. Further research can also include an analysis of snowmelt rates in burned areas to understand potential hydrologic changes following wildfire. Finally, remote sensing products can be used along with ground-based measurements to quantify snowpack distribution changes between pre- and post-wildfire periods.

While this study presents results that are relevant to the scientific community, the results also have operational implications for water managers. Water managers should anticipate changes to snow accumulation and ablation following a wildfire. They can expect earlier initiation of snowmelt and a longer snow-free season, which may impact summer streamflow and water temperatures. In addition, an overall shift of the spring snowmelt hydrograph may occur in watersheds where large fires have occurred. The pre-wildfire flow regime is likely to take more than a decade to return to pre-wildfire conditions (if it does return to pre-wildfire conditions). Therefore, long-term adjustments to reservoir operating criteria or other management activities may be necessary to account for the changes caused by wildfire.

2.7 REFERENCES

- Arkle, R. S., Pilliod, D. S., & Welty, J. L. (2012). Pattern and process of prescribed fires influence effectiveness at reducing wildfire severity in dry coniferous forests. *Forest Ecology and Management*, 276, 174–184. <https://doi.org/10.1016/j.foreco.2012.04.002>
- Baker, W. L. (2015). Are high-severity fires burning at much higher rates recently than historically in dry-forest landscapes of the western USA? *PLoS ONE*, 10(9), 1–26. <https://doi.org/10.1371/journal.pone.0136147>
- Barnett, T. P., Adam, J. C., & Lettenmaier, D. P. (2005). Potential impacts of a warming climate on water availability in snow-dominated regions. *Nature*, 438(7066), 303–309. <https://doi.org/10.1038/nature04141>
- Barnhart, T. B., Molotch, N. P., Livneh, B., Harpold, A. A., Knowles, J. F., & Schneider, D. (2016). Snowmelt Rate Dictates Streamflow. *Update Citation When Published*, 1–11. <https://doi.org/10.1002/2016GL069690>
- Bradley, C. M., Hanson, C. T., & DellaSala, D. A. (2016). Does increased forest protection correspond to higher fire severity in frequent-fire forests of the western United States? *Ecosphere*, 7(10), 1–13. <https://doi.org/10.1002/ecs2.1492>
- Broxton, P., Dawson, N., & Zeng, X. (2016). Linking snowfall and snow accumulation to generate spatial maps of SWE and snow depth. *Earth and Space Science*, 3, 246–256. <https://doi.org/10.1002/2016EA000174>.Received
- Burles, K., & Boon, S. (2011). Snowmelt energy balance in a burned forest plot, Crowsnest Pass, Alberta, Canada. *Hydrological Processes*, 25, 3012–3029. <https://doi.org/10.1002/hyp.8067>
- Burrill, E. A., Wilson, A. M., Turner, J. A., Pugh, S. A., Menlove, J., Christiansen, G., Conkling,

- B. L., & David, W. (2018). The Forest Inventory and Analysis Database: database description and user guide version 8.0 for Phase 2. In *U.S. Department of Agriculture, Forest Service*. (Vol. 2). <http://www.fia.fs.fed.us/library/database-documentation/>
- Clow, D. W. (2010). Changes in the timing of snowmelt and streamflow in Colorado: A response to recent warming. *Journal of Climate*, 23(9), 2293–2306.
<https://doi.org/10.1175/2009JCLI2951.1>
- Curry, C. L., & Zwiers, F. W. (2018) Examining controls on peak annual streamflow and floods in the Fraser River Basin of British Columbia. *Hydrology and Earth System Sciences*, 22(4), 2285–2309. <https://doi.org/10.5194/hess-22-2285-2018>
- Dennison, P. E., Brewer, S. C., Arnold, J. D., & Moritz, M. A. (2014). Large wildfire trends in the western United States, 1984-2011. *Geophys. Res. Lett.*, 41, 2928–2933.
- Doesken, N., & Judson, A. (1996). *The Snow Booklet: A guide to the Science, Climatology, and Measurement of Snow in the United States*.
- Du, X., Goss, G., & Faramarzi, M. (2020). Impacts of hydrological processes on stream temperature in a cold region watershed based on the SWAT equilibrium temperature model. *Water (Switzerland)*, 12(4). <https://doi.org/10.3390/W12041112>
- Eidenshink, J., Schwind, B., Brewer, K., Zhu, Z.-L., Quayle, B., & Howard, S. (2007). A Project for Monitoring Trends in Burn Severity. *Fire Ecology*, 3(1), 3–21.
<https://doi.org/10.4996/fireecology.0301003>
- Fassnacht, F. E., Schmidt-Riese, E., Kattenborn, T., & Hernández, J. (2021). Explaining Sentinel 2-based dNBR and RdNBR variability with reference data from the bird's eye (UAS) perspective. *International Journal of Applied Earth Observation and Geoinformation*,

95(October 2020), 102262. <https://doi.org/10.1016/j.jag.2020.102262>

Gleason, K. E., Mcconnell, J. R., Arienzo, M. M., Chellman, N., & Calvin, W. M. (2018). Four-fold increase in solar forcing on snow in western U.S. burned forests since 1999. *Nature Communications*, 2019, 1–8. <https://doi.org/10.1038/s41467-019-09935-y>

Gleason, K. E., & Nolin, A. W. (2016). *Charred forests accelerate snow albedo decay: parameterizing the post-fire radiative forcing on snow for three years following fire*. 3870(June), 3855–3870. <https://doi.org/10.1002/hyp.10897>

Gleason, K. E., Nolin, A. W., & Roth, T. R. (2013). Charred forests increase snowmelt : Effects of burned woody debris and incoming solar radiation on snow ablation. *Geophysical Research Letters*, 40, 4654–4661. <https://doi.org/10.1002/grl.50896>

Goeking, S. A., & Tarboton, D. G. (2020). Forests and Water Yield: A Synthesis of Disturbance Effects on Streamflow and Snowpack in Western Coniferous Forests. *Journal of Forestry*, 172–192. <https://doi.org/10.1093/jofore/fvz069>

Gupta, H. V., Kling, H., Yilmaz, K. K., & Martinez, G. F. (2009). Decomposition of the mean squared error and NSE performance criteria: Implications for improving hydrological modelling. *Journal of Hydrology*, 377(1–2), 80–91. <https://doi.org/10.1016/j.jhydrol.2009.08.003>

Harpold, A. A., Biederman, J. A., Condon, K., Merino, M., Korgaonkar, Y., Nan, T., Sloat, L. L., Ross, M., & Brooks, P. D. (2014). Changes in snow accumulation and ablation following the Las Conchas Forest Fire, New Mexico, USA. *Ecohydrology*, 7, 440–452. <https://doi.org/10.1002/eco.1363>

- Harpold, A., Brooks, P., Rajagopal, S., Heidbuchel, I., Jardine, A., & Stielstra, C. (2012). Changes in snowpack accumulation and ablation in the intermountain west. *Water Resources Research*, 48(11). <https://doi.org/10.1029/2012WR011949>
- Helsel, D. R., Hirsch, R. M., Ryberg, K. R., Archfield, S. A., & Gilroy, E. J. (2020). Statistical Methods in Water Resources Techniques and Methods 4 – A3. *USGS Techniques and Methods*.
- Hubbart, J. A., Link, T. E., & Gravelle, J. A. (2015) Forest canopy reduction and snowpack dynamics in a Northern Idaho watershed of the continental-maritime region, United States. *Forest Science*, 61(5), 882–894. <https://doi.org/10.5849/forsci.14-025>
- Jensen, J. L. R., Humes, K. S., Hudak, A. T., Vierling, L. A., & Delmelle, E. (2011). Evaluation of the MODIS LAI product using independent lidar-derived LAI: A case study in mixed conifer forest. *Remote Sensing of Environment*, 115(12), 3625–3639.
<https://doi.org/10.1016/j.rse.2011.08.023>
- Jonckheere, I., Fleck, S., Nackaerts, K., Muys, B., Coppin, P., Weiss, M., & Baret, F. (2004). Review of methods for in situ leaf area index determination Part I. Theories, sensors and hemispherical photography. *Agricultural and Forest Meteorology*, 121(1–2), 19–35.
<https://doi.org/10.1016/j.agrformet.2003.08.027>
- Keeley, J. E. (2009). Fire intensity, fire severity and burn severity: A brief review and suggested usage. *International Journal of Wildland Fire*, 18(1), 116–126.
<https://doi.org/10.1071/WF07049>
- Kolden, C. A., Smith, A. M. S., & Abatzoglou, J. T. (2015). Limitations and utilisation of Monitoring Trends in Burn Severity products for assessing wildfire severity in the USA.

International Journal of Wildland Fire, 24(7), 1023–1028.

<https://doi.org/10.1071/WF15082>

Li, D., Wrzesien, M. L., Durand, M., Adam, J., & Lettenmaier, D. P. (2017). How much runoff originates as snow in the western United States, and how will that change in the future?

Geophysical Research Letters, 44(12), 6163–6172. <https://doi.org/10.1002/2017GL073551>

Littell, J. S., Mckenzie, D., Peterson, D. L., & Westerling, A. L. (2009). Climate and wildfire area burned in western U.S. ecoprovinces, 1916-2003. *Ecological Applications*, 19(4),

1003–1021. <https://doi.org/10.1890/07-1183.1>

Mankin, J. S., Viviroli, D., Singh, D., Hoekstra, A. Y., & Diffenbaugh, N. S. (2015). The potential for snow to supply human water demand in the present and future. *Environmental*

Research Letters, 10(11). <https://doi.org/10.1088/1748-9326/10/11/114016>

Marks, D., & Winstral, A. (2001). Comparison of snow deposition, the snow cover energy balance, and snowmelt at two sites in a semiarid mountain basin. *Journal of*

Hydrometeorology, 2(3), 213–227. <https://doi.org/10.1175/1525->

7541(2001)002<0213:COSEDTS>2.0.CO;2

Maxwell, J., Call, A., & St. Clair, S. B. (2018). Wildfire and topography impacts on snow accumulation and retention in montane forests. *Forest Ecology and Management*, 432, 256–

263. <https://doi.org/10.1016/j.foreco.2018.09.021>

Maxwell, J., & St. Clair, S. B. (2019). Snowpack properties vary in response to burn severity gradients in montane forests. *Environmental Research Letters*, 14, 124094.

<https://doi.org/10.1088/1748-9326/ab5de8>

Meigs, G. W., Turner, D. P., Ritts, W. D., Yang, Z., & Law, B. E. (2011). Landscape-Scale Simulation of Heterogeneous Fire Effects on Pyrogenic Carbon Emissions, Tree Mortality,

and Net Ecosystem Production. *Ecosystems*, 14(5), 758–775.

<https://doi.org/10.1007/s10021-011-9444-8>

Mote, P. W., Li, S., Lettenmaier, D. P., Xiao, M., & Engel, R. (2018). Dramatic declines in snowpack in the western US. *Npj Climate and Atmospheric Science*, 1(1).

<https://doi.org/10.1038/s41612-018-0012-1>

Musselman, K. N., Molotch, N. P., Margulis, S. A., Kirchner, P. B., & Bales, R. C. (2012).

Influence of canopy structure and direct beam solar irradiance on snowmelt rates in a mixed conifer forest. *Agricultural and Forest Meteorology*, 161, 46–56.

<https://doi.org/10.1016/j.agrformet.2012.03.011>

Myneni, R., Knyazikhin, Y., Park, T. (2015). *MOD15A2H MODIS/Terra Leaf Area Index/FPAR 8-Day LA Global 500m SIN Grid V006* [Data set]. NASA EOSDIS Land Processes DAAC.

Accessed 2022-03-28 from <https://doi.org/10.5067/MODIS/MOD15A2H.006>

Natural Resources Conservation Service (2021). NRCS: National Water and Climate Center SNOTEL data network. U.S. Department of Agriculture, available at:

<ww.wcc.nrcs.usda.gov/snow/> , (last accessed: 16 April 2021)

Omernik, J. M., & Griffith, G. E. (2014). Ecoregions of the Conterminous United States:

Evolution of a Hierarchical Spatial Framework. *Environmental Management*, 54(6), 1249–1266. <https://doi.org/10.1007/s00267-014-0364-1>

Picotte, J. J., Bhattarai, K., Howard, D., Lecker, J., Epting, J., Quayle, B., Benson, N., & Nelson, K. (2020). Changes to the Monitoring Trends in Burn Severity program mapping production procedures and data products. *Fire Ecology*, 16(1). <https://doi.org/10.1186/s42408-020-00076-y>

- Revuelto, J., Lopez-Moreno, J. I., Azorin-Molina, C., & Vincente-Serrano, S. M. (2015). Canopy influence on snow depth distribution in a pine stand determined from terrestrial laser data. *Water Resources Research*, *51*, 3476–3489. <https://doi.org/10.1002/2014WR016496>
- Sexstone, G. A., & Fassnacht, S. R. (2014). What drives basin scale spatial variability of snowpack properties in northern Colorado? *Cryosphere*, *8*(2), 329–344. <https://doi.org/10.5194/tc-8-329-2014>
- Stevens, J. T. (2017). Scale-dependent effects of post- fire canopy cover on snowpack depth in montane coniferous forests. *ECOLOGICAL APPLICATIONS*, *27*(6), 1888–1900.
- Stevens-Rumann, C. S., & Morgan, P. (2019). Tree regeneration following wildfires in the western US: a review. *Fire Ecology*, *15*(1), 1–17. <https://doi.org/10.1186/s42408-019-0032-1>
- Stewart, I. T., Cayan, D. R., & Dettinger, M. D. (2004). Changes toward earlier streamflow timing across western North America. *Journal of Climate*, *18*(8), 1136–1155. <https://doi.org/10.1175/JCLI3321.1>
- Sturm, M., Goldstein, M. A., & Parr, C. (2017). Water and live from snow: A trillion dollar science question. *Water Resources Research*, *53*, 3534–3544. <https://doi.org/10.1029/eo064i046p00929-04>
- Tennant, C. J., Harpold, A. A., Lohse, K. A., Godsey, S. E., Crosby, B. T., Larsen, L. G., Brooks, P. D., Van Kirk, R. W., & Glenn, N. F. (2017). Regional sensitivities of seasonal snowpack to elevation, aspect, and vegetation cover in western North America. *Water Resources Research*, *53*(8), 6908–6926. <https://doi.org/10.1002/2016WR019374>
- U.S. Census Bureau, P. D. (2019). *Table 1. Annual Estimates of the Resident Population for the*

United States, Regions, States, and Puerto Rico: April 1, 2010 to July 1, 2019 (NST-EST2019-01).

- Varhola, A., Coops, N. C., Weiler, M., & Moore, R. D. (2010). Forest canopy effects on snow accumulation and ablation: An integrative review of empirical results, *J. Hydrology*, *392*, 219–233. <https://doi.org/10.1016/j.jhydrol.2010.08.009>
- Veatch, W., Brooks, P. D., Gustafson, J. R., & Molotch, N. P. (2009). ‘Quantifying the effects of forest canopy cover on net snow accumulation at a continental, mid-latitude site’, *Ecohydrology*, *2*, 115–128. <https://doi.org/10.1002/eco>
- Viviroli, D., Dürr, H. H., Messerli, B., Meybeck, M., & Weingartner, R. (2007). Mountains of the world, water towers for humanity: Typology, mapping, and global significance. *Water Resources Research*, *43*(7), 1–13. <https://doi.org/10.1029/2006WR005653>
- Vose, R. S., Easterling, D. R., Kunkel, K. E., LeGrande, A. N., & Wehner, M. F. (2017). Temperature changes in the United States. *Climate Science Special Report: Fourth National Climate Assessment, I*, 185–206. <https://doi.org/10.7930/J0N29V45.U.S>
- Westerling, A. L., Hidalgo, H. G., Cayan, D. R., & Swetnam, T. W. (2006). Warming and earlier spring increase western US forest wildfire activity. *Science*, *313*(5789), 940–943. <https://doi.org/10.1126/science.1128834>
- Xiao, Y., Li, X., Zhao, S., & Song, G. (2019). Characteristics and simulation of snow interception by the canopy of primary spruce-fir Korean pine forests in the Xiaoxing’an Mountains of China. *Ecology and Evolution*, *9*(10), 5694–5707. <https://doi.org/10.1002/ece3.5152>
- Yang, J., Tian, H., Tao, B., Ren, W., Pan, S., Liu, Y., & Wang, Y. (2015). A growing importance

of large fires in conterminous United States during 1984-2012. *Journal of Geophysical Research: Biogeosciences*, 120(12), 2625–2640. <https://doi.org/10.1002/2015JG002965>

Yang, W., Shabanov, N. V., Huang, D., Wang, W., Dickinson, R. E., Nemani, R. R., Knyazikhin, Y., & Myneni, R. B. (2006). Analysis of leaf area index products from combination of MODIS Terra and Aqua data. *Remote Sensing of Environment*, 104(3), 297–312. <https://doi.org/10.1016/j.rse.2006.04.016>

Zambrano-Bigiarini, Mauricio. (2020) hydroGOF: Goodness-of-fit functions for comparison of simulated and observed hydrological time series R package version 0.4-0. URL <https://github.com/hzambran/hydroGOF>. DOI:10.5281/zenodo.839854.

Zeng, X., Broxton, P., & Dawson, N. (2018). Snowpack Change From 1982 to 2016 Over Conterminous United States. *Geophysical Research Letters*, 45, 12,940-12,947. <https://doi.org/10.1029/2018GL079621>

CHAPTER 3 - REGIONAL SNOWPACK VULNERABILITY TO WILDFIRE AND CHANGING CLIMATE WITHIN THE WESTERN U.S.

3.1 OVERVIEW

Snowpack is important for water supply in the western U.S. where most streamflow in major watersheds is derived from snowpack. Due to increasing wildfire frequency and magnitude, the potential vulnerability of snowpack is an important consideration for water managers. However, not all locations on the landscape will experience the same changes in snowpack if a wildfire occurs. The objective of this analysis is to determine locations and conditions where the snowpack is more sensitive to wildfire occurrence in the western U.S. ecoregions. Four snowpack measures were evaluated including annual maximum snow water equivalent (SWE), annual maximum SWE normalized by winter precipitation, peak SWE date, and melt-out date. Random forest models were developed for each measure using topographic, climatic, and land cover predictor variables along with snowpack data from wildfire impacted SNOTEL sites. The results indicate terrain slope is an important variable for predicting changes in maximum SWE, while incoming shortwave radiation and aridity are important for peak SWE date and melt-out date changes, respectively. The largest spatial variability amongst all snow measures occurs for maximum SWE with a range of 5% increase to over 10% decrease due to wildfire. Spatial variability for peak SWE and melt-out dates varied between ecoregions with the largest range in the northern and mid-latitude ecoregions. Peak SWE and melt-out dates are expected to be earlier across most ecoregions, with the exception of the Arizona-New Mexico Mountains where later melt-out dates are possible. Shallow slopes were identified as the most vulnerable for maximum SWE changes from wildfire. When evaluating the combined impacts

of climate and wildfire, areas with fewer days below freezing were most vulnerable. The estimated total snow water volume difference due to wildfires occurring between 2015 through 2020 ranged from a 1% increase in the North Cascades to an 6% reduction in the Arizona-New Mexico Mountains.

3.2 INTRODUCTION

Snowpack is a critical component of water supply for the western U.S. where approximately one fourth of the country's population (U.S. Census Bureau, 2019) reside. It has been estimated that total runoff from snowmelt provides a significant majority of annual streamflow in the western U.S. The snowmelt contribution has been estimated in several publications (Barnett et al., 2005; Doesken & Judson, 1996; Li et al., 2017; Serreze et al., 1999; Stewart et al., 2004) and ranges from 53% (Li et al., 2017) to 80% (Stewart et al., 2004). Given the importance of snowmelt runoff in the region, water management activities are especially focused on snowpack processes. This focus is due to the integral parts that snow accumulation and snowmelt play for water supply, flood risk management and ecological requirements. Water supply and flood forecasting depend on snowpack information to inform prediction models used for several aspects of water management (Adams, 2016; Horn, 1968; Lea, 2008). Key variables for accurately predicting peak streamflow are timing and magnitude of peak snow water equivalent (SWE) (Clow, 2010; Curry & Zwiers, 2018). The melt rate of the snowpack is an important driver of the summer baseflow (Barnhart et al., 2016), which has both water supply and ecological implications. In addition, streamflow temperatures (Du et al., 2020) and mountain lake temperatures (Smits et al., 2020) increase with reductions in snowpack and may

have negative consequences for aquatic ecology. Decreases in runoff from snowpack also affect irrigated agriculture and result in water curtailment (Vano et al., 2010).

In recent years, air temperatures have been increasing due to climate change (see National Climate Assessment report at <https://nca2018.globalchange.gov/>). In the western U.S., air temperature increased 0.8°C during 1986-2016 compared to the baseline period of 1901-1960 (Vose et al., 2017), and this air temperature increase is higher than the national average (Vose et al., 2017). Air temperature increases can have broad implications for snow accumulation and ablation process. Peak snowpack has been declining across the western U.S. as air temperatures have increased (Grundstein & Mote, 2010; Mote et al., 2018; Pierce et al., 2008; Zeng et al., 2018). The reported decreases in peak SWE range from 15% to 31% for 01 April in the western U.S. (Mote et al., 2018). While drought and inter-annual wintertime temperature variability contribute to episodic decreases, the observed trends in snowpack can be attributed to climate change that has already occurred (Pierce et al., 2008). Vulnerable areas due to climate change that are those most sensitive to future warming and are susceptible to large changes. In the western U.S. these areas are in transitional snow zones where the mean winter temperatures are near freezing (Luce et al., 2014; Nolin & Daly, 2006). Mote (2003) found that lower elevation sites had the largest decrease in 1 April snow water equivalent (SWE) (40% decreasing trend). Similarly, Grundstein and Mote (2010) reported 80% of sites below 1000 m had statistically significant declines in snowpack compared to 62% of sites above this elevation. Several publications predict continuing decreases in peak SWE due to increasing temperatures (Cayan, 1996; Hamlet et al., 2005; Knowles et al., 2006; Luce et al., 2014; Marshall et al., 2019). A consequence of this reduction in peak SWE may be overall reduced water availability from snowmelt (Barnett et al., 2005; Fyfe et al., 2017).

Climate change has also increased the occurrence and magnitude of wildfires in the western U.S. (Dennison et al., 2014; Littell et al., 2009; Westerling et al., 2006, Yang et al., 2015), and future climate scenarios predict further increases in fire activity as extreme temperatures and droughts become more common in the region (Flannigan et al., 2000; Guyette et al., 2014; Stavros et al., 2014). The increase in wildfire activity is through increased aridity from warming air temperatures (Greve et al., 2019) and associated increases of vegetation stress, which results in lower moisture and increased flammability of the vegetation (Goodwin et al., 2021; Littell et al., 2016; Swetnam & Betancourt, 1998).

Data analysis and modeling impacts from wildfire on snowpack have been evaluated in previous studies, but most studies have focused on changes in relatively limited spatial domains (Burles & Boon, 2011; Gleason et al., 2013; Gleason & Nolin, 2016; Harpold et al., 2014; Moeser et al., 2020). These studies have also used a variety of methods to summarize and model post-wildfire snowpack or components of the snow surface energy balance. Chapter 2 summarized snowpack changes for several burned NRCS SNOw TELemetry (SNOTEL) sites across the western U.S. The results indicated earlier melt-out and peak SWE dates are likely, while changes to peak SWE are variable between northern and southern regions. Additionally, the observed snowpack changes were not sensitive to burn severity classification but did show dependence on the change in leaf-area index and the tree genus. Burles and Boon (2011) used a process-based point energy balance model to quantify differences in energy balance characteristics between burned and unburned locations in Alberta, Canada. Their model was not designed to be transferrable to other locations without requiring the full suite of input variables necessary for modeling energy fluxes for snowpack. Another modeling study by Moeser et al. (2020) applied a snowpack energy budget model at 1 m² resolution to a burned site in New

Mexico. Their model results had less than 10% bias when compared to the observed snow depth measurements, but the authors also noted those results may not be transferable to other regions. In addition, the data requirements for simulating snowpack using an energy balance model are extensive and often one of the limitations to using this method for post-wildfire snowpack analysis, especially at the high spatial resolutions. In the Northwest U.S., Gleason and Nolin (2016) used an energy balance model to test new parameterizations of post-wildfire snow albedo decay. This work was focused on a specific aspect of model parameterization and may be useful in other regions; however, the quantification of changes to snowpack would still require additional models and input data. For water managers, the limited spatial domain of the previous work presents challenges and the results may not be reliable indicators of snowpack changes over an entire burn area. As shown in Chapter 2 in Figures 3-6, observations of snowpack changes vary within western U.S. ecoregions and may have limited applicability of other areas with similar burn severity and elevation.

At regional scales, there are limited studies related to snowpack changes due to wildfire. Stevens (2017) collected snow depth measurements in the Sierra Nevada Mountains and found fire severity had a negative effect on snow depth. In their observations, the highest snow depths were found in unburned areas. They also developed statistical models to predict changes in snow depth using burn severity, canopy gaps, and topographic aspect in the Sierra Nevada Mountains. Based on the linear model parameter estimates, they found inverse relationships between burn severity and snow depth. The parameter estimates for canopy gap and northeast aspect indicate a positive relationship while southwest aspect was negative. Again, these results would have predictive power for the area from which the training data was derived, but potentially limited applicability in other regions. Another regional scale study by Micheletty et al. (2014) used

remote sensing data to evaluate the spatial variability of melt-out after fires in California. They found melt-out occurred on average 9 days earlier in burn areas based on 11 years (6 years pre-wildfire and 5 years post-wildfire) of snow cover data.

Snowpack vulnerability can be defined by the sensitivity and susceptibility of regional snowpack to changes when a wildfire occurs. While many studies have examined the impacts of individual wildfires on snowpack properties, few tools are available to help water managers plan for expected impacts of a wildfire in a particular region. The objective of this study is to determine locations and conditions where the snowpack is more sensitive to wildfire occurrences in the western U.S. This includes:

1. Determining spatial variability of wildfire impacts on SWE within ecoregions (and how representative an analysis at a select site is expected to be for an ecoregion)
2. Identifying locations within the ecoregions where snowpack is especially sensitive to wildfire and whether those sites have been preferentially burned.
3. Quantify the snow water changes across each ecoregion due to fires from 2015 through 2020.

The study uses SNOTEL data for the western U.S., which are consistently collected and reported for numerous sites across the western U.S. A random forest (RF) model was developed using pre- and post-wildfire changes at burned SNOTEL sites and associated unburned sites to predict the magnitude of snowpack change following a wildfire. The model is evaluated based on comparing RF error statistics to the variability of changes at the burned SNOTEL sites. The model is applied to several ecoregions across the western U.S. to quantify potential changes to peak SWE magnitude and date along with melt-out dates. The wildfire perimeters from the interagency fire perimeter history dataset (NIFC, 2021) are then used to quantify areas that have

burned in each ecoregion during 2015 through 2020 period. This provides information about how much snowpack has already changed due to recent wildfire activity.

3.3 DATA

3.3.1 SNOTEL Data

The ground-based data used in the vulnerability analysis are the daily reported SWE and precipitation values from the SNOTEL network sites, which are operated by the Natural Resources Conservation Service (NRCS, 2021). The sites in the analysis range from southern New Mexico (latitude 33.4° N) to the mountain ranges in northern Washington (latitude 48.9° N) (Figure 12). Quality control was completed through visual inspection of the SWE and precipitation time series. The local NRCS Snow Survey offices were consulted before removing any apparent reporting errors. To maximize the utilization of available data, only years with more than 10% of daily precipitation or SWE values missing were removed from the dataset. Of the 1500 station-years available for the burned sites, 23 years were removed.

NRCS Snow Survey Data Collection Offices have identified 43 sites that have been directly impacted by wildfires through 2019 in the western U.S. The period of record for both SWE and precipitation at each burned site is shown in Figure 13 along with the wildfire date. Comparison unburned sites were identified within the same level 3 ecoregion for each burned site. Using level 3 ecoregion as a grouping criterion allows us to compare burned and unburned sites that have similar regionally classified geology, physiography, vegetation, climate, and soils (Omernik & Griffith, 2014). At least two unburned sites were identified for each burned site. The initial matching criteria was to find unburned sites within a distance of 50 km and ± 300 m of

elevation. These criteria resulted in unburned sites for approximately 80 percent of the burned locations. Pairing for the remaining 20% of burned sites required expansion of the search radius or elevation range and are noted in the supporting data. The time series for each of the 108 unburned sites was divided based on the fire date of the associated burned location. The representativeness of the unburned sites relative to the burned locations was evaluated using the Kling-Gupta efficiency (KGE) (Gupta et al., 2009). The KGE average of 0.82 suggests the unburned sites behavior relatively similarly to the burned sites for this period.

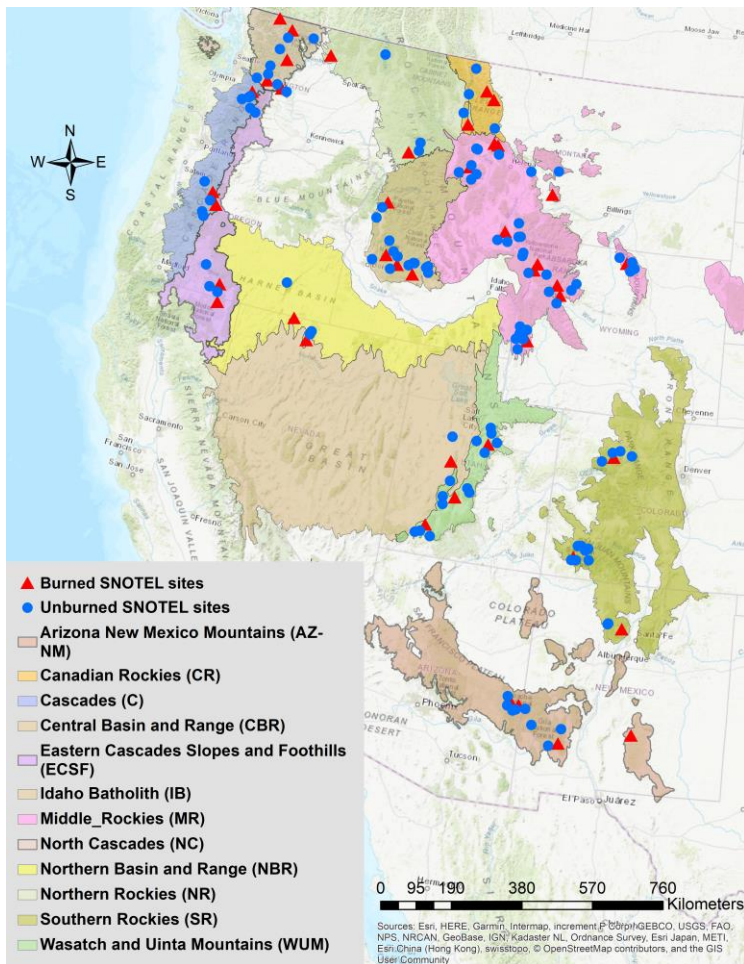


Figure 12. Map of burned (red triangles) and unburned (blue circles) SNOTEL sites in western United States along with the level 3 ecoregions (Omernik & Griffith, 2014) used in the analysis.

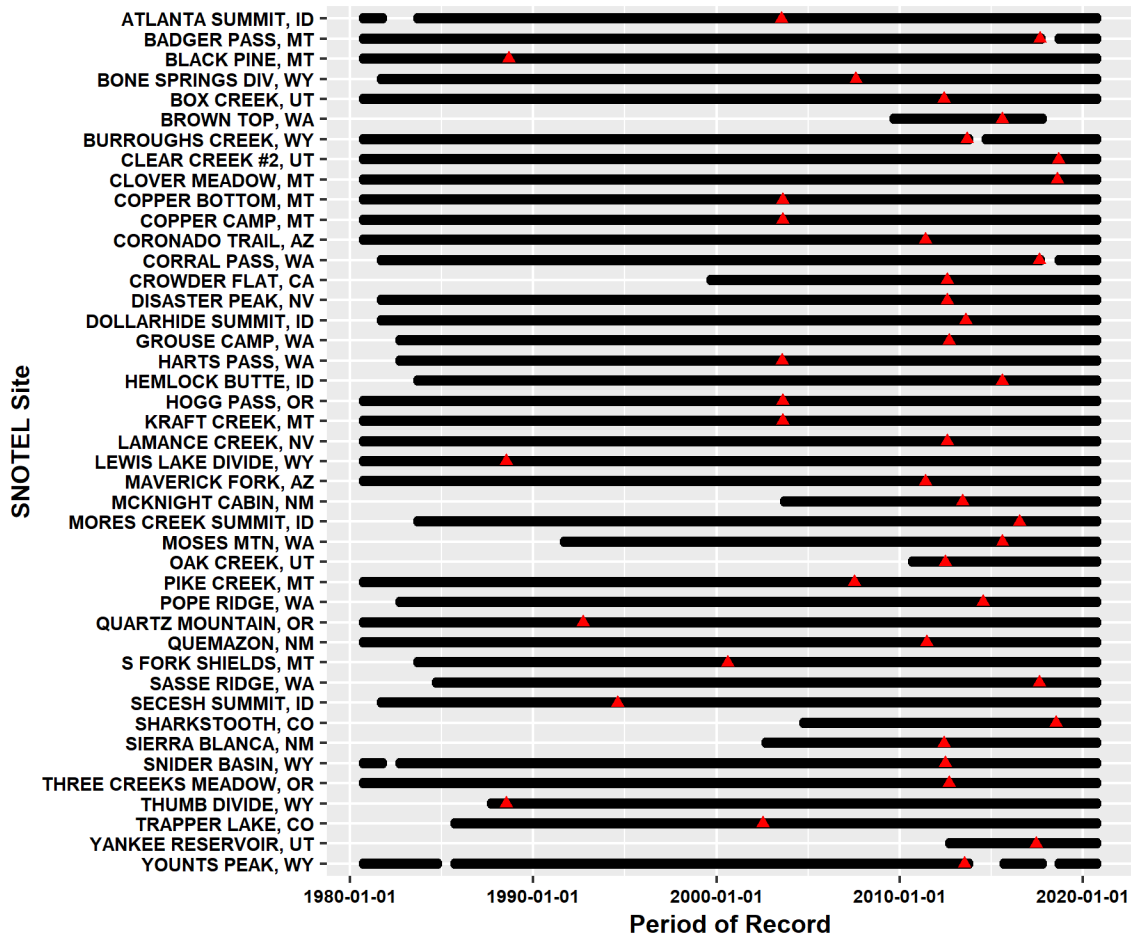


Figure 13. Period of record used for each of the 43 burned SNOTEL site. The date of the wildfire (red triangle) is shown for reference within the record.

3.3.2 Snowpack Measures

The snowpack measures used in this analysis are annual maximum SWE; annual maximum SWE normalized by dividing the maximum SWE value by the cumulative October through April precipitation (nSWE); date of annual maximum SWE (peak date); and melt-out date (Table 2). For each of these measures it is important to distinguish between the combined signal (climate plus wildfire) and the wildfire signal when considering changes in snowpack. The climate signal is estimated using the difference between post-wildfire and the pre-wildfire

snowpack measure at the unburned sites. The combined signal is the difference between the pre-wildfire and post-wildfire snowpack measure at the burned sites. Both the climate and combined signals are derived using differences between the temporal subsets of the data. The wildfire signal is then calculated as the difference between the post-wildfire to pre-wildfire changes at the burned and unburned sites. The results for this analysis focus on the snowpack changes (percent difference for SWE and days difference for dates) due to both wildfire and combined signals.

Table 2. Definitions for SWE measures used which are consistent with those defined in Chapter 2.

Measure	Description
Annual maximum SWE (SWE)	First date of maximum SWE using a 01 October through 30 September water year
Annual maximum normalized SWE (nSWE)	The annual maximum SWE value divided by the total October through April precipitation
Date of annual maximum SWE (Peak date)	Date of annual maximum SWE as defined above
Melt-out date	First daily value after the peak SWE for which SWE equaled zero

3.3.3 Topographic and Land Cover Data

Several data products from the LANDFIRE data portal (<https://landfire.gov/>) were used as candidate predictor variables in the model development. These spatially continuous datasets for the United States are produced through a shared program between the wildland fire management programs of the U.S. Department of Agriculture Forest Service and U.S. Department of the Interior. The variables from LANDFIRE include both land surface and topographic information available for the contiguous United States at 30 m spatial resolution. The topographic data includes aspect (LANDFIRE, 2016a), elevation (LANDFIRE, 2016b), and slope (LANDFIRE, 2016d). The only land cover dataset used was existing vegetation type,

which groups ecological and plant communities by similar physical environments (LANDFIRE, 2016c; NatureServe, 2009). Based on results presented Figure 7 burn severity was not considered because changes in the snow measures were not found to be sensitive to categories of burn severity. The results show in Figure 8 indicate the snow measure changes are sensitive to the leaf area index change. Changes in leaf area index were not included due to their spatial-temporal variability (Pokorný et al, 2008). A single location may have a range of potential post-wildfire leaf area index changes going into the future which will be further influenced by climate and insect mortality of forests.

3.3.4 Forest Inventory and Analysis Data

Forest metrics from the U.S. Department of Agriculture Forest Service (USDA-FS) Forest Inventory and Analysis (FIA) were used as predictor variables in the analysis. The FIA data provides consistent forest stand level data for both public and privately owned U.S. forested areas (Burrill et al., 2018). The 240 m gridded data from 2017 was used to obtain the total basal area and dominant stand density index species. Total basal area represents the sum of the cross-sectional area of trees at 1.37 m height relative to the ground over a grid cell (Bettinger, 2008). The dominant stand density index species represents the tree species with the largest basal area per number of trees for a grid cell (Woodall et al., 2003). From the dominant stand index tree species, the tree genus was determined. Updated metrics are not available throughout the period of record used in this analysis. Therefore, pre-wildfire FIA metrics associated with each burned site are not available for all wildfires. In this analysis the 2017 FIA metrics are used for all burned sites regardless of the year in which they were burned. The 240 m grids were resampled to create 30 m grids that align with other predictor variables. During the RF development, both the total basal area and tree genus were used based on the resampled 240 m grid coincident with

the burned site location. Inspection of the 30 m grid values from resampled grid was performed to ensure consistency with the original 240 m datasets at the burned sites. The genus used in this analysis include pine (*Pinus*), fir (includes both *Abies* and *Pseudotsuga*), spruce (*Picea*), hemlock (*Tsuga*) and three sites which were other genera. For analysis purposes, the hemlock and unspecified genera are grouped as “hemlock/other” to create a total of four genus classes.

3.3.5 Incoming Shortwave Radiation

The Daymet average daily incident shortwave radiation flux was also considered as a candidate predictor variable (Thornton et al., 2020). This dataset has a 1 km spatial resolution and has continuous spatial coverage for North America. The daily values for the grid cell coincident with the burned sites were averaged over the 1980-2020 for use in the RF model development. The algorithms used to develop Daymet require only air temperature and precipitation as inputs and have been shown to be representative of data collected at ground-based meteorological stations in complex terrain (Thornton et al., 2000). The 1 km spatial resolution was resampled to 30 m grids for the RF model development.

3.3.6 Climate Data

Daily precipitation and temperature values were used as candidate predictor variables in the analysis. The data are from the Parameter-elevation Regressions on Independent Slopes Model (PRISM) datasets (Daly et al., 1994) (<https://prism.oregonstate.edu/>). The daily total precipitation and mean air temperature at the 30 arc-second spatial resolution (approximately 4 km grid) were used in this analysis. PRISM precipitation dataset has been shown to be representative of ground-based precipitation measurements (Buban et al., 2020) and is used to improve model simulations for streamflow and snowpack (Gao et al., 2017; Raleigh &

Lundquist, 2012). The PRISM temperature datasets have some known biases in mountainous terrain but are still considered representative conditions on mountain slopes (Strachan & Daly, 2017). To create consistency in the spatial resolution between the climate and topographic data, a resampling of the 3-arc second grids was performed to create 30 m grids for both the daily air temperature and precipitation (PRISM, 2021). This was accomplished by using GIS software and using a resampling technique set of “nearest,” which simply divides the original PRISM grids into small pieces but does not create new or interpolated values.

3.3.7 Potential Evaporation

The daily potential evaporation (PET) was used in this study to evaluate the ratio of annual PET to annual precipitation. The PET dataset developed by Abatzoglou (2013) was used because it has been used in other studies related to snowpack modeling the western U.S. (Hammond et al., 2018; Harpold et al., 2017) and provide spatially consistent coverage for the entire study domain. The 4 km PET grids were resampled to 30 m spatial resolution for the RF model development.

3.3.8 Snowpack Data

A spatially continuous snow water equivalent dataset (<https://nsidc.org/data/nsidc-0719>) by Broxton et al. (2019) was also used in this analysis. The model developed in the current analysis from the burned SNOTEL sites estimates changes to SWE and the dataset by Broxton et al. (2016) provides spatially continuous estimates of SWE across the western U.S. The dataset by Broxton et al. (2019), hereafter referred to as UA SWE, assimilates SNOTEL and cooperative observer snow measurements to generate a 4 km spatial resolution dataset that extends from 1981 through 2020 and were resampled to 30 m spatial resolution. The UA SWE dataset has

been used in efforts to quantify SWE trends for the continuous U.S. (Zeng et al., 2018) for WY 1982-2016 and to estimate peak SWE quantiles in eastern Idaho (Giovando et al., 2021) for WY 1982-2020. The peak SWE information from this dataset was used to quantify changes in snow water from wildfires.

3.3.9 Predictor variables

The predictor variables used in the RF model development are either directly from the datasets described previously or derived from those datasets. Predictor variables directly from the datasets include longitude, latitude, elevation, slope, total basal area, tree genus, incoming radiation, mean October through April temperature, and mean October through April precipitation totals. The derived variables include seasonal climatic indices, northness, eastness, curvature, aridity, and heat load index (HLI).

Latitude and longitude were based on the burned SNOTEL site metadata provided by the NRCS. Latitude controls the solar angle and the amount of incoming radiation during accumulation season (Seyednasrollah & Kumar, 2019). Longitude was used as a predictor variable since many of the North American mountain ranges have a north-south orientation and can provide distinction of regions with similar climate and lithology.

The elevation was extracted for each burned site from the 30 m elevation file (LANDFIRE, 2016b). The relationship between snow and elevation is primarily through the orographically influenced precipitation and temperature patterns (Dingman, 1981; Sospedra-Alfonso et al., 2015). Increased SWE accumulation occurs at higher elevations (Sospedra-Alfonso et al., 2015).

Land surface slope for each burned site was determined using the 30 m dataset (LANDFIRE, 2016d). The values from the dataset are natively in degrees, but were converted to

percent slope for use in the RF model development. Slope has been shown to influence the stability of the snowpack and the input of solar radiation (Anderton et al., 2004; Varhola et al., 2010). Berndt (1965) reported steeper slopes (18%) accumulated 20-30% less snowpack compared to gentler slopes (<6%).

Total basal area and tree genus are indicators of canopy density and distribution. Tree size, shape, and crown height can have a significant influence on the amount of radiation reaching the land surface (Seyednasrollah & Kumar, 2013). In addition, snowpack accumulation and ablation have been shown to be strongly related to canopy density (Tennant et al., 2017; Varhola et al., 2010) due to increased snowfall interception and sublimation (Sexstone et al., 2018). The snowfall interception can vary by tree genus based on the efficiency of the branch tips to hold snow (Schmidt & Glun, 1991).

Incoming shortwave radiation was used in this study because radiation fluxes have been shown to be the largest contributor to snowmelt (Follum et al., 2015; Maidment, 1993). The shortwave radiation grids coincident with the burned SNOTEL sites were extracted from the 1980-2020 average values derived from the Daymet daily time series.

Air temperature and precipitation both have direct influence on both snowpack accumulation and ablation (Hamlet et al., 2005; Sospedra-Alfonso et al., 2015). Air temperature, and winter precipitation are the primary climatic forcing variables for snow processes. The precipitation and temperature seasonal variables were derived from the daily PRISM data for water years (WY) 1982-2020. The seasonally aggregated (October through April) temperature and precipitation variables are reflective of the overall winter weather. The aggregation was performed because the snow measures used in the model development represent seasonal totals (e.g., peak SWE). The precipitation predictor variable used is the mean annual October through

April precipitation total was derived from the daily PRISM data (MeanOct_Apr_tot). The temperature derived variables used the daily mean temperature from the PRISM products. The simplest of the predictor variables is the mean October through April daily temperature (MeanTemp). Several additional variables were created that follow the temperature index (TI) concept (USACE, 1956) used for snowmelt modeling. For this analysis, the TI is simply the maximum of either the daily mean temperature or zero. TI can be considered an index of daily net energy flux into the snowpack. The opposite temperature variable from TI is referred to as freezing degree-day (FDD) which is the minimum of either the daily mean temperature or zero. FDD is often used to model ice formation on water bodies (USACE, 2006). FDD would be related to the net energy out of the snowpack when daily temperature is below freezing. The TI and FDD variables are defined as:

$$TI = \max (T_a ,0) \tag{1}$$

$$FDD = \min (T_a, 0) \tag{2}$$

Where T_a is the daily mean air temperature (°C). The derived temperature variables used in the analysis are based on TI (Eq.1) and FDD (Eq. 2). Using the TI and FDD index values, several additional seasonally aggregated predictor variables related to temperature were developed. The accumulated TI (ATI) was determined for each year during the October through April season. The average of the annual ATI values was determined for the period of WY 1982-2020 to produce the MeanATI predictor variable for each burned SNOTEL site. Following a similar process, the average of the annual accumulated FDD (AFDD) was determined to produce the MeanAFDD variable for WY 1982-2020. The final temperature variable used in the RF development was the average annual number of days below freezing. This variable is similar to

AFDD in that it represents the total energy removed from the snowpack during the winter, but it is binary and excludes the magnitude of the temperature below freezing.

Land surface aspect (aspect) was extracted for all the burn sites using the LANDFIRE aspect dataset (LANDFIRE, 2016a). Aspect has been shown to be important in understanding snowpack distribution in the western U.S. (Tennant et al., 2017). Due to the continuous range of aspect (0 to 360°), it was normalized in this study by determining degree of northness and eastness. Northness is a measure of the degree to which the land surface is north-facing. Generally, northness has a positive correlation with SWE and represents areas of more persistent snow cover (Sexstone & Fassnacht, 2014). The northness follows the formulation of Molotch et al. (2005), which uses the product of the cosine of aspect (degrees) and sine of slope (degrees). Eastness is the product of the sine of aspect (degrees) and sine of slope (degrees). Eastness is the degree to which the land surface is east-facing and is related to potential snow loading in areas where west winds redistribute snow on leeward east-facing slopes (Sexstone & Fassnacht, 2014). Both of these variables control solar radiation input (Schaerer & McClung, 2006; Tennant et al., 2017).

Terrain curvature (curvature) for each of the burned sites was determined using the slope dataset and the Spatial Analysis tools within ArcGIS. Curvature is the derivative of slope and represents local relief of terrain. Local relief is related to wind drifting of snow from exposed steep slopes to gullies (Lapen & Martz, 1996). Curvature has also been considered in other studies evaluating spatial variability of snowpack (Sexstone & Fassnacht, 2014).

In this study the average aridity index (aridity) was also used as an input variable for the RF model development. The aridity index is the ratio of annual potential evaporation to annual precipitation (Greve et al., 2019). Areas with high aridity can indicate locations of higher

snowpack sublimation potential during the later winter months which could influence peak SWE magnitude and date. The average annual PET for this study was derived using the geographic locations from the burned SNOTEL sites and extracting values from the gridMet dataset (Abatzoglou, 2013). The average annual precipitation was derived from the PRISM daily totals for grids coincident with the burned sites. Table 3 summarizes predictor variables used for model development.

HLI is related to the amount of clear-sky incoming shortwave radiation by combining latitude, slope, and aspect into a single index (McCune & Keon, 2002). By combining these variables into a single index, an estimate of the incident radiation can be made for any location using only topographic information. HLI is useful when comparing locations which receive afternoon sun compared to morning sun because the same daily radiation may be occurring on similar slopes, but the potential for impacting snow process is much greater for the slope with afternoon sun (McCune & Keon, 2002). The HLI values for each burned site were processed using the LANDFIRE datasets and the R package *spatialEco* (Evans, 2021), which use the formulation of HLI specified by McCune & Keon (2002).

Table 3: Summary of predictor variables used in the development of the RF models.

Variable	Physical Basis for Snow Modeling (units)	Data Source
Latitude	Geographic location (degrees)	Natural Resources Conservation Service
Latitude	Geographic location (degrees)	Natural Resources Conservation Service
MeanOct_Apr_tot	Mean annual total precipitation between Oct-Apr; controls total annual snowpack accumulation (mm)	PRISM
MeanTemp	Mean Oct-Apr daily temperature values; index of seasonal energy flux into snowpack (°C)	PRISM
MeanATI	Mean of annual accumulated TI between Oct-Apr; index of seasonal energy flux into snowpack (°C - Days)	PRISM
MeanAFFD	Mean of annual accumulated freezing degree days between Oct-Apr; index of seasonal energy removed from snowpack (°C -Days)	PRISM
MeanLTO	Mean of annual accumulated count for days less than 0 °C between Oct-Apr; binary index of seasonal energy flux removed from snowpack (days)	PRISM
Elevation	Direct relationship to snowpack accumulation ablation based on orographic precipitation patterns and temperature (m)	LANDFIRE
Slope	Influences stability of snowpack during accumulation (m/m)	LANDFIRE
Curvature	This is the derivative of land surface slope; represents local relief which can influence accumulation and ablation	LANDFIRE (extracted from elevation file)
Northness	$\cos(\text{aspect}) \times \sin(\text{slope})$ Controls snow cover persistence and input radiation flux (degrees)	LANDFIRE (extracted from slope and aspect file)
Eastness	$\sin(\text{aspect}) \times \sin(\text{slope})$ Controls degree of snow loading from west winds and input radiation flux (degrees)	LANDFIRE (extracted from slope and aspect file)
Total Basal Area	Resampled to 30 m spatial resolution from 240 m total basal area dataset using nearest neighbor value; index of canopy density which will control snowfall interception (m ²)	Forest Inventory and Analysis
Tree Genus	Classified from resampled 30 m spatial resolution from 240 m dominant stand index species dataset using nearest neighbor value; index canopy density and branch shape which will control snowfall interception	Forest Inventory and Analysis
Incoming Radiation	Estimated incoming shortwave radiation at land surface based on 1 km ² resolution; key variable to drive snowmelt (W/m ²)	Daymet
Heat Load Index (HLI)	An index which combines both potential incoming radiation and land surface temperature from latitude, slope, and aspect; indicator of fluxes to driver snowmelt	R package (<i>spatialEco</i>) using LANDFIRE elevation
Aridity	Ratio of total annual potential evaporation (PET) to total annual precipitation; areas with higher aridity can have increased sublimation through elevated vapor pressure deficits	PET: gridMet Precipitation: PRISM

3.4 METHODS

3.4.1 Random Forest Models

Random Forest (RF), a subset of the available machine learning (ML) approaches, is a supervised ML method that uses an ensemble of decision trees to predict responses from a set of predictor variables (Breiman, 2001). RF models have been shown to be effective and accurate in modeling water resources and snow processes while providing several advantages. The advantages that are most relevant to the vulnerability analysis are the ability of RF models to: 1) capture both linear and non-linear dependencies between predictor and response variables (Boulesteix et al., 2012); and 2) effectively use small sample sizes (Biau & Scornet, 2016). A complete list of advantages for RF is succinctly outlined in Tyrallis et al. (2019). RF models have been increasingly used for water resource applications in recent years (Tyrallis et al., 2019; Yang et al., 2019; Zhang et al., 2019). Publications related to streamflow and water quality are the most common water resource applications of RF models, while there are other recent publications that directly estimate snow distribution (Tyrallis et al., 2019; Yang et al. 2019). The RF approach has been used in many applications related to estimating snow quantity or distribution. Yang et al. (2019) used a RF for snow depth reconstruction in China, while Zhang et al. (2021) used the RF approach to estimate SWE in Sweden using satellite, topographic, and land cover information. RF was also used to bias correct the Snow Data Assimilation System SWE product in Ontario, Canada to provide more accurate snowpack information to water managers (King et al., 2020).

The foundation of the RF approach is the Classification and Regression Trees (CART) described by Breiman et al. (1984). The input data to the CART are matrices of predictor variables (\mathbf{X}) and response variables (\mathbf{Y}). In this analysis \mathbf{X} is $p \times m$ matrix comprised of p

predictor variables for m SNOTEL sites. The CART process begins with determining the initial split for a single predictor variable by iteratively dividing the groups of data and predicting snow measure changes. This process continues until mean squared error (MSE) of the measured values at the burned SNOTEL sites compared to the predicted values is minimized. The minimum MSE is then used to determine the threshold value to establish a tree node with value t_n (Figure 14). Once the node of the first predictor variable is determined, the remaining predictor variables are divided based on the groups created from divisions of the first variable. This process is repeated until all predictor variables have been evaluated. The final groups, representing the leaf of the CART, generally have a small number of observations (between 1 and 5) which are not split further (Biau and Scornet, 2016).

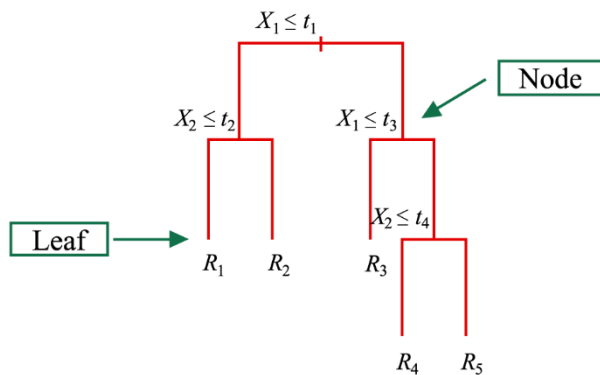


Figure 14. Example of CART which are the basis of the ensemble of decision trees used in the RF approach. The split at each node is based on binary split of the predictor variable X based on the threshold t , continuing until the groups of predictor and response variable are determined in the leaf R .

The RF approach uses an ensemble of CARTs based on four parameters that need to be specified. The ensemble is created by varying the predictor variables used for splitting at each node (Biau and Scornet, 2016). These parameters are 1) number of trained trees used in the ensemble ($ntree$); 2) number of randomly selected predictor variables used at each node to split ($mtry$); 3) number of observations used in each tree ($samplesize$), and maximum number of

observations in each leaf (*nodesize*). For the vulnerability analysis the *samplesize* and *nodesize* were set to 27 and 5 for this analysis. Sensitivity testing for these two parameters indicated the results remained similar for each of the snow measures. Due to limited size of the burned SNOTEL dataset, larger values for these parameters were not considered. Sensitivity testing was performed for slightly smaller values and the RF model accuracy was not found to be sensitive. The number of trained trees was set to 500 based on the criterion proposed by Boulesteix et al. (2012) which states RF performance increases approaches 0 for $n_{tree} \geq 250$. The assumed *n_{tree}* values was confirmed with sensitivity testing of the results to the *n_{tree}* parameter and showed no error reduction for values greater than 500. Determination of the *mtry* parameter was estimated using the lowest root-mean squared error (RMSE) for the RF model. In this analysis, the *randomForest* R package (version 4.6-14) is used for the RF model development (Breiman et al., 2021.; Liaw & Wiener, 2002).

3.4.2 Model Development

In total 8 RF models were developed for this analysis. There were several steps involved to arrive at the final RF models used for predication across each ecoregion. These steps included training each model using k-fold cross validation (James et al., 2013) with all potential predictor variables, evaluating variable importance, final selection of predictor variables, and evaluation of training error statistics to determine optimal RF parameters (i.e., *mtry*).

Due to the limited sample size available for training the model, all sites were used in the random forest model development. The model training was performed using a 5-fold cross validation process which provides a more robust estimate of the model error statistics (James et al., 2013). The 5-fold cross validation process randomly splits the initial 43 sites into five equal subsets (or as close to equal as possible), then trains the model on the four subsets and validates

the model against the remaining subset. This is repeated until all subsets are used for evaluation. The mean training error statistics for all 5 folds are used as the training error associated with that specific RF model. The validation error is calculated using the combined results from the validation folds. For example, during each fold, 35 burned sites are used for training the RF and 8 sites are used for validation. This process is repeated 5 times and the validation statistics are evaluated on the combined validation results from each fold. James et al. (2013) suggests that the number of folds (k) should be equal to 5 or 10 because these values do not result in excessively high bias or high variance for the mean squared error statistic. In addition, as the number of folds in the k -fold cross validation approaches the total sample size, the variance of the mean squared error can increase between each fold and provides a less robust estimate of the true model error (James et al., 2013). For the vulnerability analysis $k=5$ was selected because of the relatively small training dataset available for RF models.

3.4.3 Model Training and Variable Importance

The RF training and cross validation followed a two-step procedure. First, the k -fold training process was performed for all combinations of predictor variables listed in Table 3. A table of error statistics associated with each combination of predictor variables was compiled and evaluated. The final set of predictor variables used for the RF models was based on the minimum RMSE statistic for each snow measure.

The importance of the predictor variables is determined by evaluating the mean decrease in accuracy (mean increase in error) of the RF model. The mean decrease in accuracy is determined for each variable by assessing differences in errors averaged across all trees when individual predictor variables are randomly rearranged. This rearranging disassociates predictor

variable values from the snow measures for a specific burned site. As described by Biau and Scornet (2016), the important prediction variables result in larger errors when rearranged.

3.4.4 Model Application

The RF models were trained using the percent difference of in peak SWE, nSWE, and days difference for peak date and melt-out date for both the combined and wildfire signals for each of the burned SNOTEL sites. The input variables used for the RF models are derived from spatially continuous datasets for all of the western U.S. Using the spatially continuous predictor variable datasets allows for prediction of snowpack changes for both the combined and wildfire signals for all areas that may experience changes in SWE after a wildfire. Using the *raster* R package (version 3.4-5) (Hijmans, 2020), the trained RF models for all ecoregions were used to create spatially continuous predictions of snowpack changes for western U.S. ecoregions that include burned sites. The RF results were only applied to areas classified with tree cover based on the LANDFIRE Existing Vegetation Type (EVT) (LANDFIRE, 2016c) dataset. The majority of burned sites were located within or immediately adjacent to treed areas; therefore, the RF models were only applied to the tree land cover classification. Using the final RF model output, subsequent to the masking steps, the total snow water volume changes was quantified for each of the ecoregions at 30 m resolution. This was accomplished by using the fire signal annual maximum SWE percent change from the RF model multiplying them to a spatially continuous UA annual maximum SWE dataset to quantify volumes of snow water changes for post-wildfire conditions.

3.4.5 Model Evaluation

The RF model evaluation consisted of two separate performance comparisons. These comparisons use results from simple models to ensure the RF models provide more predictive information than just using the average of the SNOTEL observations. The two simple models were derived using the average snow measure change from 1) all 43 SNOTEL sites (Overall Average) and 2) the average for each ecoregion (Ecoregion Average) for each snow measure and signal. The RMSE and coefficient of determination (R^2) were then determined for the simple models for only for the purpose of comparing to the error statistics of the RF models. The RF RMSE is derived using the final predicted values from each trained RF model and the associated snow measure changes at all the 43 SNOTEL sites. The simple models were not used for any further analysis beyond comparisons of error statistics.

A second measure of performance to ensure the RF models are sufficient for predictions at burned sites are the criteria described by Moriasi et al. (2007). The ratio of RMSE-to the standard deviation of the observation (RSR) was used for each RF model. The RSR uses the model RMSE and the standard deviation of the observations to determine the relative model error. Specifically, RSR is:

$$RSR = \frac{RMSE}{STDEV_{OBS}} \quad (3)$$

In addition to RSR (Eq. 3), the Nash-Sutcliffe efficiency (NSE) (Nash & Sutcliffe, 1970) is also used by Moriasi et al. (2007) to classify model performance. Models are considered “satisfactory” for $NSE > 0.5$ and $RSR \leq 0.70$ (Moriasi et al., 2007). The Nash-Sutcliffe efficiency is defined as:

$$NSE = 1 - \left[\frac{\sum_{i=1}^n (Y_i^{obs} - Y_i^{sim})^2}{\sum_{i=1}^n (Y_i^{obs} - Y^{mean})^2} \right] \quad (4)$$

Where Y_i^{obs} is the i^{th} observation for the snow measure, Y_i^{sim} is the corresponding i^{th} simulated value and Y^{mean} is the mean of all the snow measure observations (Eq. 4).

3.5 RESULTS

3.5.1 RF Model Training and Evaluation

The model error statistics resulting from the k-fold cross validation process are shown in Table 4. Both the training and validation RMSE for the combine signal (CS) and wildfire signal (FS) SWE models are 19%. The coefficient of determination was slightly reduced for the FS SWE model as compared to the combined signal model. The CS nSWE model RMSE for training and validation are 15% and 16%, respectively. The nSWE FS model RMSE for both training and validation is 15%. The RMSE for peak SWE and melt-out date CS models is approximately 9 and 7 days, respectively. The RMSE for the FS peak SWE date and melt-out date changes are approximately 11 days and 8 days, respectively.

Table 4: Summary k-fold cross validation error statistics for both the combined and fire signal models. The SWE and nSWE error are a percentage while the peak and melt-out error is in days.

Snow Measure	CS Training (Validation) RMSE	CS Training (Validation) R ²	FS Training (Validation) RMSE	FS Training (Validation) R ²
SWE	19% (19%)	0.52 (0.45)	19 % (19%)	0.42 (0.40)
nSWE	15% (16%)	0.40 (0.15)	15% (15%)	0.38 (0.25)
Peak Date	8.7 d (8.7d)	0.46 (0.41)	10.6 d (10.9 d)	0.48 (0.18)
Melt-out Date	6.7 d (6.9 d)	0.50 (0.37)	8.1 d (8.3 d)	0.44 (0.07)

Predictions for each snow measures change at the 43 sites were made using the RF models resulting from the k-fold cross validation process. The observations were used to

compare with results from both the RF and simple models. These simple models are useful because they provide a benchmark for more complex models. The complex models should have at least the same prediction ability as using the simple models. The RF RMSE and coefficient of determination (R^2) values are improvements over the two simple models in all cases (Table 5). The coefficient of determination is zero for the simple-overall average model since the predicted snow measure changes are the same for each burned site. The simple-ecoregion average model does perform better when compared to the overall average, but still does not match the RF models.

The RSR, NSE, and model classification using the Moriasi et al. (2007) criteria are shown in Table 6. All models are “satisfactory” except for the combined signal nSWE model. Based on the RMSE values in Table 5, the combined signal nSWE model only shows a slight improvement over just using the ecoregion average for the nSWE changes at the burned SNOTEL sites. Therefore, the RSR resulting in a “unsatisfactory” classification is understandable. The combined signal nSWE model does indicate improved R^2 values relative to the simple-ecoregion average predictions.

Table 5: Summary of RMSE values comparing the combined signal (CS) and fire signal (FS) random forest models to the simple models which only use the average of the burned SNOTEL observations. The SWE and nSWE RMSE values are percentages while peak and melt-out date RMSE values are in days.

Model	SWE-FS		SWE-CS		nSWE-FS		nSWE-CS		Peak Date-FS		Peak Date-CS		Meltout Date-FS		Meltout Date-CS	
	RMSE	R2	RMSE	R2	RMSE	R2	RMSE	R2	RMSE	R2	RMSE	R2	RMSE	R2	RMSE	R2
Random Forest	0.10	0.88	0.09	0.90	0.08	0.86	0.12	0.47	4.7	0.87	3.8	0.91	4.1	0.83	3.3	0.89
Simple-Overall Average	0.25	0.00	0.25	0.00	0.18	0.00	0.17	0.00	9.3	0.00	11.3	0.00	8.4	0.00	8.7	0.00
Simple-Ecoregion Average	0.21	0.31	0.18	0.45	0.15	0.31	0.14	0.26	7.1	0.41	7.8	0.52	6.2	0.45	6.6	0.43

Table 6: Summary RSR values and model classification based on RSR and NSE ranges specified by Moriasi et al. (2007).

Model	RSR	NSE	Classification
SWE-FS	0.40	0.86	satisfactory
SWE-CS	0.36	0.85	satisfactory
nSWE-FS	0.43	0.81	satisfactory
nSWE-CS	0.73	0.75	unsatisfactory
Peak Date-FS	0.50	0.86	satisfactory
Peak Date-CS	0.33	0.89	satisfactory
Meltout Date-FS	0.48	0.76	satisfactory
Meltout Date-CS	0.37	0.86	satisfactory

3.5.2 Input Variable Importance

The predictor variables importance from the 5-fold cross validation are shown Figure 15. The most important variable for CS SWE changes is Mean LT0 (Figure 15a), while the most important variable for the FS SWE is slope (Figure 15b). This indicates when only considering wildfire impacts, topographic variables (i.e., slope, HLI, and northness) should be the focus when assessing the magnitude of SWE change. However, when evaluating the CS SWE changes, topographic information importance is reduced and mean winter climate is the key variable.

The most important variables are incoming radiation and slope for CS nSWE (Figure 15c) and FS nSWE (Figure 15d), respectively. The topographic variables for FS nSWE and FS SWE are similar, suggesting that regardless of winter precipitation totals, slope is likely key for determining SWE changes from only wildfire impacts. Other studies have found slope to be an important factor in snow accumulation (Berndt, 1965; Varhola et al., 2010). Gentler slopes were found to have increased snow accumulation especially when the canopy is removed (Berndt, 1965). Stevens (2017) found southwest facing slopes to have a negative correlation to snow depth in burned areas. The results from these studies suggest that areas of more SWE accumulation could be susceptible to larger changes in SWE following a wildfire.

The most important variable for the CS peak and melt-out date is mean winter temperature (Figure 15e and 15g). In addition, mean temperature importance is relatively much greater than other variables for both of these models. This result suggests that perhaps only mean winter temperature needs to be considered when evaluating the magnitude in date changes. The most important variable for the FS peak date model is incoming radiation (Figure 15f) while the most important variable for FS melt-out date is aridity (Figure 15h). Aridity could be an

indicator of increased sublimation post-wildfire resulting in earlier melt-out as suggested by Harpold et al. (2014).

The R^2 for the CS nSWE, FS peak date, and FS melt-out date differences decreases substantially between the training and validation output from the k-fold cross validation process (Table 4). This decrease of R^2 for the CS nSWE and FS peak date differences could be associated with the variability of incoming radiation. The coefficient of variation for incoming radiation is much greater than unity, indicating the variance in the predictor variable is much larger than the mean. Therefore, the RF model training data used for each fold of the k-fold cross validation process may not adequately capture the incoming radiation variability. The reduced R^2 for the FS melt-out date may be attributed to the importance of the individual ecoregion used by the RF model and the unbalanced sample size available with the limited number of SNOTEL sites in each ecoregion (Figure 15h).

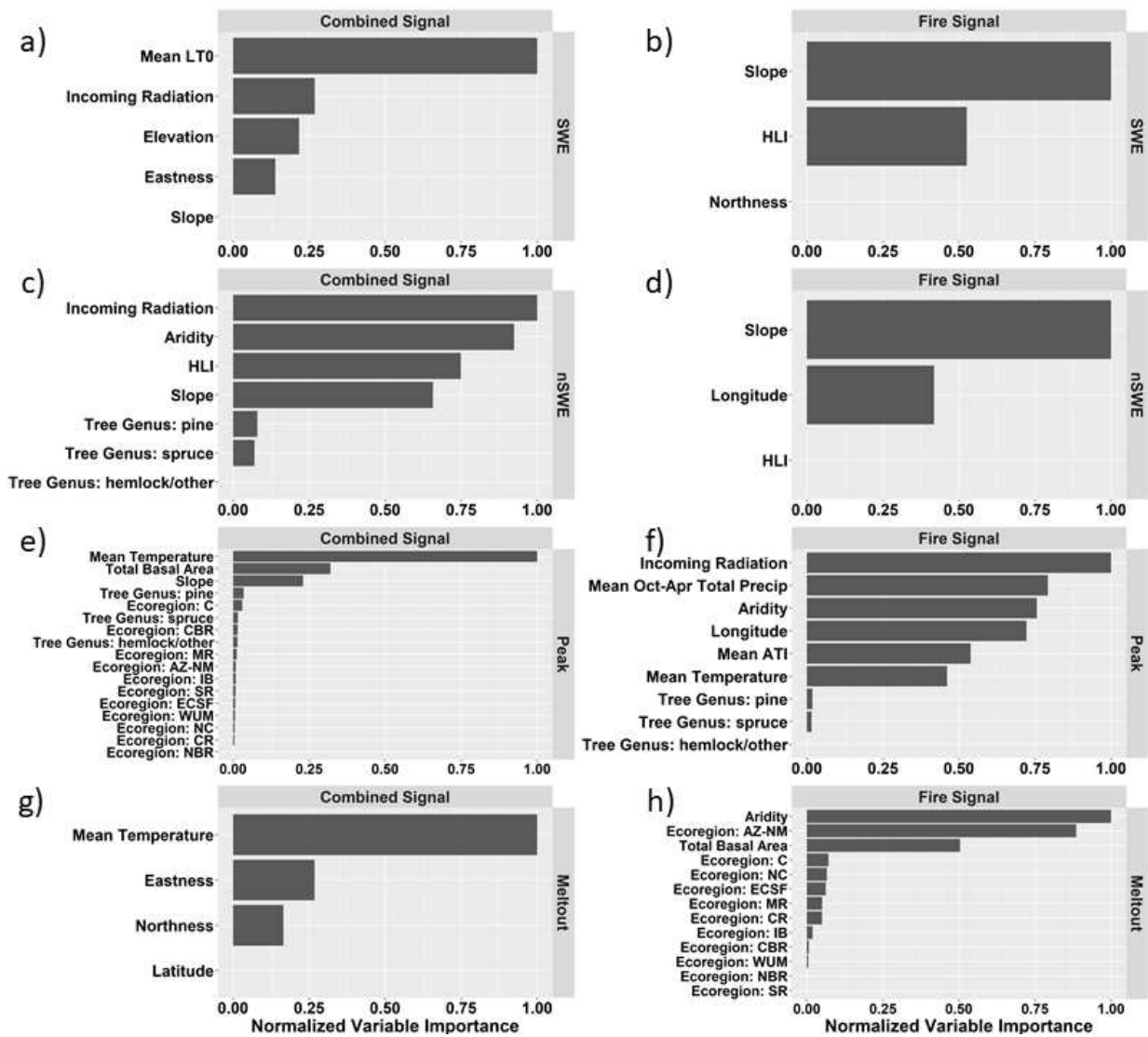


Figure 15: Variable importance for each RF model. The list of predictor variables used in the RF model along with the relative of importance for a) combined signal SWE model; b) fire signal SWE model; c) combined signal nSWE model; d) fire signal nSWE model; e) combined signal peak date model; f) fire signal peak date model; g) combined signal melt-out model; and h) fire signal melt-out model.

3.5.3 Spatial Variability

A summary of spatial results for each ecoregion and snow measure is shown in Figure 16. The overall results indicate increased spatial variability for the CS models as compared to the FS models. The inter-quartile range (IQR) values, which represent the intra-ecoregion spatial

variability for SWE, are 2-3 times larger for the CS model compared to the FS model for most ecoregions (Figure 16a). The IQR differences between CS and FS are less for nSWE (Figure 16b), which suggest spatial variability in precipitation could be contributing to the spatial variability of the CS SWE changes. The IQR for the peak and melt-out dates does indicate certain ecoregions have increased spatial variability for the CS model results compared to the FS model results (Figure 16c and 16d). The largest IQR for the CS peak and melt-out date differences occur in the Northern Rockies, North Cascades, Wasatch and Uinta Mountains and the Southern Rockies. The larger IQR values for the CS models are likely a result of the most important variables identified by RF model development process. Both MeanLT0 and MeanTemp have a relatively large distributional range for most ecoregions and could be the source of the spatial variability.

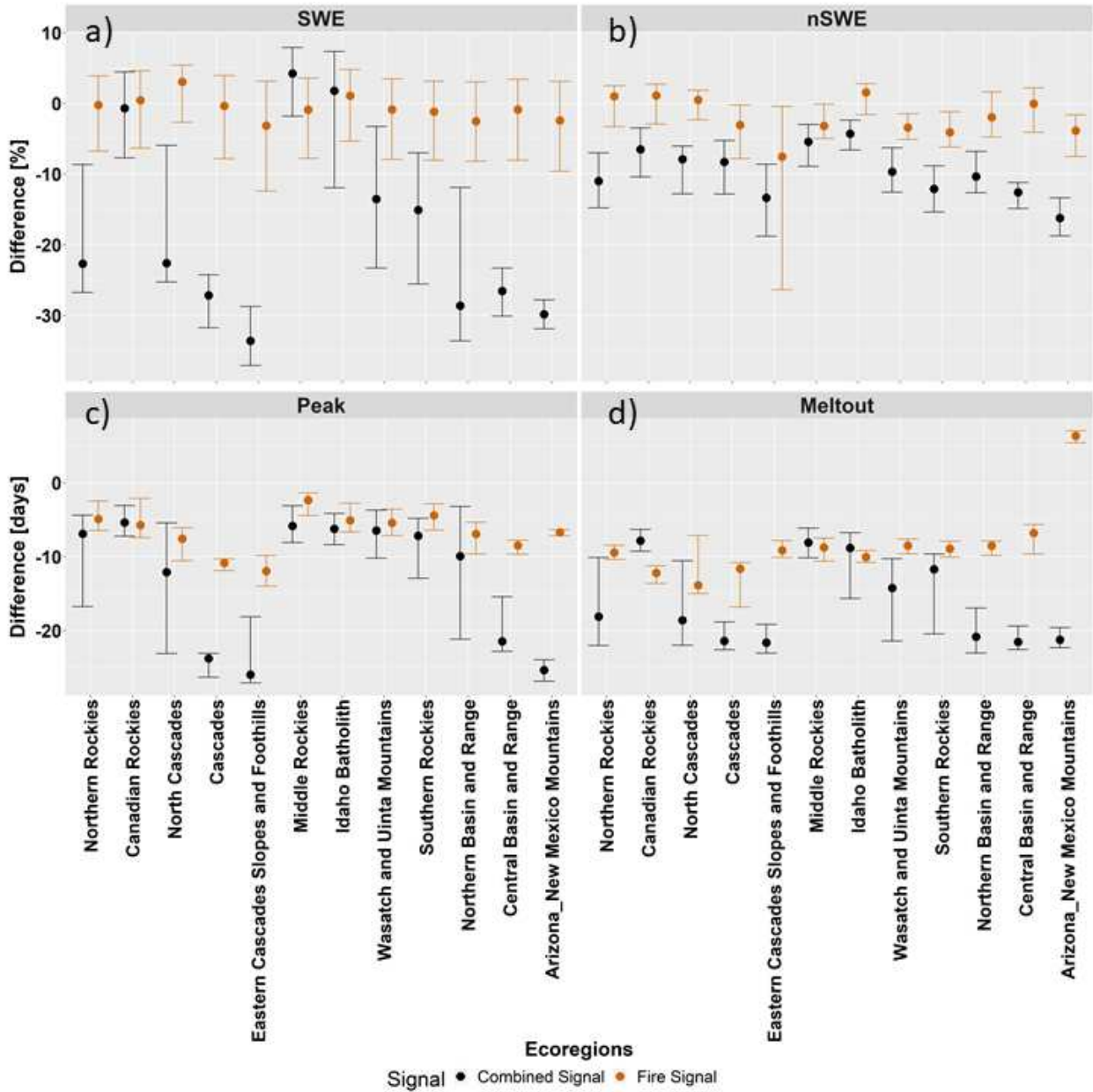


Figure 16. Ecoregion median and interquartile range (IQR) of combined and fire signal changes for a) peak SWE, b) maximum normalized SWE, c) peak SWE date, and d) melt-out date.

3.5.4 Identification and evaluation of snow vulnerable areas

The location and quantification of areas where snow is most vulnerable are based on the predicted SWE changes. Vulnerable areas within each ecoregion are those areas with predicted SWE changes exceeding the RF model training RMSE resulting from the k-fold cross validation

process (Table 4). Specifically, any areas within the ecoregions which have a predicted absolute SWE value change of greater than 19% were classified as vulnerable. An example of vulnerable areas for the Southern Rockies is shown in Figure 17 along with wildfire perimeters from this region during the 2015-2020 period. The fire perimeters are from the National Interagency Fire Center (<https://data-nifc.opendata.arcgis.com/datasets/nifc::interagency-fire-perimeter-history-all-years/about>). From Figure 17a, areas of the southern Rockies that are vulnerable from the CS are at lower latitudes. This is due to the warmer mean winter temperatures and reduced days below freezing. Zooming into the areas in southern Colorado, near La Veta, Colorado, there are large portions of the Junkins and Spring Creek burn areas that are vulnerable (Figure 17b). The majority of burned area in the Spring Creek fire perimeter is vulnerable to changes in SWE using CS model results (Figure 17c). In contrast to the CS results, the areas of vulnerability based on the FS are substantially less because they are only located in areas with shallow slope (Figure 17d). Again, zooming into areas of southern Colorado, there are limited locations with the Junkins and Spring Creek fire perimeters which are classified as vulnerable (Figure 17e). Only the west side of the Spring Creek fire perimeter has concentrations of vulnerable areas based on the fire signal RF model results (Figure 17f).

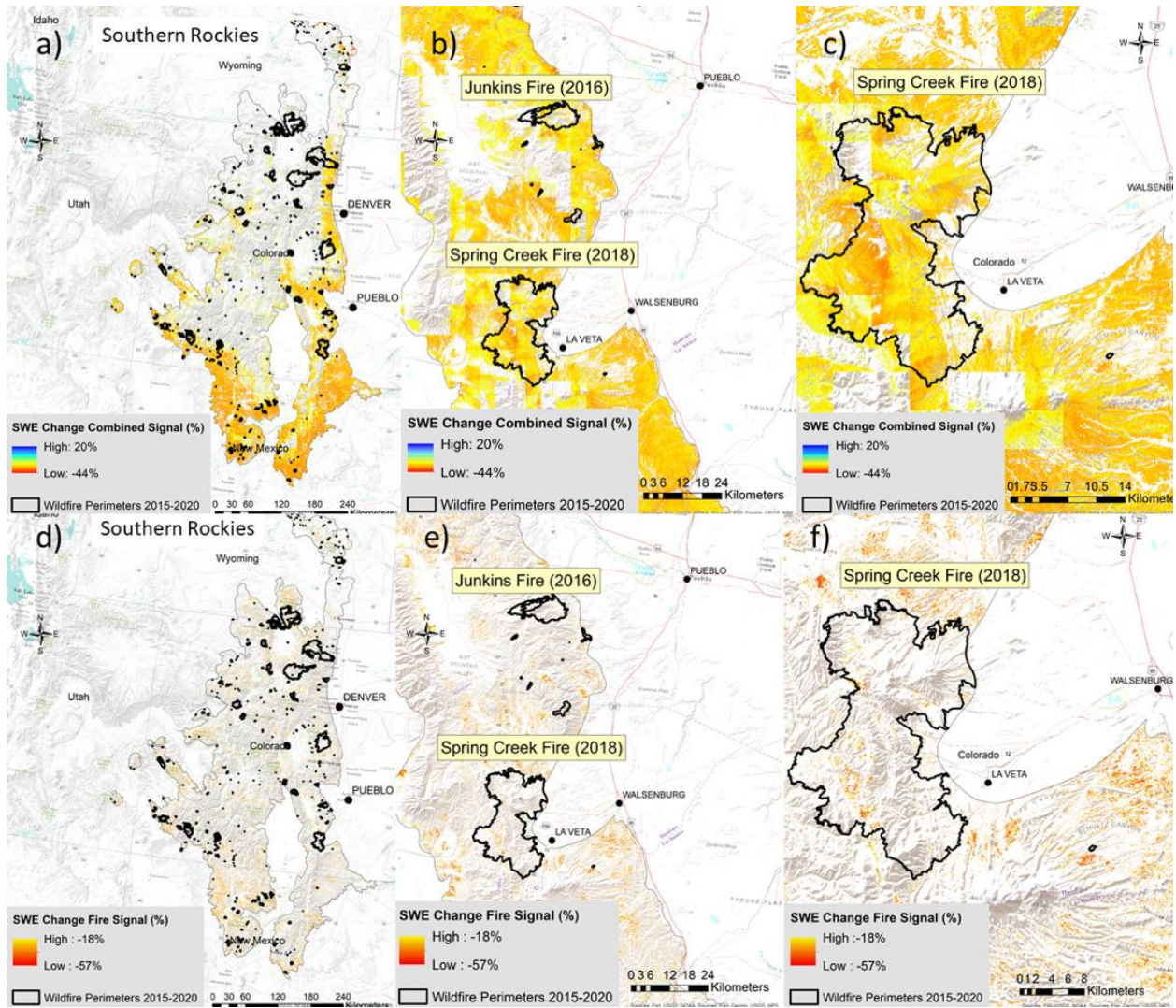


Figure 17. Vulnerable areas of Southern Rockies based on SWE change magnitude greater than model RMSE. Vulnerable areas using the combined signal SWE model for a) the Southern Rockies ecoregion; b) areas in southern Colorado; and c) areas of Spring Creek Fire from 2018. Vulnerable areas using the fire signal SWE model for d) Southern Rockies ecoregion; e) areas in southern Colorado; and f) areas of Spring Creek Fire from 2018.

Using the important variables from each RF model, the distribution of predictor variables helps further clarify the characteristics in each ecoregion where SWE vulnerability may exist. The distribution of predictor variables used in the CS SWE model are shown in Figure 18 and are sorted by variable importance. There are three distributions shown for each predictor variable. The first is the values for the entire ecoregion classified as tree cover; the second is

areas classified as tree cover within the fire 2015-2020 perimeters; and the final distribution are areas identified as vulnerable based on the percent SWE difference exceeding the model RMSE. The most important variable for the CS SWE model is MeanLT0. For the northern and mid-latitude ecoregions many areas within these ecoregions have more than 100 days of temperatures below freezing. However, the vulnerable areas are limited to lower MeanLT0 values (less than 100 days) and are a relatively small portion of the total ecoregion distribution (Figure 18a). In contrast, the MeanLT0 values for vulnerable areas for the southern ecoregions generally span the entire ecoregion distribution. This suggests that more areas are potentially vulnerable to SWE changes post-wildfire when both climate and wildfire are combined. The northern and mid-latitude ecoregions areas, where wildfires have occurred, span only a small portion of the total ecoregion range for the MeanLT0 predictor variable (Figure 18a). There is substantial variability for incoming radiation between ecoregions. Within each ecoregion, the vulnerable distributions for incoming radiation are generally within the distribution range for the entire ecoregion (Figure 18b). There are minimal differences between ecoregions and distributions within each ecoregion for eastness. The vulnerable area distribution aligns with both the entire ecoregion as well as the areas where fires have occurred (Figure 18c). The distribution of slope shows differences between ecoregions, however only there are minimal differences in the range of slope values for the entire ecoregion as compared to the vulnerable areas (Figure 18d). Using the combined model results, vulnerable areas are located in ecoregions (or portions of ecoregions) which have few winter days below freezing. This would suggest that even small changes in land surface temperatures due to wildfire would result in less seasonal snowpack accumulation, regardless of the incoming radiation and topographic position. Areas of the Cascades and Eastern Cascades Slopes and Foothills ecoregions that are susceptible to increases in temperature and considered

“at risk” for SWE decreases from climate (Nolin & Daly, 2006) may also be vulnerable to wildfire impacts on SWE.

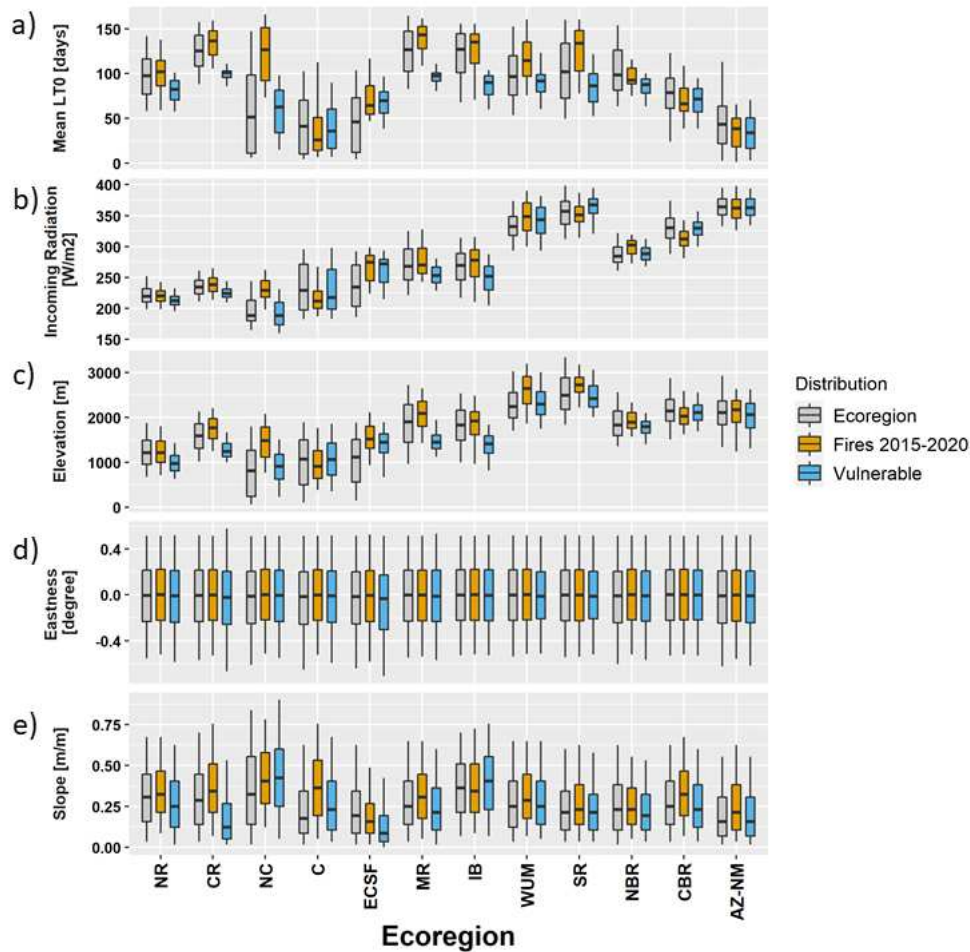


Figure 18. Distribution predictor variables used in combined signal SWE model for the ecoregion area (black), burned areas (brown), and vulnerable areas (light blue). The variables in descending order of importance are a) MeanLTO, b) incoming radiation, c) eastness, and d) slope. The median values are the heavy black line in the colored rectangle. The colored rectangle extents represent the 25th and 75th percentile. The lines extending from the colored rectangle represent the 5th and 95th percentiles.

The predictor variable distributions for the FS SWE model are shown in Figure 19. The vulnerable areas are in shallower slope areas (Figure 19a). Shallow slope areas tend to have increased SWE accumulation because areas of higher slope are subject to more wind redistribution and solar radiation depending on the aspect direction (Berndt, 1965). The HLI for

areas of vulnerability is generally consistent with the median HLI values for the entire ecoregion (Figure 19b), while the northness values for vulnerable areas are lower (more south-facing) across all ecoregions (Figure 19c). The vulnerable areas on south-facing slopes are likely due to the increased solar radiation reaching the snow surface when the canopy is removed following a wildfire. The increased radiation can result in more sublimation (Harpold et al., 2014) and therefore lower peak SWE.

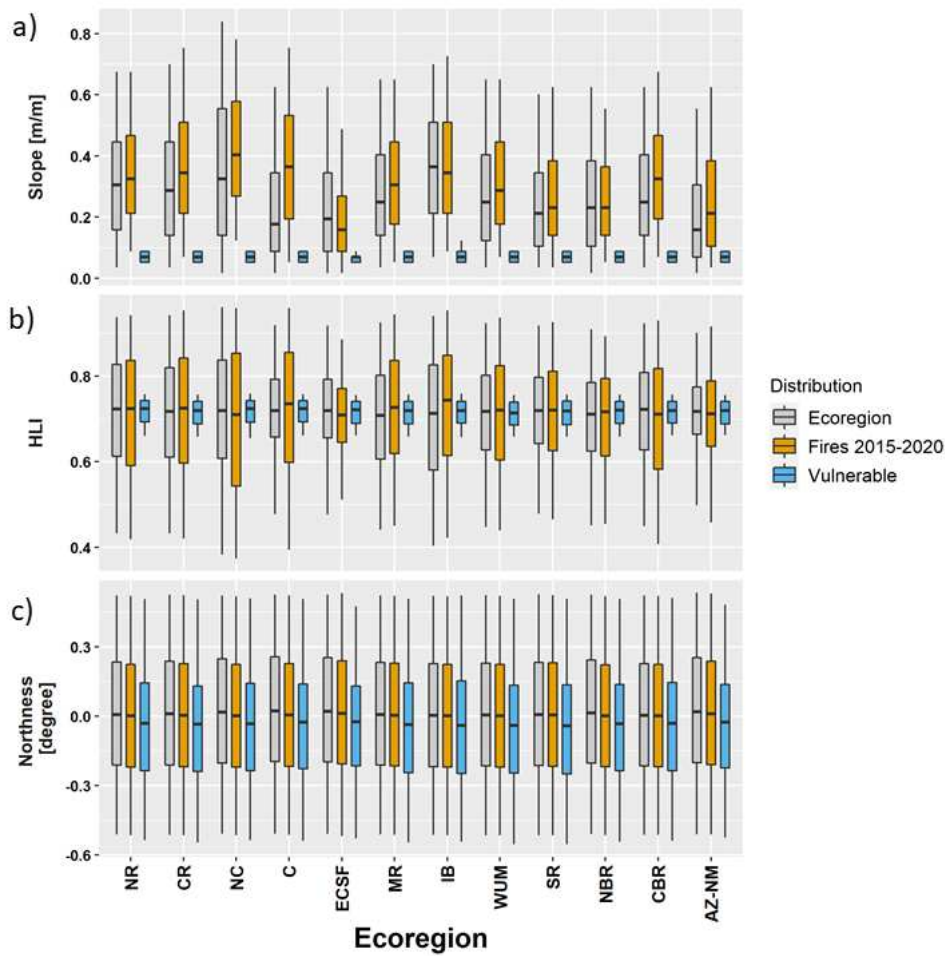


Figure 19. Distribution predictor variables used in fire signal SWE model for the ecoregion area (black), burned areas (brown), and vulnerable areas (light blue). The variables in descending order of importance are a) slope, b) HLI, and c) northness. The median values are the heavy black line in the colored rectangle. The colored rectangle extents represent the 25th and 75th percentile. The lines extending from the colored rectangle represent the 5th and 95th percentiles.

3.5.6 Snow Water volume changes due to fires from 2015-2020

The potential changes for snow measures across ecoregions is important for quantifying vulnerabilities to future wildfires. Given the increase in frequency and size of fires in recent years, it is important to also quantify snow water changes which have already occurred in each of these regions and put these differences in the context of mean annual peak snow water.

The burned area for each ecoregion summarized in Table 7. The burned areas are based the National Interagency Fire Center wildfire perimeters from 2015 through 2020. The percent of the total area burned between the 2015-2020 was less than 10% of any ecoregion. The highest burned area proportion is in the Cascades while the lowest is in the Central Basin and Range. The change in snow water depth based on the FS SWE model and recent fires is also quantified by ecoregion in Table 7. The snow water change is reported as an average depth over the spatial domain for discussion clarity. From the results, there is a range of depth differences for the burned areas between the pre- and post-wildfire periods. All depth changes are negative for the burned areas, with the exception of the Northern Rockies and North Cascades which were approximately zero and 1% difference. The largest snow water depth decreases are for the Eastern Cascades Slopes and Foothills and Arizona-New Mexico Mountains were approximately 6% for the burned areas. Considering the short duration of the previous fires evaluated (2015-2020), the changes for some of the ecoregions could be consequential for processes that depend on snowmelt (e.g. streamflow runoff volume, stream and lake temperature, etc.).

Table 7. Summary of average SWE depth along with pre- and post-wildfire SWE depth changes based on the burned areas from 2015-2020 for each ecoregion.

Ecoregion	Percent of Tree Classified Ecoregion Area Burned	Ecoregion SWE Avg. Depth [mm]	Burned Area 2015-2020 Pre-wildfire SWE Avg. Depth [mm]	Burned Area 2015-2020 Post-wildfire SWE Avg. Depth [mm]	Burned Area 2015-2020 Snow Water Change [%]
Northern Rockies	3.1	279	293	293	0
Canadian Rockies	6.2	542	553	550	-1>
North Cascades	5.3	602	585	588	1
Cascades	8.8	318	307	300	-2
Eastern Cascades Slopes and Foothills	4.1	195	190	177	-6
Middle Rockies	2.1	295	397	394	-2
Idaho Batholith	6.4	441	484	477	-1
Southern Rockies	4.5	235	230	222	-4
Wasatch and Uinta Mountains	4.6	280	319	310	-3
Central Basin and Range	1.3	82	101	100	-1
Northern Basin and Range	5.5	175	188	182	-3
Arizona-New Mexico Mountains	4.8	49	65	61	-6

3.6 DISCUSSION

The spatial variability of snowpack in unburned areas has been documented in other studies due to topographic, land cover, and climatic variables (Anderton et al., 2004; Fassnacht et al., 2017; Sexstone & Fassnacht, 2014; Sospedra-Alfonso et al., 2015; Tennant et al., 2017). The SWE model results (Figure 16a) for CS and FS demonstrate post-wildfire snowpack changes within ecoregions are also spatially variable using similar predictor variables. This suggest the spatial variability in the SWE changes are likely a direct consequence of the inherent variability of snowpack. This reasoning applies to the CS peak and melt-out results which are also quite spatially variable for several of the ecoregions and have importance placed on topographic variables. In contrast, the spatial variability of the FS peak and melt-out dates is substantially

less than the CS results. In both of these models only climatic and land cover variables are considered important. This suggests that topography would be the primary source of intra-ecoregion spatial variability for post-wildfire snow measure changes while climate and land cover are the source of inter-ecoregion variability.

Using the results from Figure 16 and in Table 1 (Chapter 2), conclusions can be made about the spatial representativeness of the SNOTEL site used in this analysis. The empirical results from the SNOTEL sites indicate all ecoregions except the Northern Rockies, Middle Rockies, and Idaho Batholith have decreasing SWE post-wildfire. By comparison the CS SWE results also indicate spatial median decreases in all of the ecoregions except the Middle Rockies and Idaho Batholith. The empirical analysis for the Northern Rockies only includes one burned SNOTEL site. This could increase uncertainty in the empirical results and therefore would not necessarily make the RF model results inconsistent with previous findings. The empirical results (Table 1) are generally consistent in the FS SWE change direction but not magnitude. This inconsistency in the magnitude of change is likely due to the spatial representativeness of the SNOTEL sites. Measurements at SNOTEL sites adequately represent the temporal evolution of snowpack (Fassnacht et al., 2014), but have limited spatial representation of the SWE distribution surrounding the site (Meromy et al., 2013; Molotch et al., 2005).

The vulnerable areas for SWE changes from wildfire are concentrated in shallow slope areas of each ecoregion (Figure 19). In many of the ecoregions the south-facing shallow slope areas are only a limited subset of the entire distribution of slope values. This indicates areas across the western U.S. vulnerable to wildfire impacts may be isolated. In contrast, SWE changes, when climate and wildfire are combined, are primarily dependent on the average number of days below freezing that occur each winter. Vulnerable areas for northern and mid-

latitude ecoregions are concentrated in areas with overall warmer winter temperatures. For the southern ecoregions the vulnerable areas from the combined effects cover substantial portions of the entire ecoregion (Figure 18). The vulnerable CS SWE results are consistent with the current statistically significant SWE trends described by Grundstein and Mote (2010) at lower elevation and presumably warmer snow measurement sites.

The changes in snow water volume due to recent fires also presents an interesting challenge for water managers. In some areas, as much as a 6% decrease may have occurred due to the cumulative effect of wildfire during 2015 through 2020. This decrease may have significant impacts to municipal and agricultural water supplies. Moreover, any SWE decrease resulting from wildfire is compounded with continuing climate change impacts which have also resulted in decreased peak SWE. The snow water volume lost due to wildfire may be a long-term effect. Figure 10 showed the differences in peak SWE do not recover quickly and in some cases were not recovered after more than 30 years post-wildfire. The potential long-term reduction of snow water volume will have several consequences including economic loss at a regional or national scale (Sturm et al., 2017), reductions in water allocations for agricultural users (Vano et al., 2010), and ecological functions (Saccone et al., 2013).

Based on two separate evaluation methods, the RF models do have predictive ability for snowpack changes post-wildfire at the burned SNOTEL sites which are used in the model development. However, there are other concerns when using ground-based stations to estimate changes over larger domains. Due to SNOTEL site characteristics, changes in interception from canopy loss due to wildfire would likely not be reflected in the SWE measurements. Sublimation from snowfall interception can be important in the overall water balance (Sexstone et al., 2018). However, changes in albedo, turbulent fluxes, and net incoming radiation reaching

the snow surface are incorporated into the measured values. Given the limited spatial representativeness and limited number of SNOTEL sites used in this analysis, the RF results do have substantial uncertainty when developing a tool for large portions of the western U.S. However, these results do lead to several testable hypothesis. The first hypothesis is the largest SWE changes in a region, when comparing burned and burned areas, will occur in relatively gentle slope areas. In contrast, locations with relatively low mean days below freezing will have the largest SWE changes when considering both climate and wildfire. Another hypothesis could be topographic variables such as slope and aspect are the key for explaining spatial variability of SWE between ecoregions. Finally, decreases in snow water in burned areas persist for several years following a wildfire.

3.7 CONCLUSIONS

In this study, there are eight RF models developed to quantify wildfire effects on snowpack across several ecoregions in the western U.S. Separate models were used to predict changes using two signal classifications (combined and fire) for four different snow measures. The data used to develop these signals is based on pre- and post-wildfire periods at 43 SNOTEL sites that have been impacted by wildfire (combined signal). Unburned comparison SNOTEL sites were identified for each of the 43 wildfire impacted locations. A total of 108 comparison sites, divided based on the same points in time as the burned sites, were used to remove climatic differences and isolate the effects of wildfire (fire signal). The snow measures include melt-out date, date of maximum SWE, maximum SWE, and maximum normalized SWE (maximum SWE divided by October through April total precipitation). The training data used in the model development was based on several predictor variables and the snow measures at each of the wildfire impacted SNOTEL sites. The predictor variables consist of several sources of

information including geographic (i.e., longitude, latitude); topographic (i.e., slope, northness, eastness, elevation, curvature); climatic information (i.e., temperature and precipitation); land surface energy fluxes (i.e., incoming shortwave radiation, HLI) and land cover (i.e., tree genus, total basal area). The RF models were used to predict areas of snow vulnerability in each ecoregion. Quantification of snow water volume changes from recent fires was also performed. The RF model development used relatively limited training data (only 43 wildfire impacted SNOTEL sites) and has training error which exceeds the median change in peak SWE. In addition, the SNOTEL sites used for training the RF models are not evenly distributed between ecoregions.

The key conclusions from the vulnerability study are:

- There is substantial spatial variability within all ecoregions for changes in maximum SWE. The largest spatial variability is in the northern and mid-latitude ecoregions. The combined signal peak SWE changes range from over 35% decrease in the Eastern Cascades Slopes and Foothills to 10% increase in the Middle Rockies. The fire signal peak SWE changes range from approximately 10% decrease to 5% increase.
- The spatial variability for the wildfire only signal is less than the combined signal, especially for peak SWE and melt-out dates.
- The most important variables for prediction maximum SWE and nSWE from only wildfire effects is terrain slope.
- The most important variable for predicting peak SWE and melt-out date changes from wildfire only effects is incoming shortwave radiation and aridity, respectively.

- The most important variables for predicting changes to maximum SWE, peak date and melt-out date changes using the combined signal data are mean days below freezing and mean winter temperature.
- Vulnerable areas for changes in SWE due to wildfire only are located in shallow sloped terrain. Areas with warmer winter temperatures (i.e., where snowfall occurs near the ice-water transition temperature) are also vulnerable to combined climate and wildfire impacts.
- The snow water volume changes for areas burned from 2015-2020 resulted in SWE decreases for all ecoregions except the Northern Rockies and North Cascades. The maximum snow water decrease was 6% for areas burned between 2015-2020 in the Eastern Cascades Slopes and Foothills and the Arizona-New Mexico Mountains.

While the results of this analysis provide an improved predictive tool over using simple average for water resource managers, there are important limitations that should be noted. Relatively few ground-based measurement sites for snowpack are available to use in the training of the RF models. In addition, the spatial representativeness of SNOTEL sites is very limited which may introduce substantial uncertainty when modeling changes over entire ecoregions. There are also limitations with the SNOTEL data from the perspective of the RF models can only predict vulnerable areas for ecoregions where training data is available. Much of the Sierra Nevada Mountains are not included in the model development for this reason. Also, there is currently no high spatial/temporal resolution remote sensing product that measures SWE. Products like the UA SWE data are based on interpolating ground-based measurements. This further limits comparisons between the model results and observations. However, this

framework can be utilized as additional data becomes available from ground-based measurements. Finally, RF models do not provide predictions in snowpack melt-rates or changes in snowmelt runoff volume, which are often most important for water management activities.

From vulnerability analysis there are several potential directions for future research. The framework for the RF model development can be used as more measurements become available which would provide additional training data. As remote sensing platforms come online which directly measure SWE at high spatial resolutions, comparisons between predicted snowpack changes from the vulnerability results comparison for large areas can be made. Another possible direction would be including snow cover area products along with the SNOTEL information. Finally, evaluating differences in snowmelt runoff from predicted vulnerable areas which have been burned recently will provide the connection from this work to the water management activities in each region. The snow vulnerability results provide an initial step to risk identification for areas before wildfires occur as well as potentially informing post-wildfire assessments and field measurement campaigns.

3.8 REFERENCES

- Abatzoglou, J. T. (2013). Development of gridded surface meteorological data for ecological applications and modelling. *International Journal of Climatology*, *33*(1), 121–131.
<https://doi.org/10.1002/joc.3413>
- Adams, T. E. (2016). Flood Forecasting in the United States NOAA/National Weather Service. In *Flood Forecasting: A Global Perspective*. Elsevier Inc. <https://doi.org/10.1016/B978-0-12-801884-2.00010-4>
- Anderton, S. P., White, S. M., & Alvera, B. (2004). Evaluation of spatial variability in snow water equivalent for a high mountain catchment. *Hydrological Processes*, *18*(3), 435–453.
<https://doi.org/10.1002/hyp.1319>
- Barnett, T. P., Adam, J. C., & Lettenmaier, D. P. (2005). Potential impacts of a warming climate on water availability in snow-dominated regions. *Nature*, *438*(7066), 303–309.
<https://doi.org/10.1038/nature04141>
- Barnhart, T. B., Molotch, N. P., Livneh, B., Harpold, A. A., Knowles, J. F., & Schneider, D. (2016). Snowmelt Rate Dictates Streamflow. *Update Citation When Published*, 1–11.
<https://doi.org/10.1002/2016GL069690>
- Berndt, H. W. (1965). Snow Accumulation and Disappearance in Lodgepole Pine Clearcut Blocks in Wyoming. *Journal of Forestry*, *63*(2), 88–91. <https://doi.org/10.1093/jof/63.2.88>
- Bettinger, P. (2008). Chapter 2: Valuing and Characterizing Forest Conditions. In *Forest Management and Planning* (pp. 17–18).
- Biau, G., & Scornet, E. (2016). A random forest guided tour. *Test*, *25*(2), 197–227.
<https://doi.org/10.1007/s11749-016-0481-7>
- Boulesteix, A. L., Janitza, S., Kruppa, J., & König, I. R. (2012). Overview of random forest

- methodology and practical guidance with emphasis on computational biology and bioinformatics. *Wiley Interdisciplinary Reviews: Data Mining and Knowledge Discovery*, 2(6), 493–507. <https://doi.org/10.1002/widm.1072>
- Breiman, L. (2001). Random Forests. *Machine Learning*, 45, 5–32. https://doi.org/10.1007/978-3-030-62008-0_35
- Breiman, L., Cutler, A., Liaw, A., & Wiener, M. (2021). *randomForest: Breiman and Culer's Random Forests for Classification and Regression* (R package version 4.6-14). [//cran.r-project.org/package=randomForest](https://cran.r-project.org/package=randomForest)
- Breiman L, Friedman JH, Olshen RA, Stone CJ (1984) Classification and regression trees. Chapman & Hall/CRC, Boca Raton.
- Broxton, P. D., van Leeuwen, W. J. D., & Biederman, J. A. (2019). Improving Snow Water Equivalent Maps With Machine Learning of Snow Survey and Lidar Measurements. *Water Resources Research*, 55(5), 3739–3757. <https://doi.org/10.1029/2018WR024146>
- Broxton, P., Dawson, N., & Zeng, X. (2016). Linking snowfall and snow accumulation to generate spatial maps of SWE and snow depth. *Earth and Space Science*, 3, 246–256. <https://doi.org/10.1002/2016EA000174>.Received
- Buban, M. S., Lee, T. R., & Baker, C. B. (2020). A comparison of the U.S. climate reference network precipitation data to the parameter-elevation regressions on independent slopes model (PRISM). *Journal of Hydrometeorology*, 21(10), 2391–2400. <https://doi.org/10.1175/JHM-D-19-0232.1>
- Burles, K., & Boon, S. (2011). Snowmelt energy balance in a burned forest plot, Crowsnest Pass, Alberta, Canada. *Hydrological Processes*, 25, 3012–3029. <https://doi.org/10.1002/hyp.8067>
- Burrill, E. A., Wilson, A. M., Turner, J. A., Pugh, S. A., Menlove, J., Christiansen, G., Conkling,

- B. L., & David, W. (2018). The Forest Inventory and Analysis Database: database description and user guide version 8.0 for Phase 2. In *U.S. Department of Agriculture, Forest Service*. (Vol. 2). <http://www.fia.fs.fed.us/library/database-documentation/>
- Cayan, D. R. (1996). Interannual Climate Variability and Snowpack in the Western United States. *Journal of Climate*, 9, 928–948.
- Clow, D. W. (2010). Changes in the timing of snowmelt and streamflow in Colorado: A response to recent warming. *Journal of Climate*, 23(9), 2293–2306.
<https://doi.org/10.1175/2009JCLI2951.1>
- Curry, C. L., & Zwiers, F. W. (2018). Examining controls on peak annual streamflow and floods in the Fraser River Basin of British Columbia. *Hydrology and Earth System Sciences*, 22(4), 2285–2309. <https://doi.org/10.5194/hess-22-2285-2018>
- Daly, C., Neilson, R. P., & Phillips, D. L. (1994). A Statistical-Topographic Model for Mapping Climatological Precipitation over Mountainous Terrain. *Journal of Applied Meteorology*, 33.
- Dennison, P. E., Brewer, S. C., Arnold, J. D., & Moritz, M. A. (2014). Large wildfire trends in the western United States, 1984-2011. *Geophys. Res. Lett.*, 41, 2928–2933.
- Dingman, S. L. (1981). Elevation: A major influence on the hydrology of New Hampshire and Vermont, USA. *Hydrological Sciences Bulletin*, 26(4), 399–413.
<https://doi.org/10.1080/02626668109490904>
- Doesken, N., & Judson, A. (1996). *The Snow Booklet: A guide to the Science, Climatology, and Measurement of Snow in the United States*.

- Du, X., Goss, G., & Faramarzi, M. (2020). Impacts of hydrological processes on stream temperature in a cold region watershed based on the SWAT equilibrium temperature model. *Water (Switzerland)*, 12(4). <https://doi.org/10.3390/W12041112>
- Evans J.S. (2021). *_spatialEco_*. R package version 1.3-6, <URL: <https://github.com/jeffrejevans/spatialEco>>.
- Fassnacht, S. R., Deitemeyer, D. C., & Venable, N. B. H. (2014). Capitalizing on the daily time step of snow telemetry data to model the snowmelt components of the hydrograph for small watersheds. *Hydrological Processes*, 28(16), 4654–4668. <https://doi.org/10.1002/hyp.10260>
- Fassnacht, S. R., López-Moreno, J. I., Ma, C., Weber, A. N., Pfohl, A. K. D., Kampf, S. K., & Kappas, M. (2017). Spatio-temporal snowmelt variability across the headwaters of the Southern Rocky Mountains. *Frontiers of Earth Science*, 11(3), 505–514. <https://doi.org/10.1007/s11707-017-0641-4>
- Flannigan, M. D., Stocks, B. J., & Wotton, B. M. (2000). Climate change and forest fires. *Science of the Total Environment*, 262(3), 221–229. [https://doi.org/10.1016/S0048-9697\(00\)00524-6](https://doi.org/10.1016/S0048-9697(00)00524-6)
- Follum, M. L., Downer, C. W., Niemann, J. D., Roylance, S. M., & Vuyovich, C. M. (2015). A radiation-derived temperature-index snow routine for the GSSHA hydrologic model. *Journal of Hydrology*, 529(P3), 723–736. <https://doi.org/10.1016/j.jhydrol.2015.08.044>
- Fyfe, J. C., Derksen, C., Mudryk, L., Flato, G. M., Santer, B. D., Swart, N. C., Molotch, N. P., Zhang, X., Wan, H., Arora, V. K., Scinocca, J., & Jiao, Y. (2017). Large near-Term projected snowpack loss over the western United States. *Nature Communications*, 8, 1–7. <https://doi.org/10.1038/ncomms14996>
- Gao, J., Sheshukov, A. Y., Yen, H., & White, M. J. (2017). Catena Impacts of alternative climate

information on hydrologic processes with SWAT : A comparison of NCDC , PRISM and NEXRAD datasets. *Catena*, 156(May), 353–364.

<https://doi.org/10.1016/j.catena.2017.04.010>

Giovando, J., Engel, C., Daly, S., Warner, M., Hamill, D., & Heisman, E. (2021). Wintertime snow and precipitation conditions in the Willow Creek watershed above Ririe Dam, Idaho. Engineer Research and Development Center (U.S.). <https://doi.org/10.21079/11681/40479>

Gleason, K. E., & Nolin, A. W. (2016). Charred forests accelerate snow albedo decay : parameterizing the post- fire radiative forcing on snow for three years following fire. *Hydrological Processes*, 30, 3855–3870. <https://doi.org/10.1002/hyp.10897>

Gleason, K. E., Nolin, A. W., & Roth, T. R. (2013). Charred forests increase snowmelt : Effects of burned woody debris and incoming solar radiation on snow ablation. *Geophysical Research Letters*, 40, 4654–4661. <https://doi.org/10.1002/grl.50896>

Goodwin, M. J., Zald, H. S., North, M., & Hurteau, M. D. (2021). Climate-Driven Tree Mortality and Fuel Aridity Increase Wildfire’s Potential Heat Flux. *Geophysical Research Letters*, 48.

Greve, P., Roderick, M. L., Ukkola, A. M., & Wada, Y. (2019). The aridity Index under global warming. *Environmental Research Letters*, 14(12), 124006. <https://doi.org/10.1088/1748-9326/ab5046>

Grundstein, A., & Mote, T. (2010). Trends in average snow depth across the Western United States. *Physical Geography*, 31(2), 172–185. <https://doi.org/10.2747/0272-3646.31.2.172>

Gupta, H. V., Kling, H., Yilmaz, K. K., & Martinez, G. F. (2009). Decomposition of the mean squared error and NSE performance criteria: Implications for improving hydrological modelling. *Journal of Hydrology*, 377(1–2), 80–91.

<https://doi.org/10.1016/j.jhydrol.2009.08.003>

- Guyette, R. P., Thompson, F. R., Whittier, J., Stambaugh, M. C., & Dey, D. C. (2014). Future fire probability modeling with climate change data and physical chemistry. *Forest Science*, *60*(5), 862–870. <https://doi.org/10.5849/forsci.13-108>
- Hamlet, A. F., Mote, P. W., Clark, M. P., & Lettenmaier, D. P. (2005). Effects of temperature and precipitation variability on snowpack trends in the Western United States. *Journal of Climate*, *18*(21), 4545–4561. <https://doi.org/10.1175/JCLI3538.1>
- Hammond, J. C., Saavedra, F. A., & Kampf, S. K. (2018). How Does Snow Persistence Relate to Annual Streamflow in Mountain Watersheds of the Western U.S. With Wet Maritime and Dry Continental Climates? *Water Resources Research*, *54*(4), 2605–2623. <https://doi.org/10.1002/2017WR021899>
- Harpold, A. A., Biederman, J. A., Condon, K., Merino, M., Korgaonkar, Y., Nan, T., Sloat, L. L., Ross, M., & Brooks, P. D. (2014). Changes in snow accumulation and ablation following the Las Conchas Forest Fire, New Mexico, USA. *Ecohydrology*, *7*, 440–452. <https://doi.org/10.1002/eco.1363>
- Harpold, A. A., Kaplan, M. L., Zion Klos, P., Link, T., McNamara, J. P., Rajagopal, S., Schumer, R., & Steele, C. M. (2017). Rain or snow: Hydrologic processes, observations, prediction, and research needs. *Hydrology and Earth System Sciences*, *21*(1), 1–22. <https://doi.org/10.5194/hess-21-1-2017>
- Hijmans, R. (2021). raster: Geographic Data Analysis and Modeling. R package version 3.5-11. <https://CRAN.R-project.org/package=raster>
- Horn, W. L. (1968). Snowpack and Water Supply. *Journal - American Water Works Association*, *60*(12), 1389–1395. <https://doi.org/10.1002/j.1551-8833.1968.tb03689.x>
- James, G., Witten, D., Hastie, T., & Tibshirani, R. (2013). *An Introduction to Statistical*

Learning with application in R. Springer.

King, F., Erler, A., Frey, S., & Fletcher, C. (2020). Application of machine learning techniques for regional bias correction of SWE estimates in Ontario, Canada. *Hydrology and Earth System Sciences Discussions*, 1–26. <https://doi.org/10.5194/hess-2019-593>

Knowles, N., Dettinger, M., & Cayan, D. R. (2006). Trends in Snowfall Versus Rainfall for the Western United States, 1949-2001. *Journal of Climate*, 19(April 2007), 4545–4559.

LANDFIRE: LANDFIRE Aspect layer. (2016a). U.S.

Department of Interior, Geological Survey, and U.S. Department of Agriculture.

[Online]. Available: <http://landfire.cr.usgs.gov/viewer/> [2020, June 8].

LANDFIRE: LANDFIRE Elevation layer. (2016b). U.S.

Department of Interior, Geological Survey, and U.S. Department of Agriculture.

[Online]. Available: <http://landfire.cr.usgs.gov/viewer/> [2020, June 8].

LANDFIRE: LANDFIRE Existing Vegetation Type layer. (2016c). U.S.

Department of Interior, Geological Survey, and U.S. Department of Agriculture.

[Online]. Available: <http://landfire.cr.usgs.gov/viewer/> [2020, June 8].

LANDFIRE: LANDFIRE Slope layer. (2016d). U.S.

Department of Interior, Geological Survey, and U.S. Department of Agriculture.

[Online]. Available: <http://landfire.cr.usgs.gov/viewer/> [2020, June 8].

Lapen, D. R., & Martz, L. W. (1996). An investigation of the spatial association between snow depth and topography in a Prairie agricultural landscape using digital terrain analysis.

Journal of Hydrology, 184(3–4), 277–298. [https://doi.org/10.1016/0022-1694\(95\)02975-3](https://doi.org/10.1016/0022-1694(95)02975-3)

Lea, J. (2008). Effect of Snowpack Changes in the Central Sierra Nevada on Water Supply Forecasts in the Truckee River Basin. *76th Annual Western Snow Conference*, 115–118.

<http://sites/westernsnowconference.org/PDFs/2008Lea.pdf>

- Li, D., Wrzesien, M. L., Durand, M., Adam, J., & Lettenmaier, D. P. (2017). How much runoff originates as snow in the western United States, and how will that change in the future? *Geophysical Research Letters*, *44*(12), 6163–6172. <https://doi.org/10.1002/2017GL073551>
- Liaw, A., & Wiener, M. (2002). Classification and Regression by randomForest. *R News*, *2*(3), 18–22.
- Littell, J. S., Mckenzie, D., Peterson, D. L., & Westerling, A. L. (2009). Climate and wildfire area burned in western U.S. ecoprovinces, 1916-2003. *Ecological Applications*, *19*(4), 1003–1021. <https://doi.org/10.1890/07-1183.1>
- Littell, J. S., Pederson, G. T., Gray, S. T., Tjoelker, M., Hamlet, A. F., & Woodhouse, C. A. (2016). Reconstructions of Columbia River Streamflow from Tree-Ring Chronologies in the Pacific Northwest, USA. *JAWRA Journal of the American Water Resources Association*, *87521*. <https://doi.org/10.1111/1752-1688.12442>
- Liu, Z., Ballantyne, A. P., & Cooper, L. A. (2019). Biophysical feedback of global forest fires on surface temperature. *Nature Communications*, *10*(1), 214. <https://doi.org/10.1038/s41467-018-08237-z>
- Luce, C. H., Lopez-Burgos, V., & Holden, Z. A. (2014). Sensitivity of snowpack storage to precipitation and temperature using spatial and temporal analog models. *Water Resources Research*, *50*, 9447–9462. <https://doi.org/10.1002/2013WR014979>.Reply
- Maidment, D. R. (1993). *Handbook of hydrology*. McGraw-Hill.
- Marshall, A. M., Abatzoglou, J. T., Link, T. E., & Tennant, C. J. (2019). Projected Changes in Interannual Variability of Peak Snowpack Amount and Timing in the Western United States. *Geophysical Research Letters*, *46*(15), 8882–8892.

<https://doi.org/10.1029/2019GL083770>

- Maxwell, J. D., Call, A., & St. Clair, S. B. (2019). Wildfire and topography impacts on snow accumulation and retention in montane forests. *Forest Ecology and Management*, 432(July 2018), 256–263. <https://doi.org/10.1016/j.foreco.2018.09.021>
- McCune, B., & Keon, D. (2002). Equations for potential annual direct incident radiation and heat load. *Journal of Vegetation Science*, 13(4), 603–606. <https://doi.org/10.1111/j.1654-1103.2002.tb02087.x>
- Meromy, L., Molotch, N. P., Link, T. E., Fassnacht, S. R., & Rice, R. (2013). Subgrid variability of snow water equivalent at operational snow stations in the western USA. *Hydrological Processes*, 27(17), 2383–2400. <https://doi.org/10.1002/hyp.9355>
- Micheletty, P. D., Kinoshita, A. M., & Hogue, T. S. (2014). Application of MODIS snow cover products : wildfire impacts on snow and melt in the Sierra Nevada. *Hydrology and Earth System Sciences Discussions*, 18, 4601–4615. <https://doi.org/10.5194/hess-18-4601-2014>
- Moeser, C. D., Broxton, P. D., Harpold, A., & Robertson, A. (2020). Estimating the Effects of Forest Structure Changes From Wild fire on Snow Water Resources Under Varying Meteorological Conditions. *Water Resources Research*, 56, 1–23. <https://doi.org/10.1029/2020WR027071>
- Molotch, N. P., Colee, M. T., Bales, R. C., & Dozier, J. (2005). Estimating the spatial distribution of snow water equivalent in an alpine basin using binary regression tree models: The impact of digital elevation data and independent variable selection. *Hydrological Processes*, 19(7), 1459–1479. <https://doi.org/10.1002/hyp.5586>
- Moriasi, D. N., Arnold, J. G., Liew, M. W. Van, Bingner, R. L., Harmel, R. D., & Veith, T. L. (2007). Model Evaluation Guidelines for Systematic Quantification of Accuracy in

- Watershed Simulations. *American Society of Agricultural and Biological Engineers*, 50(3), 885–900.
- Mote, P. W. (2003). Trends in snow water equivalent in the Pacific Northwest and their climatic causes. *Geophysical Research Letters*, 30(12). <https://doi.org/10.1029/2003GL017258>
- Mote, P. W., Li, S., Lettenmaier, D. P., Xiao, M., & Engel, R. (2018). Dramatic declines in snowpack in the western US. *Npj Climate and Atmospheric Science*, 1(1). <https://doi.org/10.1038/s41612-018-0012-1>
- Nash, J. E., & Sutcliffe, J. V. (1970). River flow forecasting through conceptual models part I - A discussion of principles. *Journal of Hydrology*, 10(3), 282–290. [https://doi.org/10.1016/0022-1694\(70\)90255-6](https://doi.org/10.1016/0022-1694(70)90255-6)
- NatureServe. (2009). *Descriptions of Ecological Systems for Modeling of LANDFIRE Biophysical Settings*. http://downloads.natureserve.org/get_data/data_sets/veg_data/nsDescriptions.pdf
- Natural Resources Conservation Service (2021). NRCS: National Water and Climate Center SNOTEL data network. U.S. Department of Agriculture, available at: <http://www.wcc.nrcs.usda.gov/snow/> , (last accessed: 16 April 2021)
- Nolin, A. W., & Daly, C. (2006). Mapping “at risk” snow in the Pacific Northwest. *Journal of Hydrometeorology*, 7(5), 1164–1171. <https://doi.org/10.1175/JHM543.1>
- Omernik, J. M., & Griffith, G. E. (2014). Ecoregions of the Conterminous United States: Evolution of a Hierarchical Spatial Framework. *Environmental Management*, 54(6), 1249–1266. <https://doi.org/10.1007/s00267-014-0364-1>
- Pierce, D. W., Barnett, T. P., Hidalgo, H. G., Das, T., Bonfils, C., Santer, B. D., Bala, G., Dettinger, M. D., Cayan, D. R., Mirin, A., Wood, A. W., & Nozawa, T. (2008). Attribution

- of declining Western U.S. Snowpack to human effects. *Journal of Climate*, 21(23), 6425–6444. <https://doi.org/10.1175/2008JCLI2405.1>
- Pokorný, R., Tomášková, I., & Havránková, K. (2008). Temporal variation and efficiency of leaf area index in young mountain Norway spruce stand. *European Journal of Forest Research*, 127(5), 359–367. <https://doi.org/10.1007/s10342-008-0212-z>
- PRISM Climate Group, Oregon State University, <https://prism.oregonstate.edu>, data created 4 Jan 2021, accessed 6 Feb 2021.
- Raleigh, M. S., & Lundquist, J. D. (2012). Comparing and combining SWE estimates from the SNOW-17 model using PRISM and SWE reconstruction. *Water Resources Research*, 48(1), 1–16. <https://doi.org/10.1029/2011WR010542>
- Saccone, P., Morin, S., Baptist, F., Bonneville, J. M., Colace, M. P., Domine, F., Faure, M., Geremia, R., Lochet, J., Poly, F., Lavorel, S., & Clément, J. C. (2013). The effects of snowpack properties and plant strategies on litter decomposition during winter in subalpine meadows. *Plant and Soil*, 363(1–2), 215–229. <https://doi.org/10.1007/s11104-012-1307-3>
- Schaerer, P., & McClung, D. (2006). *The avalanche handbook*. The Mountaineers Books.
- Schmidt, R. A., & Glun. (1991). Snowfall interception on branches of three conifer species. *Canadian Journal of Forest Research*, 21, 1262–1269.
- Serreze, M. C., Clark, M. P., Armstrong, R. L., McGinnis, D. A., & Pulwarty, R. S. (1999). Characteristics of the western United States snowpack from snowpack telemetry (SNOTEL) data. *Water Resources Research*, 35(7), 2145–2160. <https://doi.org/10.1029/1999WR900090>
- Sexstone, G. A., & Fassnacht, S. R. (2014). What drives basin scale spatial variability of snowpack properties in northern Colorado? *Cryosphere*, 8(2), 329–344.

<https://doi.org/10.5194/tc-8-329-2014>

Sexstone, Graham A., Clow, D. W., Fassnacht, S. R., Liston, G. E., Hiemstra, C. A., Knowles, J. F., & Penn, C. A. (2018). Snow Sublimation in Mountain Environments and Its Sensitivity to Forest Disturbance and Climate Warming. *Water Resources Research*, *54*(2), 1191–1211.

<https://doi.org/10.1002/2017WR021172>

Seyednasrollah, B., & Kumar, M. (2013). Effects of tree morphometry on net snow cover radiation on forest floor for varying vegetation densities. *Journal of Geophysical Research Atmospheres*, *118*(22), 12,508–12,521. <https://doi.org/10.1002/2012JD019378>

Seyednasrollah, B., & Kumar, M. (2019). How surface radiation on forested snowpack changes across a latitudinal gradient. *Hydrology*, *6*(3). <https://doi.org/10.3390/hydrology6030062>

Smits, A. P., MacIntyre, S., & Sadro, S. (2020). Snowpack determines relative importance of climate factors driving summer lake warming. *Limnology and Oceanography Letters*, *5*(3), 271–279. <https://doi.org/10.1002/lol2.10147>

Sospedra-Alfonso, R., Melton, J. R., & Merryfield, W. J. (2015). Effects of temperature and precipitation on snowpack variability in the Central Rocky Mountains as a function of elevation. *Geophysical Research Letters*, *42*, 4429–4428.

Stavros, E. N., Abatzoglou, J. T., McKenzie, D., & Larkin, N. K. (2014). Regional projections of the likelihood of very large wildland fires under a changing climate in the contiguous Western United States. *Climatic Change*, *126*(3–4), 455–468.

<https://doi.org/10.1007/s10584-014-1229-6>

Stevens, J. T. (2017). Scale-dependent effects of post-fire canopy cover on snowpack depth in montane coniferous forests. *ECOLOGICAL APPLICATIONS*, *27*(6), 1888–1900.

- Stewart, I. T., Cayan, D. R., & Dettinger, M. D. (2004). Changes in Snowmelt Runoff Timing in Western North America under a 'Business as Usual' Climate Change Scenario. *Climatic Change*, 62(1), 217–232. <https://doi.org/10.1023/B:CLIM.0000013702.22656.e8>
- Strachan, S., & Daly, C. (2017). Testing the daily PRISM air temperature model on semiarid mountain slopes. *Journal of Geophysical Research*, 122(11), 5697–5715. <https://doi.org/10.1002/2016JD025920>
- Sturm, M., Goldstein, M. A., & Parr, C. (2017). Water and life from snow: A trillion dollar science question. *Water Resources Research*, 53, 3534–3544. <https://doi.org/10.1002/2017WR020840>.Received
- Swetnam, T. W., & Betancourt, J. L. (1998). Mesoscale Disturbance and Ecological Response to Decadal Climatic Variability in the American Southwest. *Journal of Climate*, 41, 329–359. https://doi.org/10.1007/978-90-481-8736-2_32
- Tennant, C. J., Harpold, A. A., Lohse, K. A., Godsey, S. E., Crosby, B. T., Larsen, L. G., Brooks, P. D., Van Kirk, R. W., & Glenn, N. F. (2017). Regional sensitivities of seasonal snowpack to elevation, aspect, and vegetation cover in western North America. *Water Resources Research*, 53(8), 6908–6926. <https://doi.org/10.1002/2016WR019374>
- Thornton, M. M., Shrestha, R., Wei, Y., Thornton, P. E., Kao, S., & Wilson, B. E. (2020). *Daymet: Daily Surface Weather Data on a 1-km Grid for North America, Version 4*. ORNL Distributed Active Archive Center. <https://doi.org/10.3334/ORNLDAAAC/1840>
- Thornton, P. E., Hasenauer, H., & White, M. A. (2000). Simultaneous estimation of daily solar radiation and humidity from observed temperature and precipitation: An application over complex terrain in Austria. *Agricultural and Forest Meteorology*, 104(4), 255–271. [https://doi.org/10.1016/S0168-1923\(00\)00170-2](https://doi.org/10.1016/S0168-1923(00)00170-2)

- Tyrallis, H., Papacharalampous, G., & Langousis, A. (2019). A brief review of random forests for water scientists and practitioners and their recent history in water resources. *Water (Switzerland)*, *11*(5). <https://doi.org/10.3390/w11050910>
- USACE (U.S. Army Corps of Engineers). (2006). Engineering and design: ice engineering. *EM 1110-2-1612*, 2–8.
- USACE (U.S. Army Corps of Engineers). (1956). *Snow Hydrology*. Portland, OR: U.S. Army Corps of Engineers.
- U.S. Census Bureau. (2019). *Table 1. Annual Estimates of the Resident Population for the United States, Regions, States, and Puerto Rico: April 1, 2010 to July 1, 2019 (NST-EST2019-01)*.
- Vano, J. A., Scott, M. J., Voisin, N., Stöckle, C. O., Hamlet, A. F., Mickelson, K. E. B., Elsner, M. M. G., & Lettenmaier, D. P. (2010). Climate change impacts on water management and irrigated agriculture in the Yakima River Basin, Washington, USA. *Climatic Change*, *102*(1–2), 287–317. <https://doi.org/10.1007/s10584-010-9856-z>
- Varhola, A., Coops, N. C., Weiler, M., & Moore, R. D. (2010). *Forest canopy effects on snow accumulation and ablation : An integrative review of empirical results*. *392*, 219–233. <https://doi.org/10.1016/j.jhydrol.2010.08.009>
- Vose, R. S., Easterling, D. R., Kunkel, K. E., LeGrande, A. N., & Wehner, M. F. (2017). Temperature changes in the United States. *Climate Science Special Report: Fourth National Climate Assessment, I*, 185–206. <https://doi.org/10.7930/J0N29V45>.U.S.
- Westerling, A. L., Hidalgo, H. G., Cayan, D. R., & Swetnam, T. W. (2006). Warming and earlier spring increase western US forest wildfire activity. *Science*, *313*(5789), 940–943. <https://doi.org/10.1126/science.1128834>

- Woodall, C. W., Fiedler, C. E., & Milner, K. S. (2003). Stand density index in uneven-aged ponderosa pine stands. *Canadian Journal of Forest Research*, 33(1), 96–100.
<https://doi.org/10.1139/x02-168>
- Yang, J., Jiang, L., Luo, J., Pan, J., Lemmetyinen, J., Takala, M., & Wu, S. (2019). Snow Depth Estimation and Historical Data Reconstruction Over China Based on a Random Forest Machine Learning Approach. *The Cryosphere Discussions*, 1–35.
<https://doi.org/10.5194/tc-2019-161>
- Yang, J., Tian, H., Tao, B., Ren, W., Pan, S., Liu, Y., & Wang, Y. (2015). A growing importance of large fires in conterminous United States during 1984-2012. *Journal of Geophysical Research: Biogeosciences*, 120(12), 2625–2640. <https://doi.org/10.1002/2015JG002965>
- Zeng, X., Broxton, P., & Dawson, N. (2018). Snowpack Change From 1982 to 2016 Over Conterminous United States. *Geophysical Research Letters*, 45, 12,940-12,947.
<https://doi.org/10.1029/2018GL079621>
- Zhang, J., Pohjola, V. A., Pettersson, R., Norell, B., Marchand, W. D., Clemenzi, I., & Gustafsson, D. (2021). Improving the snowpack monitoring in the mountainous areas of Sweden from space: A machine learning approach. *Environmental Research Letters*, 16(8).
<https://doi.org/10.1088/1748-9326/abfe8d>

CHAPTER 4 - WILDFIRE IMPACTS FOR TEMPERATURE INDEX SNOWPACK MODEL PARAMETERS

4.1 OVERVIEW

The continued trend for increased wildfire activity in the western U.S. has resulted in federal, state, and local governments performing more post-wildfire risk assessments. These assessments include watersheds that have snowmelt as part of the hydrologic regime. The current gap in generalized recommendations for water managers related to parameter adjustments in snow models presents challenges for water managers performing these risk assessments. The objectives of this analysis are to (1) quantify pre- and post-wildfire changes to melt-rate functions and P_x temperature parameters commonly used by temperature index snow models, and (2) develop equations for snow modelers to use in adjusting temperature index parameters in post-wildfire analysis. In this snow model parameter analysis, 42 SNOTEL sites that have been impacted by wildfire are used to estimate changes in melt-rates and snowfall threshold temperature. The observed changes from pre- and post-wildfire periods at each SNOTEL site are used to develop a suite of general linear models (GLMs) to create snow model parameter adjustments for melt-rate factors and temperature. The GLM inputs include readily available topographic, climatic, and land cover information to estimate changes. The results indicate melt-rates generally increase after a wildfire, especially for periods later in the ablation season. The snowfall threshold temperatures are more variable and site dependent, although the statistically significant changes suggest increases in the threshold temperature will occur post-wildfire. The coefficients from the suite of models suggest that changes to the vegetation canopy are most important for estimating melt-rate and threshold temperature differences beginning immediately after the fire event though approximately 10 years post-wildfire. After vegetation

canopy, other important input variables include air temperature regime and topographic characteristics (i.e., elevation, northness, and eastness).

4.2 INTRODUCTION

Wildfires are part of the western United States ecology and have been for millennia. Large wildfires have been documented going back 2000 years through analyzing lake sediments in mountainous regions (Calder et al., 2015). Accordingly, wildfire is important in western U.S. ecosystem functions such as vegetation composition and landscape heterogeneity (Agee, 1993). In addition, specific ecosystems like ponderosa pine forests are highly reliant on wildfire for tree regeneration (Korb et al., 2019; Stevens-Rumann & Morgan, 2019). Fire suppression during the last century has resulted in increased fire severity (Steel et al., 2015) and climate change is expected to continue to increase the size of wildfires (Littell et al., 2018).

While long-term ecosystem function depends on wildfire, the impacts to watersheds can produce abrupt changes to land surface energy and water balances (Burles & Boon, 2011; Gleason et al., 2019), which can present substantial challenges for water resources managers. One of the most consistent changes to the energy balance after a wildfire is increased ground surface temperature which is associated with decreased sensible heat flux and net radiation (Liu et al., 2005). Fires result in increased surface temperature regardless of pre-burn vegetation type and latitude due to additional net shortwave radiation flux at the surface (Liu et al., 2019). The magnitude of change for other turbulent energy fluxes (i.e., sensible and latent heat) depends on latitude and pre-burn vegetation type because solar radiation and soil-water availability are significant factors for partitioning of those fluxes. Liu et al. (2005) reported that in post-wildfire areas of Alaska the annual net radiation declined by 31% for sites that were burned 15 years or less compared to another site that had burned over 80 years ago. The decline in net radiation is

mostly attributed to ground surface albedo differences. In addition, the sensible heat fluxes were reduced by over 50% by comparison for those same locations. Annual ET values (latent heat exchange) were also decreased by over 30% for more recent fire locations as compared to older burn areas. In the Great Basin of the western U.S., soil temperatures were increased for sagebrush communities that were replaced by invasive grassland communities following wildfire. Net radiation was again decreased along with sensible heat flux (Prater & Delucia, 2006). Another study by Sanches et al. (2015) used remote sensing to evaluate change in energy fluxes after wildfires in Spain. The location had both shrub and pine vegetation prior to the fire. Their analysis indicated that 6-7 years after the fire there were increases in ground and sensible heat fluxes while latent heat flux decreased.

There are several aspects of the water balance that are impacted by wildfires including infiltration, evapotranspiration, surface runoff, and snowmelt processes (Hallema et al., 2017). The impact of wildfire on soil infiltration rate has been a topic of much interest to foresters, ecologists, and hydrologists. Several studies have evaluated the post-wildfire infiltration at various locations around the western U.S. (Balfour & Woods, 2013; Hubbert et al., 2012; Robichaud et al., 2016; Wieting et al., 2017). Enhanced soil-water repellency due to heating of the soil is the commonly cited reason for reduced infiltration (Ebel & Moody, 2013, Shillito et al., 2020). Infiltration in fire affected soils may approach zero immediately following the event resulting in increased excess precipitation and thus increased surface runoff (Ebel & Moody, 2013).

Watershed scale evapotranspiration is reduced following wildfire (Dore et al., 2010; Montes-helu et al., 2009). The reduction includes both bare ground evaporation and transpiration from vegetation. Transpiration from vegetation can decrease up to 36% depending

on the burn severity immediately after the wildfire (Poon & Kinoshita, 2018). Reduced infiltration rates in burned areas result in decreased soil water content even after multiple precipitation events (Ebel et al., 2012). The decreased soil water content reduces the soil evaporation.

The alteration of the water balance generally results in increased streamflow from wildfire effected watersheds (Ebel et al., 2012; Moody & Martin, 2001; Neary, Gottfried, & Ffolliott, 2003; Stoof et al., 2012). As the revegetation process begins, the changes to overall water supply and mean annual streamflow are more site specific. It was found that following fires in the Gila River watershed in Arizona, mean annual streamflow increased (controlling for climate and snowpack variability) while there was no evidence of an increase in the Jemez River watershed in New Mexico (Wine & Cadol, 2016). The relationship between streamflow and spatial extents of burned areas has also been explored. In the Cache La Poudre River watershed following the 2012 High Park, it was found that a 75% increase in runoff occurred for certain subbasins, while the hydrologic response at the watershed scale was minimally impacted (Havel et al., 2018). Increases in post-wildfire peak streamflow are also well documented (Hallema et al., 2017; Moody & Martin, 2001; Wagenbrenner, 2013) and range from 120% (Seibert et al., 2010) to over 1000% (Chen et al., 2013).

In forested areas, the vegetation canopy influences the surface energy and water balance (Burles & Boon, 2011; Varhola et al., 2010) mainly through differences in incoming shortwave radiation and turbulent fluxes. Forest canopies also influence snowpack accumulation and ablation (Roth & Nolin, 2017) through interception. Consequently, when a significant disturbance like wildfire occurs, the snow regime will be impacted. Table 1 from Chapter 2, shows peak SWE decreased and melt-out dates are shifted earlier at SNOTEL sites that have

been impacted by wildfire for ecoregions in the western U.S. In addition, increased snowmelt rates have been observed due to a 30% increase in available energy for snowmelt in burned areas compared with nearby unburned areas (Burles & Boon, 2011). Along with the increased available energy at the snow surface, decreases in albedo (Gleason & Nolin, 2016) will also affect the energy balance of the snowpack. Increased melt-rates have been reported for burned watersheds in the Cascade Mountains in Washington (Gleason et al., 2013; Seibert et al., 2010).

Snowmelt is a critical component to the overall water supply for the western U.S. (Doesken & Judson, 1996) and changes in magnitude and timing of snow accumulation and melt could have trillions of dollars of economic impact in the western U.S. (Sturm et al., 2017). Therefore, it is important to model potential snowpack changes in burned watersheds for quantifying potential social, economic, and ecological impacts. A range of models have been developed to estimate changes in peak SWE and snowmelt following a wildfire. Moeser et al. (2020) used the SnowPALM model to estimate post-wildfire changes in peak SWE and melt-out dates for areas in northern New Mexico. The model was developed to simulate mass and energy balances for snowpack at an hourly timestep and 1 m² spatial resolution. The goal of this work was to estimate impacts from canopy structural changes and did not include any decreased albedo from black carbon on the snow surface. The results of their modeling focused on changes in peak SWE and melt-out dates. The model generally predicted increases for peak SWE although over 30% of the area was predicted to have decreased peak SWE. The model also predicted later melt-out dates for the study area. While they do not directly report melt-rates, the increased peak SWE and later melt-out dates could result in lower overall melt-rates. Based on field observations of peak SWE and melt-out date, their high temporal and spatial resolution model results generally match observations, although the authors indicate that their results are

likely not transferable to other regions. Another detailed energy balance snow model was developed by Burles and Boon (2011) for southwestern Alberta. The spatial extents for their study were two 2500 m² plots in burned and unburned forest stands. They used hourly meteorological data collected at both plots to simulate snow accumulation and ablation. Both the modeled and measured melt-rates were increased when compared to the unburned study plot. Seibert et al. (2010) used a snowmelt runoff model to determine parameter changes between burned and unburned watersheds in western Washington. Due to the equifinality of model parameterization process, they used a Monte Carlo technique to calibrate observed streamflow and quantify parameter changes for the burned watersheds. Through the Monte Carlo parameter evaluation, they report higher melt-rates in the burned watersheds and decreased rain-snow threshold values. Based on these previous studies melt-rates in northern watersheds are likely to increase post-wildfire, while decreased melt-rates are likely in the southwestern U.S.

Temperature index (TI) snowmelt models are still commonly used for operational forecasting (USACE 2017; Duan et al., 2019) and planning studies for major infrastructure (USACE 2020). The TI model is based on an assumption of linearity between snowmelt and air temperature (USACE 1956). Two important parameters for snow accumulation and ablation included in most TI models are the rain-snow threshold (P_x temperature) for snow accumulation and melt-rate functions (either time-varying function or constant value) used during the ablation season. There are limited studies that have explored how these parameters change following a wildfire. Post-wildfire snowmelt modeling was performed in Oregon following the 2020 fire season (USACE 2021a) to estimate potential changes in peak streamflow. Only the sensitivity of melt-rate functions was tested in their analysis for simulating rain-on-snow runoff events. They used double and quadrupled snowmelt rates combined with large historical rain events to

evaluate flood risk downstream of the burn area. In the USACE (2021a) study, the rain-snow threshold temperature was calibrated to match observed snow accumulation and no quantification of post-wildfire changes was made. The post-wildfire change for the P_x temperature parameter change reported by Seibert et al. (2010) was calibrated only for their specific watershed which doesn't allow for generalizations except for watersheds in western Washington.

Currently there are still several unresolved questions about how to model snowpack in burned watersheds. The objective of the parameter analysis is to quantify melt-rate function and P_x temperature threshold changes which are used for parameterization of TI snow models. This includes:

- 1) Quantifying pre- and post-wildfire changes for melt-rate functions and rain-snow threshold temperature by ecoregions in the western U.S.
- 2) Develop a suite of equations for parameter adjustments that can be implemented by modelers to simulate snowpack in wildfire affected watersheds.

The pre- and post-wildfire snowmelt data from 42 SNOTEL sites which have been impacted by wildfire were used to estimate both changes in melt-rate values and P_x temperatures for several post-wildfire periods. The quantified differences between fire periods are then used to train generalized linear models (GLMs) to predict adjustments for these two key snow model parameters commonly used in TI models. The data types were considered in development of the GLMs. These data included land cover, burn severity, topographic, and climatic data. Trained GLMs are developed for several post-wildfire periods including 0-5, 5-10, and 10-20 years after the wildfire occurs.

4.3 DATA

4.3.1 SNOTEL Data

The snowpack data used in this analysis is from SNOTEL network sites operated by the Natural Resources Conservation Service (NRCS, 2021). Burned locations were determined based on information provided by each NRCS Snow Survey Data Collection Office and are distributed from northern Washington to southern New Mexico (Figure 20). Through 2019, 42 sites out of the entire SNOTEL network were identified as being directly impacted by wildfires and had daily snowpack, precipitation, and temperature data for both pre- and post-wildfire periods. The same number of sites could not be used as the RF model development because air temperature was not available at the Thumb Divide SNOTEL site for the pre-wildfire period. Figure 21 shows the periods when both SWE, precipitation, and air temperature data are available for each burned site.

Quality control was performed on the daily data through visual inspection of the SWE, precipitation, and air temperature time series. Reporting errors were removed following discussions with local NRCS Snow Survey offices. Any years with more than 10% of daily values missing for any of these variables were removed from the dataset. Of the 1401 station-years available for the burned sites, 7 years were removed. The average pre-wildfire period is approximately 19 years with over 81% of the sites having at least 10 years. The average post-wildfire period is approximately 12 years with 38% of the sites having at least 10 years.

Additional quality control was performed on the SNOTEL air temperature time series. Based on other work by Oyler et al. (2015) SNOTEL air temperature has been shown to have inconsistencies coinciding with air temperature sensor changes which occurred from the mid-1990s through mid-2000s. In order to homogenize the temperature data, the correction presented

in Ma et al. (2019) was used to make the earlier air temperature values consistent with the more recent period. A list of dates when each burned SNOTEL had the air temperature sensor change was obtained from the NRCS and the correction was applied for all daily values prior to the change.

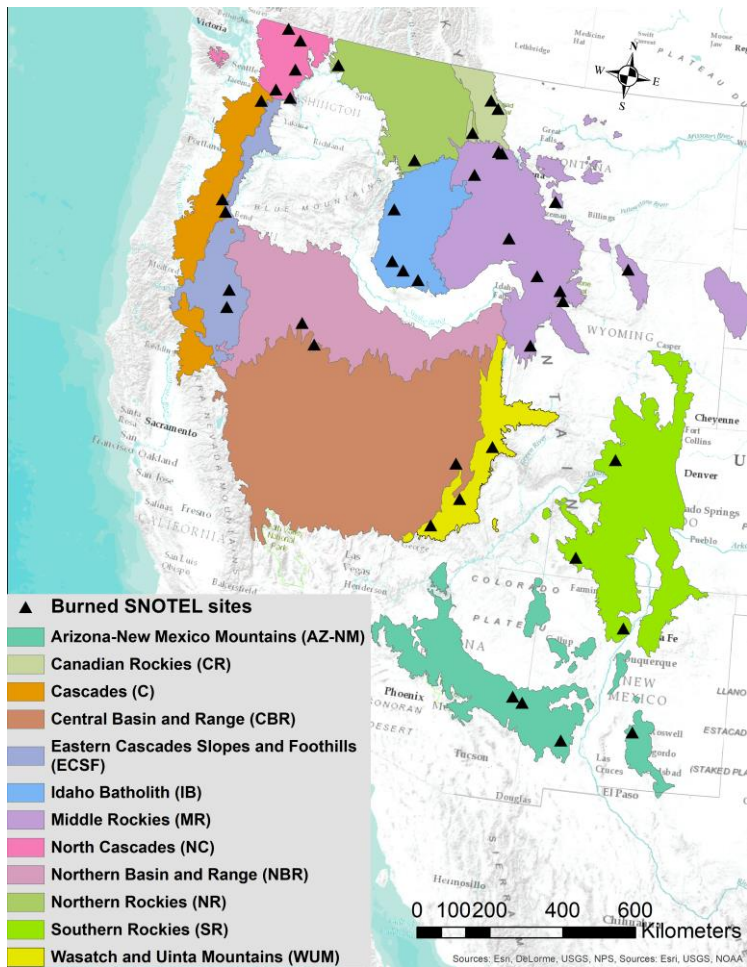


Figure 20. Map of 42 burned (black triangles) SNOTEL sites in western United States shown with level 3 ecoregions used in this analysis.

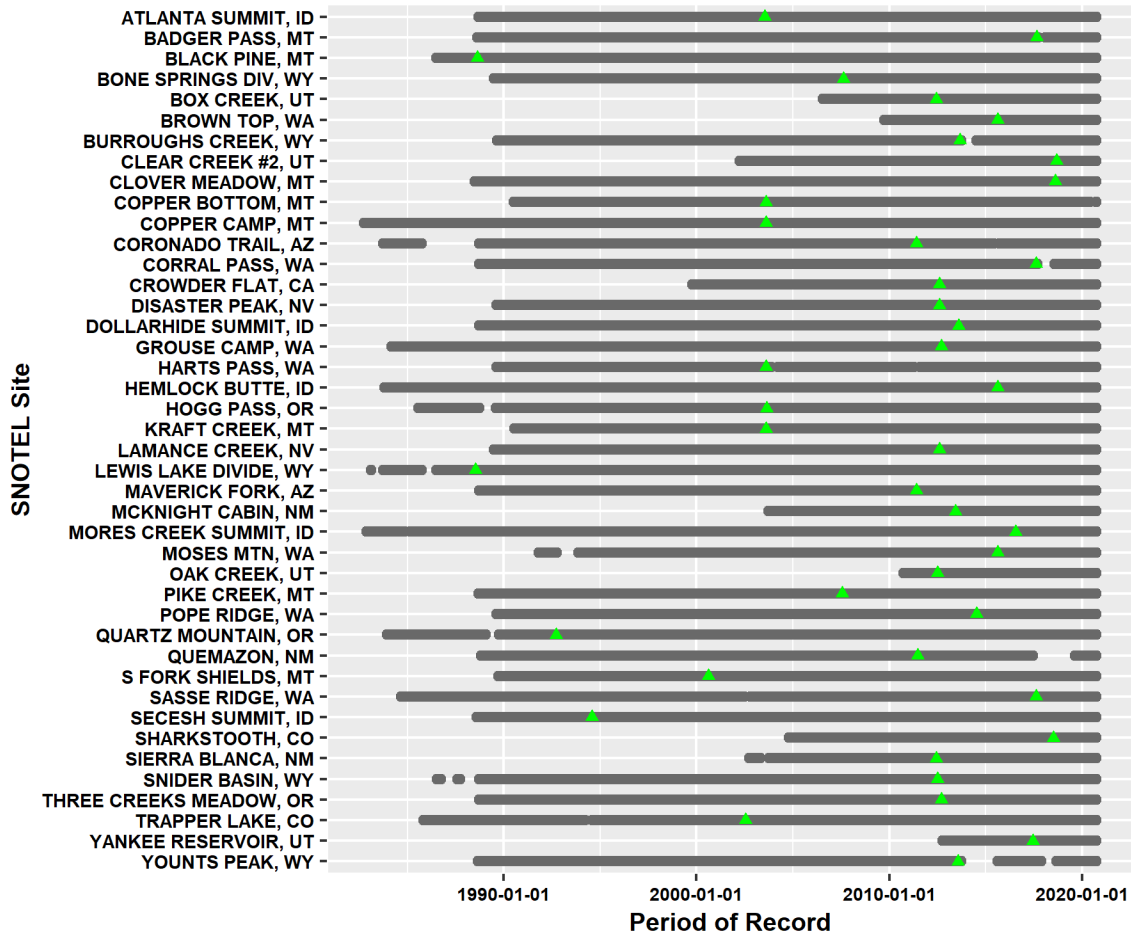


Figure 21. Period of record used for each 41 burned SNOTEL site used in this analysis. The date of the fire (green triangle) is shown for reference within the record.

4.3.2 Land Cover Data

The level 3 ecoregion associated with each SNOTEL site was included as a potential explanatory variable for observed changes. A level 3 ecoregion represents a region that is similar in geology, physiography, vegetation, climate, and soils (Omernik & Griffith, 2014). Other land cover variables included in the parameter analysis are pre-wildfire tree genus, total basal area, and leaf-area index. The dominant tree genus for the area around each SNOTEL location was sourced from the U.S. Department of Agriculture Forest Service (USDA-FS) Forest Inventory and Analysis (FIA) program data from 2017 (Burrill et al., 2018). The FIA data was

not available at each burned site for every pre-wildfire period in the dataset. In this analysis the 2017 tree genus was used in the GLM development. The FIA data does provide consistent forest stand level data on the extent, distribution and forest type composition for forested areas in the U.S. (Burrill et al., 2018). The dominant tree genus was determined through spatial analysis using a 1 km² box centered on the burned site location. Based on the FIA data the tree genus classification results for the 32 sites were 17 fir (includes both *Abies* and *Pseudotsuga*), 11 pine (*Pinus*), 8 spruce (*Picea*), 3 hemlock (*Tsuga*), and three sites were other genera. For analysis purposes, the hemlock and other genera are grouped as “hemlock/other.” Along with the dominant tree genus, the total basal area values provided by FIA was also used. The basal area represents the total cross-sectional area of larger diameter trees in each grid cell. These values are averaged using the same bounding box for each SNOTEL site. Both tree genus and basal area are not direct measures of canopy density but can be used as a potential predictors of changes to the surface energy balance which can impact snowpack melt-rate and Px temperature values.

The MODIS 8-day 500 m (MCD15A2H) leaf-area index (LAI) product (Myneni et al., 2015) was used to quantify canopy density changes. MODIS LAI has been demonstrated to have good agreement when compared with ground-based measurements of LAI (Jensen et al., 2011). LAI information was not available for 7 sites because the fires occurred prior to 2003. During the GLM development, if LAI was used as input, these 7 sites were excluded from the input dataset. Due to the annual phenology of the canopy and the seasonal nature of snowpack, the winter LAI is most relevant (Xiao et al., 2019). The MODIS imagery LAI values from the beginning of October were used for all locations to represent canopy density at the beginning of the snow accumulation season. The LAI change was evaluated by subtracting the October LAI

from the year in which the fire occurred from the year previous to the fire. The difference in LAI represents canopy density changes which again may influence both snow accumulation and ablation through differences in energy and water balance components.

4.3.3 Burn Severity

Burn severity information was obtained from the inter-agency Monitoring Trends in Burn Severity program (MTBS) (<https://www.mtbs.gov/project-overview>). The goal of MTBS is to provide consistent categorized burn severity information for all fires since 1984 (Eidenshink et al., 2007). The burn severity information from MTBS has been used in other studies for quantifying patterns and impacts of burn severity on the landscape (Arkle et al., 2012; Baker, 2015; Bradley et al., 2016). For the parameter analysis, both the categorical burn severity information (i.e., low, moderate, and high) and differenced Normalized Burn Ratio (dNBR) were used in the analysis. The dNBR values are based on the differenced (pre- and post-wildfire) for Normalized Burn Ratio which is derived using bands 4 and 7 from Landsat Thematic Mapper imagery (Eidenshink et al., 2007). Burn severity and dNBR are related to changes in canopy due to the wildfire (Eidenshink et al., 2007) and can influence snow accumulation and ablation (Tennant et al., 2017).

4.3.4 Topographic Data

Topographic variables have been used in previous studies to explain snowpack distribution (Fassnacht et al., 2003) and to quantify variability in snowpack properties (Sexstone & Fassnacht, 2014). A similar suite of topographic variables is used in the melt-rate function and Px temperature parameter analysis and are summarized in Table 1. The longitude and latitude were provided by the NRCS for each SNOTEL site used in this analysis. Using this information, elevation was extracted for the SNOTEL sites using a 30 m digital elevation model

(DEM) (LANDFIRE, 2016b). Through orographic precipitation patterns and air temperature differences, elevation has been shown to be a key variable in snow accumulation (Dingman, 1981).

Land surface slope affects the stability of snowpack during both the accumulation and ablation seasons (Anderton et al., 2004). The land surface slope in degrees was extracted directly from a separate file (LANDFIRE, 2016c) based on the geographic coordinates of each SNOTEL site. The slope values were converted to a percent slope for input to the GLM development.

Northness and eastness are two measures that combine both land surface aspect and slope (degrees) and have been shown to have high correlation with snowpack (Sexstone & Fassnacht, 2014). Northness represents the degree to which the land surface faces north while eastness is the degree facing east. Steep slopes that face north will have values approaching unity. The aspect for each SNOTEL site was extracted from the same source as both the elevation and slope files (LANDFIRE, 2016a). The northness formulation used in this analysis is the product of the cosine of aspect and sine of slope (Molotch et al., 2005). We expect a positive correlation with SWE because north facing slopes tend to have more persistent snowpack (Sexstone & Fassnacht, 2014). Eastness can also be positively correlated with snowpack because snow loading can occur from windward slopes in areas of dominant west winds (Sexstone & Fassnacht, 2014).

Terrain curvature, which is the derivative of slope, was determined using the 30 m DEM information in ArcGIS. The combined profile (parallel to maximum slope) and planform curvature (perpendicular to maximum slope) produced by ArcGIS was used in the analysis. Curvature represents the local relief (i.e., concavity or convexity) and has been shown to be

important for modeling variability in snowpack characteristics, especially in areas of substantial wind redistribution (Sexstone & Fassnacht, 2014).

4.3.5 Climatic Data

Air temperature and precipitation are primary forcing variables associated with snowpack accumulation and ablation. Daily Parameter-elevation Regressions on Independent Slopes Model (PRISM) average air temperature and total precipitation grids coincident with each burned SNOTEL site were used (PRISM, 2021). Several derived variables were also included in the parameter analysis based on temperature index (Hock, 2003) and freezing degree-day (USACE 2005) formulations evaluated with daily data. In this study, the variable TI is defined as the maximum of either the daily average air temperature ($^{\circ}\text{C}$) or zero. This results in TI always being greater than or equal to zero for any day. Conversely, the freezing degree-day (FDD) variable is defined as the minimum of either zero or the average daily air temperature. Therefore, FDD is always less than or equal to zero for any day. From these variables, the seasonal accumulations of TI and FDD are referred to as accumulated temperature index (ATI) and accumulated freezing degree-days (AFDD), respectively. The seasonal accumulation was from October through April of each year. ATI is a proxy for the seasonal accumulation of energy into the snowpack, which is important during the ablation. In contrast, AFDD is associated with the removal of energy from the snowpack and is used as a proxy for the cold content of the snowpack. The mean period of record value for each site was calculated using the annual average daily air temperature, ATI, and AFDD during October through April. An additional variable related to the cold content of the snowpack is the number of days below freezing (LT0). Unlike AFDD, the LT0 is simply a binary response on each day based on whether or not the air temperature is at or below zero. This count was summed each year during

the October through April period for each site. Again, the mean annual average over the period of record was used as an input variable the GLM development.

The snow model parameter analysis for melt-rate function and Px temperature changes used two variables related to precipitation. The first variable is the mean period of record average October through April total precipitation accumulation from PRISM. The second variable is aridity which is the ratio of annual total potential evapotranspiration to annual total precipitation (Greve et al., 2019). To provide consistency with other temperature and precipitation variables, PRISM total annual precipitation values were used. The total annual potential evapotranspiration for each site was taken from gridMet (Abatzoglou 2013) which is based on the Penman-Montieth method for reference evaporation.

Following a wildfire event, changes to surface energy balance are expected (Burles & Boon, 2011; Liu et al., 2005). Therefore two radiation related variables were included in the suite of input variables for the GLMs. These include incoming shortwave radiation from DayMet (Thorton et al, 2021). The DayMet time series was extracted for the locations coincident with each SNOTEL site and an average was evaluated for the daily October through April values for the 1980-2020 period. The final climatic variable we used was heat load index (HLI). This variable is derived from elevation data using the *spatialEco* R package (Evans, 2021). HLI is a measure of direct incident radiation reaching the earth surface. HLI differs from shortwave radiation in that it is not time varying because it is a function of latitude, slope, and aspect. In addition, HLI accounts for the occurrence of higher surface temperature on slopes that receive afternoon sun as compared to morning sun (McCune & Keon, 2002). A summary of predictor variables used for the GLM development are listed in Table 8.

Table 8. Summary of predictor variables used in development of GLMs to estimate changes in melt-rate function and P_x temperature.

Type	Variable Name	Source
Land cover	Ecoregion	U.S. Environmental Protection Agency Level 3
Land cover	Tree Genus	U.S. Department of Agriculture FIA database
Land cover	Total Basal Area	U.S. Department of Agriculture FIA database
Land cover	LAI 1-Year Pre-wildfire	MODIS
Land cover	LAI 1-Year Post-wildfire	MODIS
Land cover	LAI Percent Change	MODIS
Burn severity	Burn Severity Classification	MTBS
Burn severity	dNBR	MTBS
Topographic	Longitude	NRCS data converted to Albers
Topographic	Latitude	NRCS data converted to Albers
Topographic	Elevation	30-m elevation raster (LANDFIRE 2016)
Topographic	Slope	30-m slope raster (LANDFIRE 2016)
Topographic	Northness	$\cos(\text{aspect}) \times \sin(\text{slope})$
Topographic	Eastness	$\sin(\text{aspect}) \times \sin(\text{slope})$
Topographic	Curvature	ArcGIS function using 30-m elevation raster
Climatic	Mean Temperature	PRISM
Climatic	Mean ATI	PRISM
Climatic	Mean AFDD	PRISM
Climatic	Mean LT0	PRISM
Climatic	Mean Oct-Apr Precipitation	PRISM
Climatic	Aridity	gridMet and PRISM
Climatic	Incoming Solar Radiation	DayMet
Climatic	HLI	30-m elevation raster processed using R package <i>spatialEco</i>

This step of the process distills temperature and SWE changes during the ablation season into melt-rate functions. Figure 23 describes a general process for how melt-rate functions are estimated for TI models. Estimating the melt-rate function used in TI models has the basic goal of determining the amount of snowmelt expected to occur given a specific ATI value. Variations of this process exist depending on how the exact parameterization of the snow model is required. For example, Fassnacht et al. (2017) developed estimates of melt-rates from daily mean temperatures for several SNOTEL sites in Colorado. Rango & Martinec (1995) used accumulated degree-day values to estimate melt-rate coefficients. For this study, the process outlined by U.S. Army Corps of Engineers for development of real-time snowmelt runoff forecasting model was used (USACE, 2021b). The initial step in the melt-rate function estimation process is to use the niveograph for each water year and SNOTEL site (Figure 23a) and extract the ablation period starting at annual peak SWE value (Figure 23b) going through melt-out. The daily air temperature values during the ablation season are then used (Figure 23c) to determine ATI values from peak SWE to melt-out date (Figure 23d). Plotting the daily SWE values and ATI values together shows the melt versus temperature (Figure 23e). The melt-rate function values are the derivative of these plots (Figure 23f).

Melt-rate Function Estimation

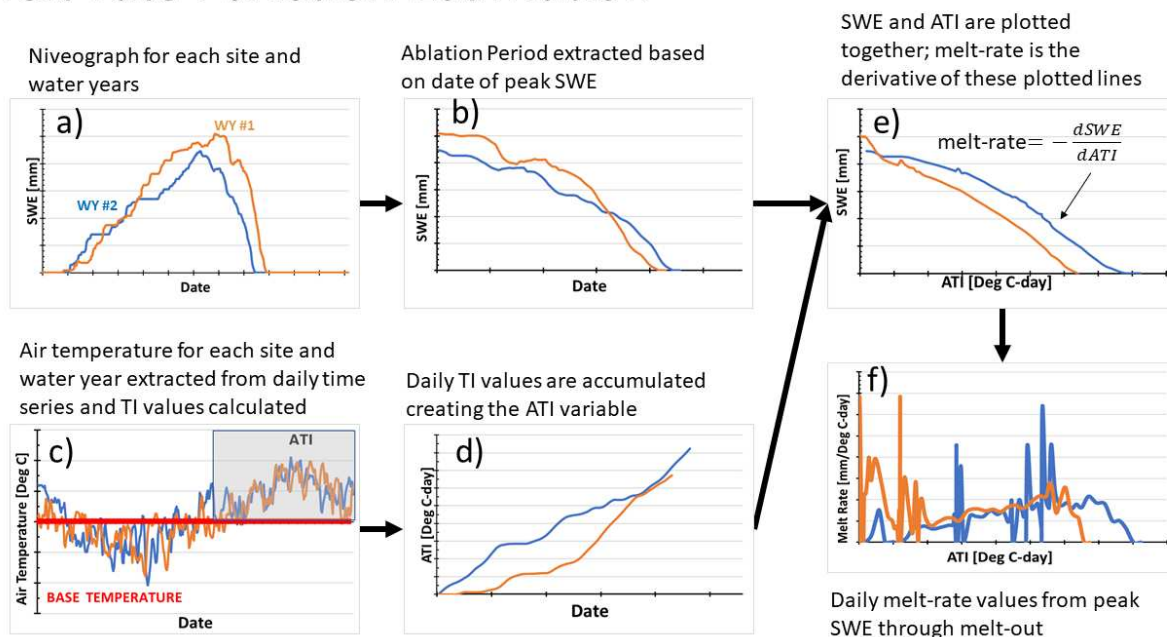


Figure 23. Melt-rate function estimate process using mean daily air temperature and SWE measurements.

Step 3: Determination of Melt-rate Function Structure.

While individual water year melt-rate relationships are available through the procedure described in Figure 23, parameterization of melt-rate functions in TI models requires determining a simplified functional relationship (or structure) of melt-rates to be parametrized into the snow model. The simplified structure should provide a reasonable approximation to the continuous derivative. This simplification is accomplished by fitting a function to the SWE versus ATI plots shown in Figure 24 which reduces the variability of melt-rates (Figure 23f). Several function structures were evaluated including linear, piece-wise continuous linear, and non-linear (i.e., quadratic and log-linear). The overall best fit function structure was evaluated using the Akaike Information Criterion (AIC) to select the best function structure for all of the water years at all sites. The piecewise linear function with a single change point has the best

overall fit (lowest AIC) to the annual melt pattern for all years at all SNOTEL sites. This function structure results in three components of the melt-rate function. The components consist of the initial melt-rate slope (Slope 1), an inflection point (Change Point) as the ATI increases, and a secondary melt-rate slope (Slope 2) (Figure 24).

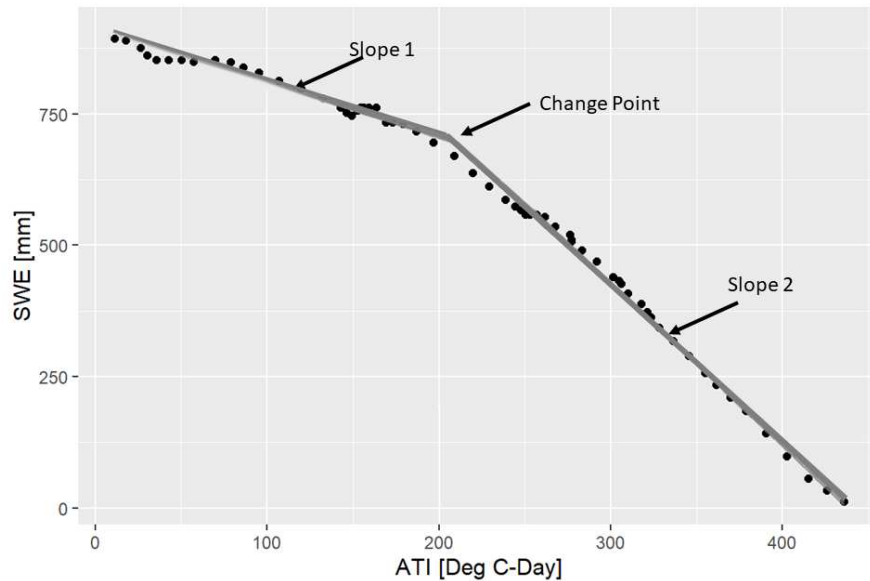


Figure 24. Melt-rate function structure used for burned SNOTEL sites to determine differences between pre- and post-wildfire periods.

Step 4: Calculate mean melt-rates for pre- and post-wildfire periods at each site.

Fitted functions for each year in the period of record were determined using the function structure determined in Step 3 (Figure 22). Based on the fire year at the individual SNOTEL sites, the pre- and post-wildfire mean values for each melt-rate function component were determined. The percent change is the difference between the post-wildfire and pre-wildfire mean melt-rate for each component divided by the pre-wildfire mean melt-rate component. The total range of years included in the data is 1 to 32 years, and the planning horizons used for model development are less than 5 years (<5 yrs), between 5 and 10 years (5-10 yrs), between 10 and 20 years (10-20 yrs) and any duration (All). The mean post-wildfire melt-rate is based using

the only data from years within planning horizon interval. For example, if a site has a period of record ending in 2019 and was burned in 2003, and the planning horizon is less than 5 years, then data from WY2004-2008 is used for determining the mean post-wildfire melt-rate function component for that site, from which the pre-wildfire melt-rate is then subtracted. Using this same site and fire year, the mean post-wildfire melt-rate function component for 5-10 yrs planning horizon would include WY2009-2013, which would produce a different change between pre- and post-wildfire periods. Following this same process, the mean post-wildfire melt-rate information would use WY2014-2019 for the planning horizon 10-20 yrs. In the latter planning horizon only 4 years are used in the mean post-wildfire value calculation due to the total period of record available.

The percent change was converted to a multiplying factor (MF) by adding one to all of the percent change values for each SNOTEL site. The MF is specifically defined as:

$$MF = \frac{PC_i}{100} + 1 \quad (5)$$

Where PC_i is the individual melt-rate function component percent change value in Equation 5. This conversion is advantageous for the GLM development because negative changes in melt-rates (i.e., lower melt-rates) are normalized to be greater than zero. Therefore, multiplying factors between zero and one represent decreases in melt-rates, while factors greater than one represent increases. Included in this step was testing for statistically significant differences between pre- and post-wildfire mean melt-rate values. The non-parametric Wilcoxon Sum Rank test (Helsel et al., 2020) was applied to assess the significance of the changes from the

pre- and post-wildfire periods from each of the melt-rate function components. A p-value of 0.05 was used for significance testing.

Step 5: Develop predictive model of post-wildfire melt-rate changes.

The final step in the process is development of predictive models to estimate MF for pre-wildfire melt-rate function components. This is most directly accomplished through linear regression because linear model coefficients can be reported and reused easily without additional software or programming code. To achieve transferability to practitioners, generalized linear model (GLM) coefficients for the MF for each melt-rate function component were developed using the topographic, climatic, and land cover variables. An exhaustive evaluation of input variable combinations was performed using a GLM in the *leaps* package in R (Lumley, 2020). The GLM model development included a k-fold cross validation process to determine the model evaluation RMSE. The combination of variables that minimize the k-fold cross validation RMSE were selected for use in the final model formulation. The data used in the exhaustive search consisted all sites due to the limited total sites available for this analysis. The k-fold process used 5-folds which have been shown to produce robust model training error statistics for datasets with high variance (James et al., 2013). The coefficient of variation for all the melt-rate function components are much greater than one, thus indicating relatively high variance in the data. Besides providing a robust estimate of error statistics, an additional advantage of the k-fold cross validation process is the data is iteratively split between training and validation data during each fold of the process. The 5-fold selection results in 80% of the SNOTEL sites being used for determining GLM coefficients while 20% is used for evaluating the trained model during each iteration. This process is repeated 5 times to provide robust error estimates from the final GLM coefficients. Separate models were developed for each component and duration of years since

the fire occurred at the site. A total of 12 GLMs were developed to provide estimated MF for four different planning horizons and each of the three melt-rate function components.

4.4.2 Px Temperature

The other TI snow model parameter considered in the snow model parameter analysis is the Px temperature. The process for finding the post-wildfire Px temperature adjustments is similar to the melt-rate function and diagramed in Figure 25.

Post-Wildfire Px Temperature Estimation Process

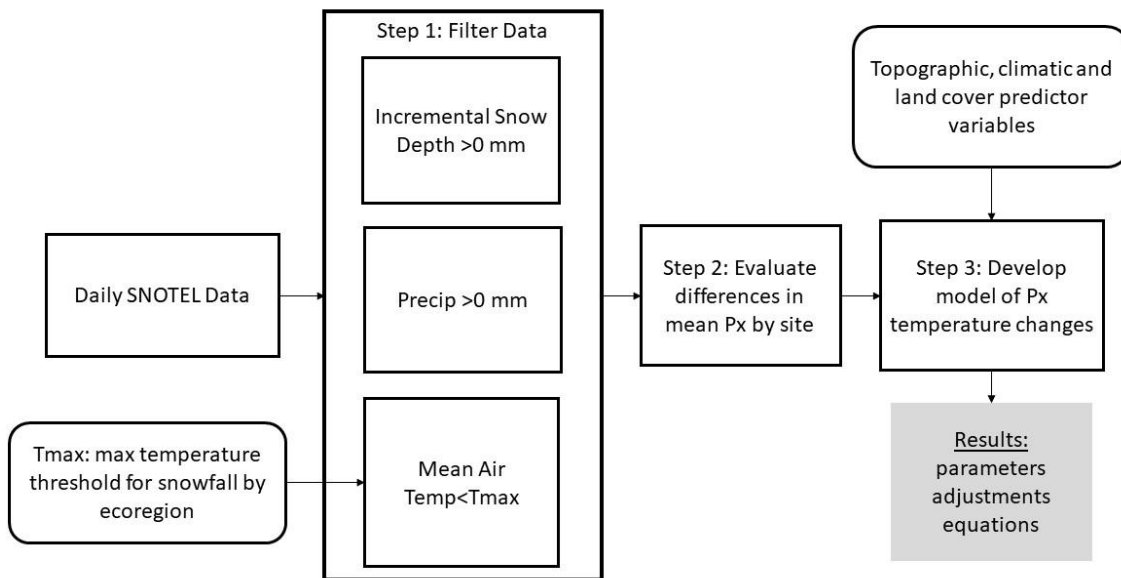


Figure 25. Px temperature parameter adjustment equations using mean daily air temperature, snow depth, and precipitation measurements.

Step 1: Filtering Data

The determination of a representative Px temperature was determined for period of record at each SNOTEL site using three filtering criteria (Figure 25). These criteria include days when the snow depth increased, precipitation was positive, and air temperature was below a maximum threshold. The first two criteria ensure only days when snowfall occurs are considered in the

analysis, which is a necessary condition for determining P_x temperature. The temperature threshold uses the maximum temperature threshold (T_{max}) for snowfall determined by Rajagopal & Harpold (2016) for the western U.S. ecoregions. Above this temperature threshold only rainfall will occur, while below this threshold snowfall or a mix of rain and snow can occur. They used a total of 502 SNOTEL sites across the western U.S. and a minimum of 10 sites per ecoregion. The process they used was independent of air temperature, thus the influence of P_x temperature changes at burned SNOTEL sites contained within their ecoregion results is not a factor. A summary of their findings for T_{max} in the coincident ecoregions from the current analysis is presented in Table 9. The daily P_x temperature is then determined by filtering all the daily temperature values for the period of record at each site by the criteria shown in Step 1 of Figure 25. The subsets of daily temperatures at each site are the P_x temperatures used for the remaining steps of this process.

Table 9. Maximum snow day temperature estimate by ecoregion reproduced from Rajagopal and Harpold (2016).

Level III Ecoregion	T_{max} [°C]
Northern Rockies	0.4
North Cascades	1.1
Canadian Rockies	-0.2
Cascades	1.7
Eastern Cascades Slopes and Foothills	1.2
Idaho Batholith	1.1
Middle Rockies	-0.2
Wasatch and Uinta Mountains	-0.4
Southern Rockies	-0.7
Northern Basin and Range	0.8
Central Basin and Range	-0.1
Arizona-New Mexico Mountains	1.7

Step 2: Determining Difference of mean Px temperature values pre- and post-wildfire.

After the data filtering, the average of the Px temperature values were determined for both the pre- and post-wildfire periods at each site. The difference of the mean values was then determined. The Wilcoxon Sum Rank test was also applied to the Px Temperature differences to determine significance using a p-value of 0.05.

Step 3: Develop predictive model of post-wildfire Px temperature changes.

The development of the GLM to predict changes in Px temperature was very similar to the process used for the melt-rate function. The predictor variables producing the lowest 5-fold cross validation RMSE were utilized. Again, the process was repeated for the subsets of sites based on duration since the wildfire occurred at that location. All sites were used in the 5-fold cross validation process due to the limited number of sites available in this analysis. The post-wildfire Px temperature used a similar process as the melt-rate analysis and evaluated the mean post-wildfire Px temperature at each site based on the various planning horizon intervals relative to the fire year associated with the site.

4.4.3 Model evaluation

Evaluating GLM model performance can be challenging depending on the metrics being used, and criteria should be established a priori to model development (Knoben et al., 2019). In this study, two criteria were used to evaluate the performance of the GLMs. The first criterion is comparing the Kling-Gupta efficiency (KGE) (Gupta et al., 2009) and the second is the ratio of the RMSE to the standard deviation of the observations (RSR). Specifically, RSR is

$$RSR = \frac{RMSE_{model}}{SD_{obs}} \quad (6)$$

The benefit of RSR (Eq. 6) is the normalization of a commonly presented model training statistic (RMSE) by the variation in the observed dataset (SD_{obs}) (Moriiasi et al., 2007). A

perfectly fit model would have an RSR value of zero. The criterion using RSR is presented by Moriasi et al. (2007) which specifies that RSR values less than 0.5 are considered “very good”; values between $0.5 \leq \text{RSR} \leq 0.6$ are “good”; and values $0.6 \leq \text{RSR} \leq 0.7$ are “satisfactory” for model performance. This analysis used the same intervals with the addition of $0.7 < \text{RSR}$ resulting in “unsatisfactory” model performance.

A perfectly fit model using KGE would have a value of unity. As the model fit declines, the KGE values will decrease and can go below zero. When this occurs, it can be difficult to judge the sufficiency of the model for prediction purposes. Knoben et al. (2019) have proposed that KGE values above the mean model benchmark have some ability to relate input and response variables. The benchmark formulation is based on using the mean of the observations within the KGE formula which results in $\text{KGE}_{\text{benchmark}} \approx -0.41$ (Knoben et al., 2019). Therefore, even if the KGE is negative, a comparison can be made to the benchmark for evaluating model performance.

4.5 RESULTS

4.5.1 Variable Correlation

The Pearson correlation coefficients for all input variables, melt-rate components, and P_x temperature differences are shown in Figure 26. Topographic variables including elevation, northness, and eastness are included as predictors in several of final GLM listed in Table A1. Elevation has a strong positive correlation with incoming radiation, while a moderate negative correlation with northness. This indicates the incoming radiation, which is a component of the snow surface energy balance, will depend on topographic variables. HLI, which is another variable related to incident solar radiation, is moderately correlated to slope, northness, and curvature. Both slope and aspect are used to determine HLI and northness, therefore the correlation is likely due to these two topographic variables.

Burn severity, specifically dNBR, is positively correlated with total basal area and the mean October through April precipitation. Areas with high precipitation are more likely to have dense vegetation. Therefore, when a wildfire occurs there is potential for large differences in canopy density between pre- and post-wildfire conditions.

Climatic variables such as Mean LTO and Mean October through April precipitation are positively correlated with latitude while negatively correlated with Mean Temperature and Mean ATI. These results follow earth's temperature gradient when moving towards the extreme latitudes. Aridity is strongly correlated to the climatic variables, but in the opposite direction. Aridity is a function of potential evapotranspiration which increases with air temperature. Tree genus also has moderate correlations with climatic variables due to the plant physiology and soil water requirements of different genus.

The strongest positive correlations for the Change Point component are curvature, LAI one-year post-wildfire, and the percent change in LAI. The strongest negative correlation for the Change Point is based on ecoregion (i.e., Cascades, Idaho Batholith). Overall, the correlations between the input variables and Slope 1 were relatively weak. The strongest positive correlations for Slope 1 are HLI and the years since the fire occurred, while there were only small negative correlations for incoming shortwave radiation and the tree genus fir (includes both *Abies* and *Pseudotsuga*). The correlations between Slope 2 and the input variables showed greater strength (both positive and negative) overall relative to the other melt-rate components. The strongest positive correlations for Slope 2 are latitude, high burn severity, dNBR, Mean LTO and Mean October through April total precipitation. Conversely, the strongest negative correlations are aridity, low burn severity, mean temperature, mean ATI, mean AFDD, incoming shortwave radiation, and ecoregion (i.e., Arizona-New Mexico Mountains, Central Basin and

Range). The correlations between Px Temperature and input variables are relatively weak and only a few input variables show any notable correlation strength. Both longitude and total basal area are positively correlated, while dNBR, years since the fire, the tree genus hemlock (*Tsuga*) and ecoregions (i.e., Canadian Rockies, Central Basin and Range, Middle Rockies).

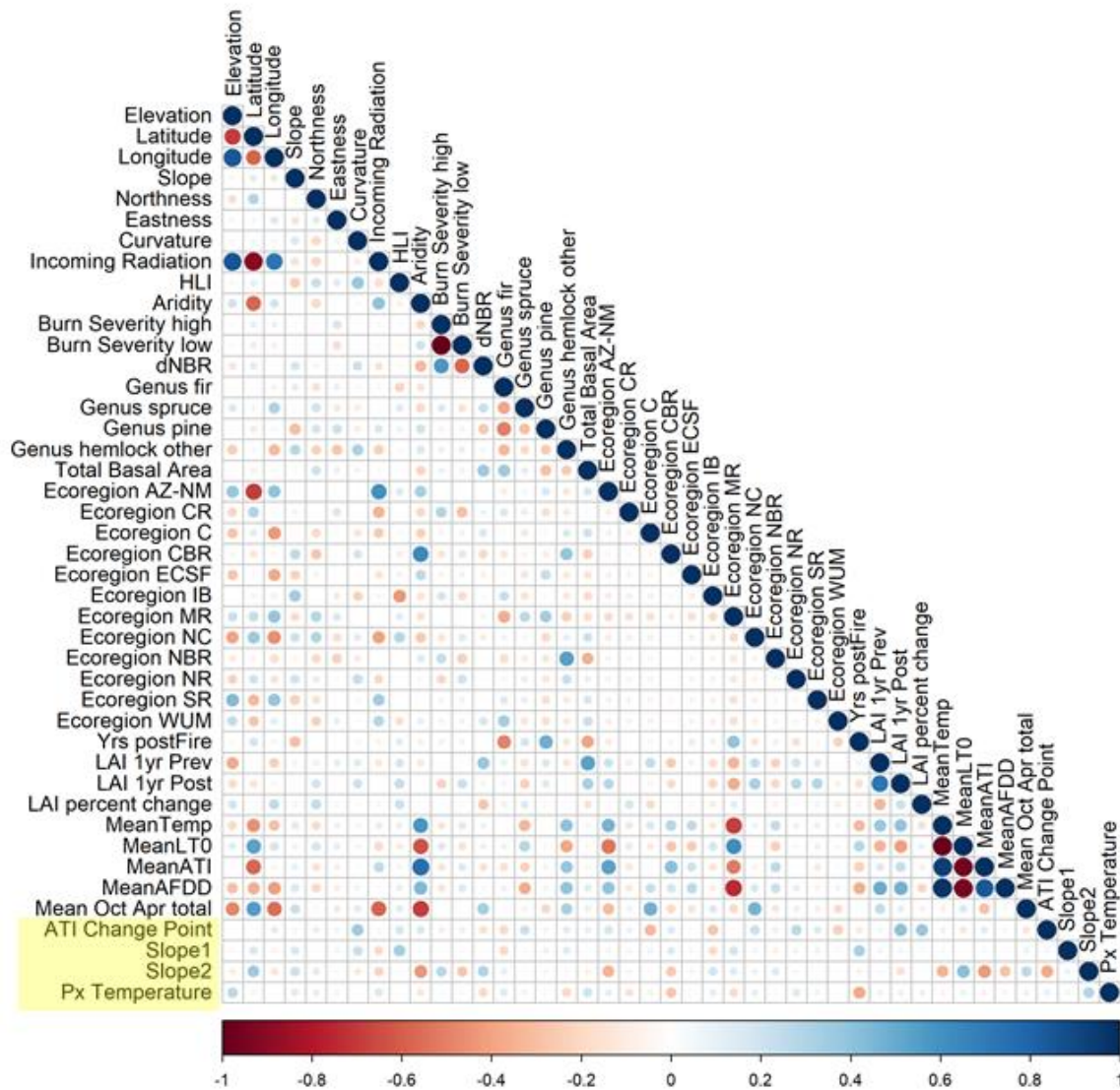


Figure 26. Pearson correlation coefficient for input variables compared to melt-rate function components (Slope 1, Slope 2, and ATI Change Point) and Px temperature (highlighted). The strength of the correlation is reflected in the circle size with larger circles resulting from higher correlation coefficient values. The sign of the correlation is based on the circle colors with red indicating negative correlation and blue positive correlation.

4.5.2 Melt-rate function component changes

Using the assumed melt-rate function structure described previously, the mean pre- and post-wildfire changes for the two slope segments and the change point at each SNOTEL site were quantified using the entire post-wildfire period (Figure 27). The sites are ordered approximately north to south using level 3 ecoregion (Omernik & Griffith, 2014) grouping. The pre-and post-wildfire difference for Slope 1 indicates most of the northern sites have increasing slopes (Figure 27a). Conversely, there is a shift in this pattern in the Middle Rockies, and most sites have a decreasing melt-rate slope. Only three sites have statistically significant changes in the mean Slope 1 values between pre- and post-wildfire. Two of the statistically significant sites are in the Middle Rockies ecoregion, while the third is in the Arizona-New Mexico Mountains.

The direction of melt-rate differences for Slope 2 varies substantially across sites, except for the southernmost sites where these locations have constantly decreasing post-wildfire melt-rate differences (Figure 27b). There are eleven sites with statistically significant pre- and post-wildfire changes for the mean Slope 2 magnitudes. Within the subset of sites that have statistically significant changes, all but two of them indicate a positive (increasing) melt-rate change. The magnitude of Slope 2 differences also varies with larger differences in the northern ecoregions.

The change point component of the melt-rate function has a relatively consistent pattern of decreasing values except for the northern and southern most ecoregions (Figure 27c). There are two sites with statistically significant changes in the mean Change Point value between pre- and post-wildfire periods. The direction and magnitude for these sites differ and do not provide insight to geographic patterns in the Change Point component. However, the average magnitude of negative Change Point differences (decreasing ATI values) is larger than the average positive

values for the northern and southern ecoregions (Figure 27c). The negative differences in Change Points indicate lower accumulated TI values (few days with above freezing temperatures) necessary to transition from the Slope 1 melt-rate to Slope 2 melt-rate in the post-wildfire areas.

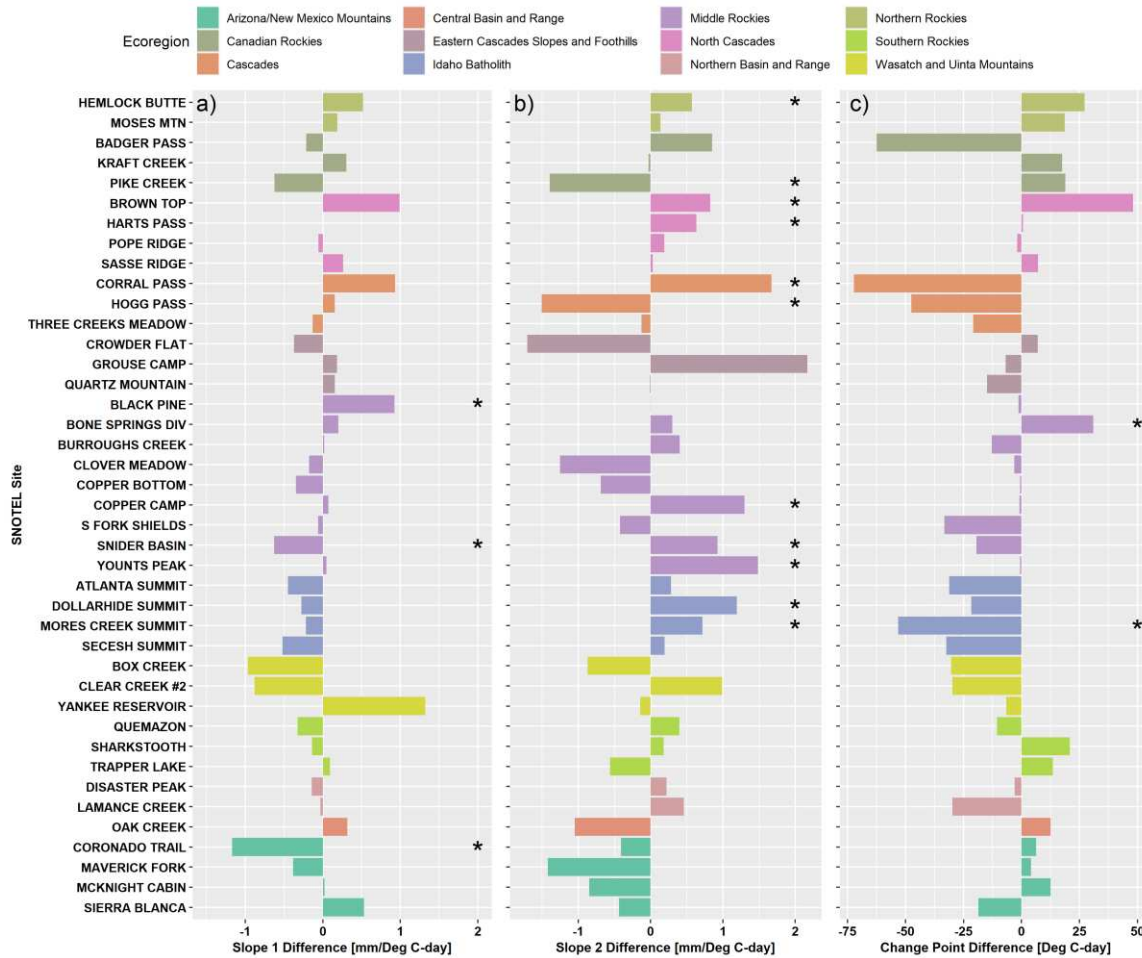


Figure 27. Post-wildfire minus pre-wildfire changes in melt-rate function components from SNOTEL data between pre- and post-wildfire for a) slope 1 (early season melt), b) slope 2 (late season melt), and c) change point (ATI value for transition from slope 1 to slope 2). Statistically significant changes ($p \leq 0.05$) between the mean pre- and post-wildfire periods are shown with an asterisk.

4.5.3 Px Temperature Differences

The differences in mean Px temperature between pre- and entire post-wildfire periods varies between ecoregions and sites within the same ecoregion (Figure 28). Most statistically significant changes are positive, which indicates the Px Temperature increased post-wildfire. Regardless of the direction of change, most changes are less than 0.5 °C. There are five sites with statistically significant differences. These occur within the Cascades, Eastern Cascades Slopes and Foothills, and the Idaho Batholith ecoregions. While there is substantial variability in the direction of change, the largest magnitude differences are negative. Moreover, the overall largest magnitude change is statistically significant and negative at Hogg Pass SNOTEL, which has over 1 °C in Px Temperature difference.

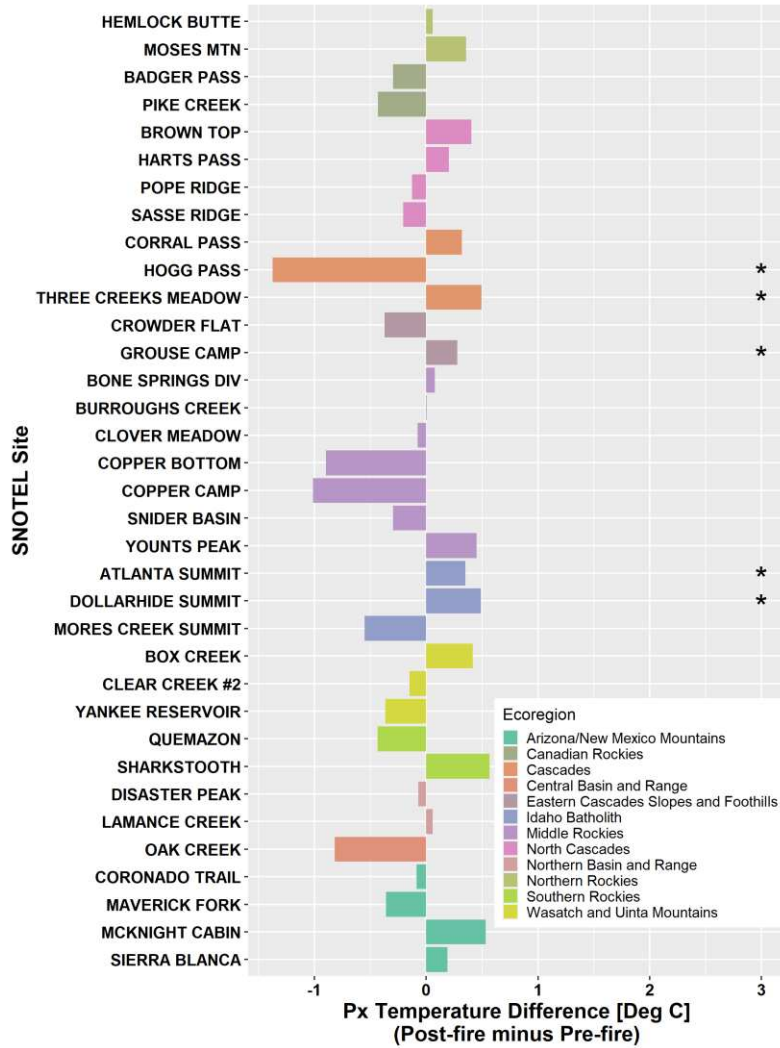


Figure 28. Changes in Px temperature from SNOTEL data between pre- and post-wildfire. Statistically significant changes ($p \leq 0.05$) between the mean pre- and post-wildfire periods are shown with an asterisk.

4.5.4 Models for Estimating Melt-rate changes post-wildfire

Using the measured melt-rate changes from the burned SNOTEL sites and the input variables described previously, GLMs were produced which can be used to estimate the factors snowmelt modelers need to adjust melt-rate components post-wildfire. Figure 29 shows the results comparing the final factor values each GLM produced with the observed changes.

Factors above unity represent increases to pre-wildfire component values (i.e., increased ATI values and higher melt-rates). The GLMs for melt-rate components for periods less than 5 years since the fire occurred are shown in Figure 29a through 29c. The training and validation statistics from the 5-fold cross validation process are shown on each of the panels. The majority of SNOTEL sites have a Change Point factor of below unity (Figure 29a) which indicates lower ATI values between melt-rate slopes. There is an even distribution of Slope 1 (Figure 29b) and Slope 2 (Figure 29c) factors above and below unity.

The GLMs for the 5-10 year period since the wildfire occurred have coefficient of determination (R^2) values between the predictive and observed components approximately equal to 0.70 for all three components with Slope 1 model having the lowest RMSE value (Figure 29d – 29f). Again, the majority of Change Point factors (Figure 29d) for the sites are below unity, while the Slope 1 (Figure 29e) and Slope 2 model (Figure 29f) results are evenly distributed above and below unity. The results of the GLMs for the 10-20 year period since the wildfire occurred are shown in Figures 29g through 29i. These models indicate agreement between the predicted and observed component values; however, these models were developed using a very limited subset of the total burned SNOTEL sites. Even with this limitation, the distribution of component values from the models is consistent with other post-wildfire periods.

The final set of GLMs developed for the melt-rate components include data from all 42 sites used for this study (Figures 29j-29l). The GLM for the Change Point factor (Figure 29j) has moderate agreement (based on R^2) between the predicted and observed values while the models for the Slope 1 (Figure 29k) and Slope 2 (Figure 29l) melt-rate function components have stronger agreement. The distribution of factors for the Change Point shows most sites would have values at or below unity (Figure 29j). The Slope 1 factors are more evenly distributed with

a slight majority below unity (Figure 29k) and the Slope 2 factors are evenly distributed above and below unity (Figure 29l). The GLM model coefficients for the melt-rate function components are listed in Table A1 in Appendix A.

4.5.5 Models for Estimating Px Temperature changes post-wildfire

The results for the final set of GLMs developed for Px temperature adjustments are shown in Figure 30. There are some differences between the observed Px temperature change and the modeled for planning horizons less than 5 years (Figure 30a). There is better agreement (higher R^2) for the longer planning horizons (Figure 30b and 30c) and for the GLM trained using all the SNOTEL sites (Figure 30d). The results indicate the Px temperature is likely to decrease for periods less than 5 years since the wildfire (Figure 30a) while increase be close to 0 °C change for periods 5-10 years after the fire (Figure 30b). The larger magnitude changes for Px temperature are negative when using the model results trained on all SNOTEL sites (Figure 30d). The GLM coefficients for the Px temperature adjustment models are listed in Table A2 in Appendix A.

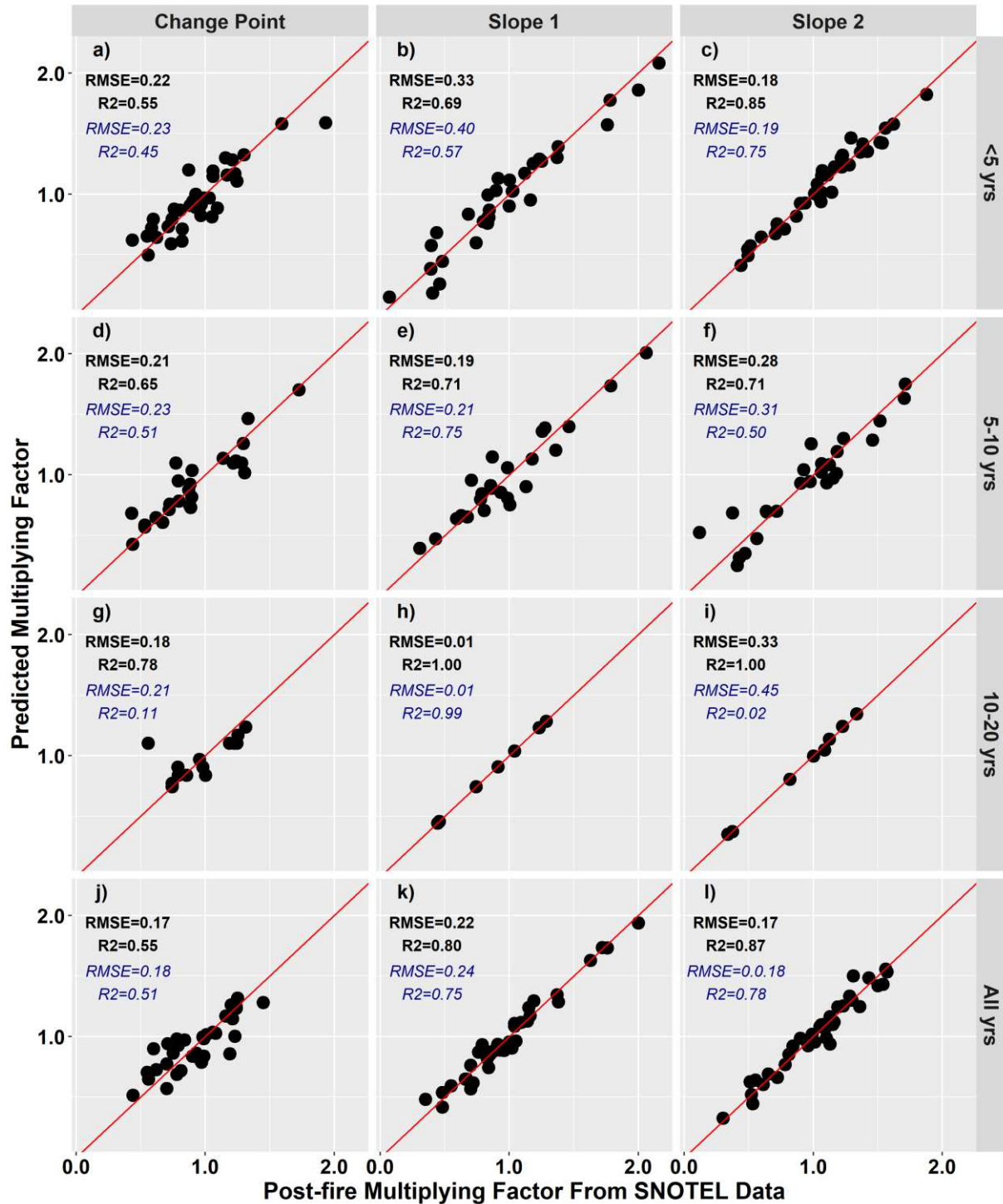


Figure 29. GLM results for melt-rate component multiplying factor for a)-c) less than 5 years since fire occurred; d)-f) 5 to 10 years since fire occurred; g)-i) 10 to 20 years since fire occurred; and j)-l) all sites regardless of time since fire. The 5-fold cross validation training RMSE and R² results are shown in black while the validation results for all folds are in blue italic. The 1:1 line is shown in red and black circles are the predicted values based on the final coefficients from the k-fold training.

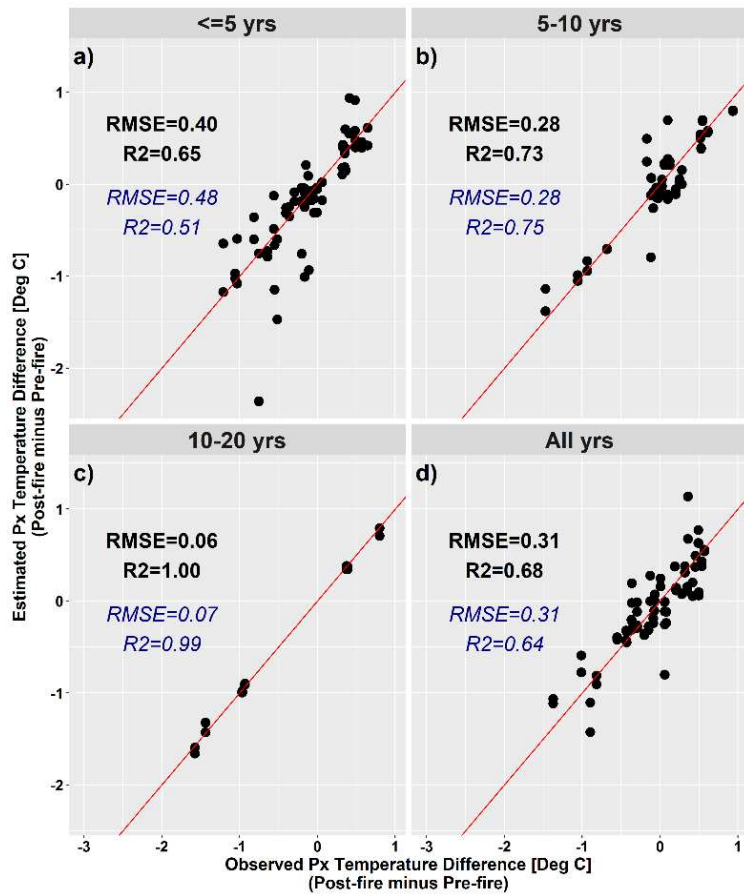


Figure 30. GLM results for melt-rate component multipliers for a)-c) less than 5 years since fire occurred; d)-f) 5 to 10 years since fire occurred; g)-i) 10 to 20 years since fire occurred; and j)-l) all sites regardless of time since fire. The 5-fold cross validation training RMSE and R^2 results are shown in black while the validation results for all folds are in blue italic. The 1:1 line is shown in red and black circles are the predicted values based on the final coefficients from the k-fold training.

4.5.6 Model Evaluation

The evaluation of model performance for each melt-rate component GLM is summarized in Table 10. The RSR and KGE are based on comparing the values produced by the GLMs using the final coefficients determined through the k-fold cross validation process. The majority of the models are classified as “very good” based on the RSR and KGE values. The Change Point GLM developed for the $10 \leq$ year planning horizon was classified as “unsatisfactory” even though the RSR was only slightly outside the defined range. For this model the KGE value is

well above the $KGE_{\text{benchmark}}$ of -0.41 which indicates the model does produce results better than a mean value of the observations. Again, models for this planning horizon were developed with very limited data and should be used with that consideration in mind. Results from using a similar process to evaluate the Px Temperature models is summarized in Table 11. Based on the RSR and KGE values all models were classified as “very good” in the snow parameter analysis. Tables A1 and A2 in the Appendix A summarizes the coefficients for the GLMs that can be used by snow modelers to adjust melt-rate functions and Px Temperatures, respectively. A linear combination of the coefficients can be used with values of the associated input variables for development of parameter adjustments.

Table 10. Evaluation of GLM performance for melt-rate components based on RSR and KGE values.

Planning Horizon	Component	RMR	KGE	Performance Summary
≤5 years	Change Point	0.44	0.85	very good
	Slope 1	0.25	0.95	very good
	Slope 2	0.20	0.97	very good
5-10 years	Change Point	0.41	0.87	very good
	Slope 1	0.31	0.93	very good
	Slope 2	0.35	0.90	very good
10-20 years	Change Point	0.71	0.54	unsatisfactory
	Slope 1	0.01	1.00	very good
	Slope 2	0.05	1.00	very good
All Data	Change Point	0.53	0.78	good
	Slope 1	0.19	0.97	very good
	Slope 2	0.22	0.96	very good

Table 11. Evaluation of GLM performance for Px Temperature based on RSR and KGE values.

Planning Horizon	RMR	KGE	Summary
≤5 years	0.17	0.98	very good
5≤ years	0.27	0.95	very good
10≤ years	0.01	1.00	very good
All Data	0.38	0.89	very good

4.6 DISCUSSION

The assumed melt-rate function structure used in this analysis has a physical basis. Slope 1 represents early season melt when albedo is relatively high and net shortwave radiation at the snow surface is high. During this period turbulent fluxes and downwelling longwave radiation will be the primary energy inputs to melt snowpack (Bilish et al., 2018; Mioduszewski et al., 2015). Since net incoming shortwave radiation is relatively low during early season melt, the total available energy for melt is less and therefore resulting in Slope 1 melt-rate magnitudes being lower. Further into the ablation season the combination of albedo decay as snow ages (Aguado, 1985) and increased hours of illumination result in the net shortwave radiation decreasing (more energy into the snowpack). During the Slope 2 period of melt, the dominant energy flux becomes incoming shortwave radiation which drives the secondary melt-rate through the remainder of the ablation season. The magnitude of shortwave radiation flux into the snowpack provides a substantially greater total energy input and thus the Slope 2 melt-rates are higher.

There are several key input variables with relatively strong correlations to melt-rate function components. The Change Point difference has higher correlations with curvature and LAI percent change. Both of these input variables influence the early season energy input into the snowpack. The LAI changes are directly related to canopy density difference pre- and post-wildfire and canopy has direct impacts on the surface energy balance (Hotovy & Jenicek, 2020;

Suzuki & Ohta, 2003). Curvature has been found to be important in modeling SWE spatial distribution (Sexstone & Fassnacht, 2014) and accumulation due to wind redistribution (Blöschl et al., 1991). Locations of high curvature may also have larger differences in the surface energy balance due to canopy losses which could result in increased energy into the snowpack and thus lower Change Point values between melt-rates.

The difference in Slope 1 magnitude is most strongly correlated with HLA and years since the fire occurred. An increase in melt-rate magnitudes for area of larger HLI is consistent with increased energy reaching the snow surface following a wildfire. The slightly positive correlation with the number of years since the fire occurred presents an interesting and potentially counter-intuitive result. However, vegetation recovery to pre-wildfire conditions takes time. Liu et al. (2005) demonstrated that surface temperatures are still elevated 15 years after a wildfire relative to 80-year-old forest stands in Alaska. Therefore, increased melt-rates can persist for several years after a wildfire occurs.

The Slope 2 difference has several variables with relatively high correlations. These variables can generally be categorized by temperature, precipitation, incoming radiation, and burn severity. The negative correlation with temperature variables indicates that the largest difference in Slope 2 magnitudes will be associated with colder regions. This is because net shortwave radiation will be the largest driver of melt during the late winter and early spring compared to areas that have higher air temperatures and increased turbulent fluxes. Conversely there is a positive correlation with winter precipitation. This indicates areas with high winter precipitation will have larger differences in the Slope 2 melt-rate following a wildfire likely due to the pre-wildfire canopy density commonly associated with areas of higher precipitation. Therefore, after a wildfire and the canopy is removed, a greater increase of incoming radiation

reaching the snow surface occurs. This same reasoning can also be applied to the correlation with burn severity. High burn severity will result in reduced canopy loss and thus more incoming radiation reaching the snow surface which drives higher melt-rates.

The Px Temperature is a challenging parameter to determine due to both time and space variation (Rajagopal & Harpold, 2016). Part of the space dimension is the vertical distance from the ground surface this temperature is applied. Snowfall may be occurring higher up in the atmosphere above the canopy but as the snow crystals get closer to the ground surface, longwave radiation from the vegetation along with turbulent fluxes can influence the mixture of snow and liquid precipitation. Keeping these complexities in mind, the results indicate the highest correlations for Px temperature with pre-wildfire total basal area and years since the fire occurred. The pre-wildfire total basal area is a measure of large vegetation in the area. The larger vegetation will have more influence on the surface fluxes which will impact the threshold temperature at which snow occurs near the surface. Conversely, the years since the fire occurred will be a proxy for the vegetation recovery which will again influence the magnitude of longwave radiation occurring from the canopy and the potential threshold temperature for snowfall.

The majority of GLMs developed to estimate changes in both melt-rate components and Px Temperature are classified as “very good” based on the RSR and KGE evaluation criteria. Only the Change Point GLM for the $10 \leq$ year planning horizon was classified as “satisfactory” due to the RSR value slightly exceeding the defined threshold. The results indicate that even with limited data, models were produced that perform substantially better than using average values derived from the SNOTEL data. The process used in this analysis includes an exhaustive evaluation of input variable combination to determine the best set of inputs for each melt-rate

component. From the model development process, information about commonly selected inputs selected across all planning horizons can be gleaned. The most commonly used input is LAI measured 1-year post-wildfire. This is consistent with the known influence that canopy density has on snow accumulation and ablation (Varhola et al., 2010). Second most commonly used inputs are longitude and dNBR. Longitude is likely associated with the north-south orientation of mountain ranges found in North America. Burn severity, based on the dNBR values, is also a direct measure of vegetation canopy reduction. Again, this is consistent with known influences the canopy has on snow accumulation. There are several input variables which are tied for the next most commonly used. These inputs include northness, eastness, mean temperature, mean ATI, and the tree genus spruce (*Picea*). Sextstone & Fassnacht have shown that both northness and eastness are important for snow distribution, while air temperature will be directly associated with snowfall. The association with spruce trees is consistent with field observations which found Engelmann spruce (*Picea engelmannii*) had increased snowfall interception compared to other conifer species (Schmidt & Glun, 1991).

The most commonly used input variable for the GLMs related to Px Temperature is Mean LT0 which represents the average number of days below freezing for a site. Since air temperature will have a direct influence on the Px temperature, the inclusion of this variable is consistent with previous work (Harpold et al., 2017). Several other input variables are included in at least two of the four GLMs developed for Px Temperature. Within this subset of commonly used variables with the GLMs are elevation, dNBR, and specific ecoregions. Elevation has been shown to be an important predictor of snowpack due to orographic precipitation effects (Fassnacht et al., 2003). Burn severity, as measured by dNBR, will impact the density of the canopy and thus change the net downwelling longwave radiation which could impact the

snowfall threshold temperature. The inclusion of specific ecoregions for various planning horizons would indicate the post-wildfire response to Px Temperature changes is not consistent across the entire western U.S. which is also apparent from the differences in Figure 28.

A limitation of evaluating melt-rate and Px temperature changes by planning horizon is the variable fire year of each site. Some sites do not have data available for all years specified by the planning horizon interval. However, as burned sites continue to gain years since the fire occurred, the melt-rate and Px temperature analyses can be updated to better refine the relative differences between post-wildfire and pre-wildfire mean values.

4.7 CONCLUSIONS

The need for generalized recommendations on snow model parameter adjustments following wildfire continues to increase each year as more and large wildfires occur. Differences between pre- and post-wildfire melt-rates and Px temperature were evaluated using 42 SNOTEL sites that have been impacted by wildfire. Using the differences of the mean values between each fire period, a suite of GLMs was developed using a k-fold cross validation process. Included in this process was an exhaustive evaluation of input variable combinations. These models can be used by water resource managers and hydrologic modelers to estimate parameter changes for snow modeling. The GLMs provide information on parameter adjustments by the number of years since the fire occurred, which provides modelers various planning horizons to assess the impact to snow accumulation and ablation in a watershed. The key conclusions from this analysis include:

- A melt-rate function structure with a single change point and two slopes provides the best overall function form for melt-rates at the SNOTEL sites used in the snow model parameter study.

- Differences in slopes indicate dependence on ecoregion based on the SNOTEL data; the Slope 2 magnitudes are generally positive (increased melt-rate) except in the most southern ecoregions.
- Differences in Px temperature direction and magnitude vary by SNOTEL site and ecoregion which indicates these changes are localized and should not be considered uniform over larger areas.
- Predictor variables related to changes in canopy density (e.g., LAI percent change, burn severity, etc.), temperature, and solar radiation are most often included in the GLM equations to predict parameter changes.
- The melt-rate factors produced by the GLMs show predictive ability especially for planning horizons immediately after the wildfire extending to 10 years post-wildfire.
- The majority of Slope 1 melt-rates decrease while the majority of Slope 2 melt-rates increase post-wildfire due to the shifts in energy fluxes reaching the snow surface.
- The Px temperature adjustments produced by the GLMs show predictive ability especially for planning horizons immediately after the wildfire extending to 10 years post-wildfire.

The snow model parameter study objective included development of generalized recommendations for model parametrization due to the lack of this type of information currently available in the literature. While this objective has been accomplished using methods that are reproducible and readily updated by practitioners, there are some important limitations to this work. The first is the number of sites available to use for model development is limited. Next, the spatial representativeness of the SNOTEL sites is limited and extrapolation to other areas with no data has not been thoroughly investigated. Finally, the variables considered in this

analysis are all documented as being important either from the snow accumulation and ablation perspective or for the overall energy and water balance. However, there may be other input variables, in combination with those used in the current analysis, which could improve the predictive ability of the parameter adjustment models.

The next steps for research related to post-wildfire parameter adjustments include testing methods for spatially distributing the melt-rate adjustment factors along with the P_x Temperature differences. Included in this effort could be additional data collection in areas recently impacted by wildfire to validate the differences predicted by the GLMs. Testing the snow model parameters adjustment results in burned areas would also prove useful and could inform subsequent analysis that are necessary. Finally, additional analysis to provide recommendations for other parameters commonly used in temperature index snow models would help water managers and practitioners during post-wildfire assessments. While further testing and analysis should be performed, this is an important first step to provide modeling guidance to water managers performing risk assessments following wildfires.

4.7 REFERENCES

- Abatzoglou, J. T. (2013), Development of gridded surface meteorological data for ecological applications and modelling. *Int. J. Climatol.*, 33: 121–131.
- Agee, J. M. (1993). Fire Ecology of Pacific Northwest Forests. In *Fire Ecology of Pacific Northwest Forests*. Island Press. <https://doi.org/10.5070/g31710279>
- Aguado, E. (1985). Radiation Balances of Melting Snow Covers at an Open Site in the Central Sierra Nevada, California. *Water Resources Research*, 21(11), 1649–1654.
<https://doi.org/10.1029/WR021i011p01649>
- Anderton, S. P., White, S. M., & Alvera, B. (2004). Evaluation of spatial variability in snow water equivalent for a high mountain catchment. *Hydrological Processes*, 18(3), 435–453.
<https://doi.org/10.1002/hyp.1319>
- Arkle, R. S., Pilliod, D. S., & Welty, J. L. (2012). Pattern and process of prescribed fires influence effectiveness at reducing wildfire severity in dry coniferous forests. *Forest Ecology and Management*, 276, 174–184. <https://doi.org/10.1016/j.foreco.2012.04.002>
- Baker, W. L. (2015). Are high-severity fires burning at much higher rates recently than historically in dry-forest landscapes of the western USA? *PLoS ONE*, 10(9), 1–26.
<https://doi.org/10.1371/journal.pone.0136147>
- Balfour, V. N., & Woods, S. W. (2013). The hydrological properties and the effects of hydration on vegetative ash from the Northern Rockies, USA. *Catena*, 111, 9–24.
<https://doi.org/10.1016/j.catena.2013.06.014>
- Bilish, S. P., McGowan, H. A., & Callow, J. N. (2018). Energy balance and snowmelt drivers of a marginal subalpine snowpack. *Hydrological Processes*, 32(26), 3837–3851.
<https://doi.org/10.1002/hyp.13293>

- Blöschl, G., Kirnbauer, R., & Gutknecht, D. (1991). Distributed Snowmelt Simulations in an Alpine Catchment: 1. Model Evaluation on the Basis of Snow Cover Patterns. *Water Resources Research*, 27(12), 3171–3179. <https://doi.org/10.1029/91WR02250>
- Bradley, C. M., Hanson, C. T., & DellaSala, D. A. (2016). Does increased forest protection correspond to higher fire severity in frequent-fire forests of the western United States? *Ecosphere*, 7(10), 1–13. <https://doi.org/10.1002/ecs2.1492>
- Burles, K., & Boon, S. (2011). Snowmelt energy balance in a burned forest plot, Crowsnest Pass, Alberta, Canada. *Hydrological Processes*, 25, 3012–3029. <https://doi.org/10.1002/hyp.8067>
- Burrill, E. A., Wilson, A. M., Turner, J. A., Pugh, S. A., Menlove, J., Christiansen, G., Conkling, B. L., & David, W. (2018). The Forest Inventory and Analysis Database: database description and user guide version 8.0 for Phase 2. In *U.S. Department of Agriculture, Forest Service*. (Vol. 2). <http://www.fia.fs.fed.us/library/database-documentation/>
- Calder, W. J., Parker, D., Stopka, C. J., Jiménez-Moreno, G., & Shuman, B. N. (2015). Medieval warming initiated exceptionally large wildfire outbreaks in the Rocky Mountains. *Proceedings of the National Academy of Sciences of the United States of America*, 112(43), 13261–13266. <https://doi.org/10.1073/pnas.1500796112>
- Chen, L., Berli, M., & Chief, K. (2013). Examining modeling approaches for the rainfall-runoff process in wildfire-affected watersheds: Using San Dimas Experimental Forest. *Journal of the American Water Resources Association*, 49(4), 851–866. <https://doi.org/10.1111/jawr.12043>
- Dingman, S. L. (1981). Elevation: A major influence on the hydrology of New Hampshire and Vermont, USA. *Hydrological Sciences Bulletin*, 26(4), 399–413. <https://doi.org/10.1080/02626668109490904>

- Doesken, N., & Judson, A. (1996). *The Snow Booklet: A guide to the Science, Climatology, and Measurement of Snow in the United States*.
- Dore, S., Kolb, T. E., Montes-Helu, M., Eckert, S. E., Sullivan, B. W., Hungate, B. A., Kaye, J. P., Hart, S. C., Koch, G. W., & Finkral, A. (2010). Carbon and water fluxes from ponderosa pine forests disturbed by wildfire and thinning. *Ecological Applications*, 20(3), 663–683. <https://doi.org/10.1890/09-0934.1>
- Duan, Q., Pappernberger, F., Wood, A., Cloke, H. L., & Schaake, J. C. (2019). Handbook of Hydrometeorological Ensemble Forecasting. In *Handbook of Hydrometeorological Ensemble Forecasting*. <https://doi.org/10.1007/978-3-642-40457-3>
- Ebel, B. A., & Moody, J. A. (2013). Rethinking infiltration in wildfire-affected soils. *Hydrological Processes*, 27(10), 1510–1514. <https://doi.org/10.1002/hyp.9696>
- Ebel, B. A., Moody, J. A., & Martin, D. A. (2012). Hydrologic conditions controlling runoff generation immediately after wildfire. *Water Resources Research*, 48(3), 1–13. <https://doi.org/10.1029/2011WR011470>
- Eidenshink, J., Schwind, B., Brewer, K., Zhu, Z.-L., Quayle, B., & Howard, S. (2007). A Project for Monitoring Trends in Burn Severity. *Fire Ecology*, 3(1), 3–21. <https://doi.org/10.4996/fireecology.0301003>
- Evans J.S. (2021). `_spatialEco_`. R package version 1.3-6, <URL: <https://github.com/jeffrejevans/spatialEco>>.
- Fassnacht, S. R., Dressler, K. A., & Bales, R. C. (2003). Snow water equivalent interpolation for the Colorado River Basin from snow telemetry (SNOTEL) data. *Water Resources Research*, 39(8), 1–10. <https://doi.org/10.1029/2002WR001512>

- Fassnacht, S. R., López-Moreno, J. I., Ma, C., Weber, A. N., Pfohl, A. K. D., Kampf, S. K., & Kappas, M. (2017). Spatio-temporal snowmelt variability across the headwaters of the Southern Rocky Mountains. *Frontiers of Earth Science, 11*(3), 505–514.
<https://doi.org/10.1007/s11707-017-0641-4>
- Gleason, K. E., McConnell, J. R., Arienzo, M. M., Chellman, N., & Calvin, W. M. (2018). Four-fold increase in solar forcing on snow in western U.S. burned forests since 1999. *Nature Communications, 2019*, 1–8. <https://doi.org/10.1038/s41467-019-09935-y>
- Gleason, K. E., & Nolin, A. W. (2016). Charred forests accelerate snow albedo decay : parameterizing the post- fire radiative forcing on snow for three years following fire. *Hydrological Processes, 30*, 3855–3870. <https://doi.org/10.1002/hyp.10897>
- Gleason, K. E., Nolin, A. W., & Roth, T. R. (2013). Charred forests increase snowmelt : Effects of burned woody debris and incoming solar radiation on snow ablation. *Geophysical Research Letters, 40*, 4654–4661. <https://doi.org/10.1002/grl.50896>
- Greve, P., Roderick, M. L., Ukkola, A. M., & Wada, Y. (2019). The aridity Index under global warming. *Environmental Research Letters, 14*(12), 124006. <https://doi.org/10.1088/1748-9326/ab5046>
- Gupta, H. V., Kling, H., Yilmaz, K. K., & Martinez, G. F. (2009). Decomposition of the mean squared error and NSE performance criteria: Implications for improving hydrological modelling. *Journal of Hydrology, 377*(1–2), 80–91.
<https://doi.org/10.1016/j.jhydrol.2009.08.003>
- Hallema, D. W., Sun, G., Bladon, K. D., Norman, S. P., Caldwell, P. V., Liu, Y., & McNulty, S. G. (2017). Regional patterns of postwildfire streamflow response in the Western United

- States: The importance of scale-specific connectivity. *Hydrological Processes*, 31(14), 2582–2598. <https://doi.org/10.1002/hyp.11208>
- Harpold, A. A., Kaplan, M. L., Zion Klos, P., Link, T., McNamara, J. P., Rajagopal, S., Schumer, R., & Steele, C. M. (2017). Rain or snow: Hydrologic processes, observations, prediction, and research needs. *Hydrology and Earth System Sciences*, 21(1), 1–22. <https://doi.org/10.5194/hess-21-1-2017>
- Havel, A., Tasdighi, A., & Arabi, M. (2018). Assessing the hydrologic response to wildfires in mountainous regions. *Hydrology and Earth System Sciences*, 22(4), 2527–2550. <https://doi.org/10.5194/hess-22-2527-2018>
- Helsel, D. R., Hirsch, R. M., Ryberg, K. R., Archfield, S. A., & Gilroy, E. J. (2020). Statistical Methods in Water Resources Techniques and Methods 4 – A3. *USGS Techniques and Methods*.
- Hock, R. (2003). Temperature index melt modelling in mountain areas. *Journal of Hydrology*, 282(1–4), 104–115. [https://doi.org/10.1016/S0022-1694\(03\)00257-9](https://doi.org/10.1016/S0022-1694(03)00257-9)
- Hotovy, O., & Jenicek, M. (2020). The impact of changing subcanopy radiation on snowmelt in a disturbed coniferous forest. *Hydrological Processes*, 34(26), 5298–5314. <https://doi.org/10.1002/hyp.13936>
- Hubbert, K. R., Wohlgemuth, P. M., Beyers, J. L., Narog, M. G., & Gerrard, R. (2012). Post-fire soil water repellency, hydrologic response, and sediment yield compared between grass-converted and chaparral watersheds. *Fire Ecology*, 8(2), 143–162. <https://doi.org/10.4996/fireecology.0802143>
- James, G., Witten, D., Hastie, T., & Tibshirani, R. (2013). *An Introduction to Statistical Learning with application in R*. Springer.

- Jensen, J. L. R., Humes, K. S., Hudak, A. T., Vierling, L. A., & Delmelle, E. (2011). Evaluation of the MODIS LAI product using independent lidar-derived LAI: A case study in mixed conifer forest. *Remote Sensing of Environment*, *115*(12), 3625–3639.
<https://doi.org/10.1016/j.rse.2011.08.023>
- Knoben, W. J. M., Freer, J. E., & Woods, R. A. (2019). Technical note: Inherent benchmark or not? Comparing Nash-Sutcliffe and Kling-Gupta efficiency scores. *Hydrology and Earth System Sciences*, *23*(10), 4323–4331. <https://doi.org/10.5194/hess-23-4323-2019>
- Korb, J. E., Fornwalt, P. J., & Stevens-Rumann, C. S. (2019). What drives ponderosa pine regeneration following wildfire in the western United States? *Forest Ecology and Management*, *454*(October), 117663. <https://doi.org/10.1016/j.foreco.2019.117663>
- LANDFIRE: LANDFIRE Aspect layer. (2016a). U.S. Department of Interior, Geological Survey, and U.S. Department of Agriculture. [Online]. Available: <http://landfire.cr.usgs.gov/viewer/> [2020, June 8].
- LANDFIRE: LANDFIRE Elevation layer. (2016b). U.S. Department of Interior, Geological Survey, and U.S. Department of Agriculture. [Online]. Available: <http://landfire.cr.usgs.gov/viewer/> [2020, June 8].
- LANDFIRE: LANDFIRE Slope layer. (2016c). U.S. Department of Interior, Geological Survey, and U.S. Department of Agriculture. [Online]. Available: <http://landfire.cr.usgs.gov/viewer/> [2020, June 8].
- Li, D., Wrzesien, M. L., Durand, M., Adam, J., & Lettenmaier, D. P. (2017). How much runoff originates as snow in the western United States, and how will that change in the future? *Geophysical Research Letters*, *44*(12), 6163–6172. <https://doi.org/10.1002/2017GL073551>

- Littell, J. S., McKenzie, D., Wan, H. Y., & Cushman, S. A. (2018). Climate Change and Future Wildfire in the Western United States: An Ecological Approach to Nonstationarity. *Earth's Future*, 6(8), 1097–1111. <https://doi.org/10.1029/2018EF000878>
- Liu, H., Randerson, J. T., Lindfors, J., & Iii, F. S. C. (2005). *Changes in the surface energy budget after fire in boreal ecosystems of interior Alaska : An annual perspective*. 110(January), 1–12. <https://doi.org/10.1029/2004JD005158>
- Liu, Z., Ballantyne, A. P., & Cooper, L. A. (2019). Biophysical feedback of global forest fires on surface temperature. *Nature Communications*, 10(1), 214. <https://doi.org/10.1038/s41467-018-08237-z>
- Lumley T. (2020). *leaps: Regression Subset Selection*. R package version 3.1. <https://CRAN.R-project.org/package=leaps>
- Ma, C., Fassnacht, S. R., & Kampf, S. K. (2019). How Temperature Sensor Change Affects Warming Trends and Modeling: An Evaluation Across the State of Colorado. *Water Resources Research*, 55(11), 9748–9764. <https://doi.org/10.1029/2019WR025921>
- McCune, B., & Keon, D. (2002). Equations for potential annual direct incident radiation and heat load. *Journal of Vegetation Science*, 13(4), 603–606. <https://doi.org/10.1111/j.1654-1103.2002.tb02087.x>
- Mioduszewski, J. R., Rennermalm, A. K., Robinson, D. A., & Wang, L. (2015). Controls on spatial and temporal variability in Northern Hemisphere terrestrial snow melt timing, 1979–2012. *Journal of Climate*, 28(6), 2136–2153. <https://doi.org/10.1175/JCLI-D-14-00558.1>
- Moeser, C. D., Broxton, P. D., Harpold, A., & Robertson, A. (2020). Estimating the Effects of Forest Structure Changes From Wild fire on Snow Water Resources Under Varying

Meteorological Conditions. *Water Resources Research*, 56, 1–23.

<https://doi.org/10.1029/2020WR027071>

Molotch, N. P., Colee, M. T., Bales, R. C., & Dozier, J. (2005). Estimating the spatial distribution of snow water equivalent in an alpine basin using binary regression tree models: The impact of digital elevation data and independent variable selection. *Hydrological Processes*, 19(7), 1459–1479. <https://doi.org/10.1002/hyp.5586>

Montes-helu, M. C., Kolb, T., Dore, S., Sullivan, B., Hart, S. C., Koch, G., & Hungate, B. A. (2009). Persistent effects of fire-induced vegetation change on energy partitioning and evapotranspiration in ponderosa pine forests. *Agricultural and Forest Meteorology*, 149, 491–500. <https://doi.org/10.1016/j.agrformet.2008.09.011>

Moody, J. A., & Martin, D. A. (2001). Post-fire, rainfall intensity-peak discharge relations for three mountainous watersheds in the Western USA. *Hydrological Processes*, 15(15), 2981–2993. <https://doi.org/10.1002/hyp.386>

Moriasi, D. N., Arnold, J. G., Liew, M. W. Van, Bingner, R. L., Harmel, R. D., & Veith, T. L. (2007). Model Evaluation Guidelines for Systematic Quantification of Accuracy in Watershed Simulations. *American Society of Agricultural and Biological Engineers*, 50(3), 885–900.

Myneni, R., Knyazikhin, Y., Park, T. (2015). MCD15A3H MODIS/Terra+Aqua Leaf Area Index/FPAR 4-day L4 Global 500m SIN Grid V006. NASA EOSDIS Land Processes DAAC. <http://doi.org/10.5067/MODIS/MCD15A3H.006>

Natural Resources Conservation Service (2021). NRCS: National Water and Climate Center SNOTEL data network. U.S. Department of Agriculture, available at: www.wcc.nrcs.usda.gov/snow/ , (last accessed: 16 April 2021)

- Neary, D. G., Gottfried, G. J., & Ffolliott, P. F. (2003). Post-Wildfire Watershed Flood Responses. *Second International Fire Ecology and Fire Management Congress, Orlando, Florida, 16-20 November 2003, Paper 1B7*, 1–8.
- Omernik, J. M., & Griffith, G. E. (2014). Ecoregions of the Conterminous United States: Evolution of a Hierarchical Spatial Framework. *Environmental Management*, 54(6), 1249–1266. <https://doi.org/10.1007/s00267-014-0364-1>
- Oyler, J. W., Dobrowski, S. Z., Ballantyne, A. P., Klene, A. E., & Running, S. W. (2015). Artificial amplification of warming trends across the mountains of the western United States. *Geophysical Research Letters*, 42(1), 153–161. <https://doi.org/10.1002/2014GL062803>
- Picotte, J. J., Bhattarai, K., Howard, D., Lecker, J., Epting, J., Quayle, B., Benson, N., & Nelson, K. (2020). Changes to the Monitoring Trends in Burn Severity program mapping production procedures and data products. *Fire Ecology*, 16(1). <https://doi.org/10.1186/s42408-020-00076-y>
- Poon, P. K., & Kinoshita, A. M. (2018). Spatial and temporal evapotranspiration trends after wildfire in semi-arid landscapes. *Journal of Hydrology*, 559, 71–83. <https://doi.org/10.1016/j.jhydrol.2018.02.023>
- Prater, M. R., & Delucia, E. H. (2006). Non-native grasses alter evapotranspiration and energy balance in Great Basin sagebrush communities. *Agricultural and Forest Meteorology*, 139, 154–163. <https://doi.org/10.1016/j.agrformet.2006.08.014>.
- PRISM Climate Group, Oregon State University, <https://prism.oregonstate.edu>, data created 4 Jan 2021, accessed 6 Feb 2021.

- Rajagopal, S., & Harpold, A. A. (2016). Testing and Improving Temperature Thresholds for Snow and Rain Prediction in the Western United States. *JAWRA Journal of the American Water Resources Association*, 89503, 1–13. <https://doi.org/10.1111/1752-1688.12443>
- Rango, A., & Martinec, J. (1995). Revisiting the Degree-Day Method for. *Water Resources Bulletin*, 31(4).
- Robichaud, P. R., Wagenbrenner, J. W., Pierson, F. B., Spaeth, K. E., Ashmun, L. E., & Moffet, C. A. (2016). Infiltration and interrill erosion rates after a wild fire in western Montana, USA. *Catena*, 142, 77–88. <https://doi.org/10.1016/j.catena.2016.01.027>
- Roth, T. R., & Nolin, A. W. (2017). *Forest impacts on snow accumulation and ablation across an elevation gradient in a temperate montane environment*. 5427–5442.
- Sanches, J. M., Bisquert, M., Rubio, E., & Caselles, V. (2015). Impact of Land Cover Change Induced by a Fire Event on the Surface Energy Fluxes Derived from Remote Sensing. *Remote Sensing*, 7, 14899–14915. <https://doi.org/10.3390/rs71114899>
- Sexstone, G. A., & Fassnacht, S. R. (2014). What drives basin scale spatial variability of snowpack properties in northern Colorado? *Cryosphere*, 8(2), 329–344. <https://doi.org/10.5194/tc-8-329-2014>
- Schmidt, R. A., & Glun. (1991). Snowfall interception on branches of three conifer species. *Canadian Journal of Forest Research*, 21, 1262–1269.
- Seibert, J., McDonnell, J. J., & Woodsmith, R. D. (2010). Effects of wildfire on catchment runoff response: A modelling approach to detect changes in snow-dominated forested catchments. *Hydrology Research*, 41(5), 378–390. <https://doi.org/10.2166/nh.2010.036>

- Shillito, R. M., Berli, M., & Ghezzehei, T. A. (2020). Quantifying the Effect of Subcritical Water Repellency on Sorptivity : A Physically Based Model Water Resources Research. *Water Resources Research*, 1921, 1–13. <https://doi.org/10.1029/2020WR027942>
- Steel, Z. L., Safford, H. D., & Viers, J. H. (2015). The fire frequency-severity relationship and the legacy of fire suppression in California forests
<http://www.esajournals.org/doi/pdf/10.1890/ES14-00224.1>. *Ecosphere*, 6(1).
<https://doi.org/10.1890/ES14-00224.1>
- Stevens-Rumann, C. S., & Morgan, P. (2019). Tree regeneration following wildfires in the western US: a review. *Fire Ecology*, 15(1), 1–17. <https://doi.org/10.1186/s42408-019-0032-1>
- Stoof, C. R., Vervoort, R. W., Iwema, J., Elsen, E. van den, Ferreira, A. J. D., & Ritsema, C. J. (2012). Hydrological response of a small catchment burned by experimental fire. *Hydrology and Earth System Sciences*, 16, 267–285. <https://doi.org/10.5194/hess-16-267-2012>
- Sturm, M., Goldstein, M. A., & Parr, C. (2017). Water and live from snow: A trillion dollar science question. *Water Resources Research*, 53, 3534–3544.
<https://doi.org/10.1029/eo064i046p00929-04>
- Suzuki, K., & Ohta, T. (2003). Effect of larch forest density on snow surface energy balance. *Journal of Hydrometeorology*, 4(6), 1181–1193. [https://doi.org/10.1175/1525-7541\(2003\)004<1181:EOLFDO>2.0.CO;2](https://doi.org/10.1175/1525-7541(2003)004<1181:EOLFDO>2.0.CO;2)
- Thornton, P.E., R. Shrestha, M. Thornton, S.C. Kao, Y. Wei, and B.E. Wilson. 2021. Gridded daily weather data for North America with comprehensive uncertainty quantification. Scientific Data. 8(1): <https://doi.org/10.1038/s41597-021-00973-0>

- USACE (U.S. Army Corps of Engineers). (2021a). HEC-HMS Tutorials and Guides, Hydrologic Engineering Center, viewed 15 November 2021, <<https://www.hec.usace.army.mil/confluence/hmsdocs/hmsguides/modeling-snowmelt/using-the-snowmelt-modeling-capabilities-within-hec-hms>>
- USACE (U.S. Army Corps of Engineers). (2021b). McKenzie River Basin-Post Wildfire Hydrologic Assessment. Portland, OR: U.S. Army Corps of Engineers.
- USACE (U.S. Army Corps of Engineers). (2020). Garrison Dam Probable Maximum Flood Update. Omaha, NE: U.S. Army Corps of Engineers.
- USACE (U.S. Army Corps of Engineers). (2017). Folsom Dam and Lake Water Control Manual. Sacramento, CA: U.S. Army Corps of Engineers.
- USACE (U.S. Army Corps of Engineers). 2006. *Engineering and Design: Ice Engineering*. EM 1110-2-1612, Washington, D.C.: Department of the Army, U.S. Army Corps of Engineers.
- USACE (U.S. Army Corps of Engineers). (1956). Snow Hydrology. Portland, OR: U.S. Army Corps of Engineers.
- Varhola, A., Coops, N. C., Weiler, M., & Moore, R. D. (2010). Forest canopy effects on snow accumulation and ablation: An integrative review of empirical results. *Journal of Hydrology*, 392(3–4), 219–233. <https://doi.org/10.1016/j.jhydrol.2010.08.009>
- Wagenbrenner, J. W. (2013). Post-fire Stream Channel Process: Changes in Runoff Rates, Sediment Delivery Across Spatial Scales, and Mitigation Effectiveness [Washington State University]. In *doctoral dissertation* (Issue July). <http://gradworks.umi.com/3598132.pdf#page=71>
- Wieting, C., Ebel, B. A., & Singha, K. (2017). Quantifying the effects of wildfire on changes in soil properties by surface burning of soils from the Boulder Creek Critical Zone

Observatory. *Journal of Hydrology: Regional Studies*, 13(April), 43–57.

<https://doi.org/10.1016/j.ejrh.2017.07.006>

Wine, M. L., & Cadol, D. (2016). Hydrologic effects of large southwestern USA wildfires significantly increase regional water supply: Fact or fiction? *Environmental Research Letters*, 11(8). <https://doi.org/10.1088/1748-9326/11/8/085006>

Xiao, Y., Li, X., Zhao, S., & Song, G. (2019). Characteristics and simulation of snow interception by the canopy of primary spruce-fir Korean pine forests in the Xiaoxing'an Mountains of China. *Ecology and Evolution*, 9(10), 5694–5707.

<https://doi.org/10.1002/ece3.5152>

CHAPTER 5 – CONCLUSIONS

5.1 SUMMARY OF RESULTS

In this study, SWE data from 45 SNOTEL sites that were impacted by wildfire were used to quantify the changes of snow phenology measures from both wildfire and climate changes. These sites range from southern New Mexico to Alaska. An additional 110 unburned SNOTEL sites were used as comparison sites for the burned locations. Overall, climate has a strong influence on SWE and should be considered when quantifying the wildfire signal. Wildfires produced earlier melt-out dates for nearly all ecoregions and on average, the wildfires advanced the melt-out date by 9 days for the ecoregions considered. Wildfires produced earlier peak SWE dates for most ecoregions and on average, the wildfires advanced the peak SWE date by 7 days for the ecoregions considered. Wildfires produced lower maximum SWE values for most ecoregions. On average, wildfires reduced peak SWE by approximately 13% for the ecoregions considered. However, part of the reduction was likely due to localized precipitation patterns occurring over some of the unburned sites. Nonetheless, increases in peak nSWE were observed for several of the northern ecoregions. When the climate and wildfire signals are combined, the largest changes in SWE timing and depth occurred in the Cascades, Eastern Cascades Slopes and Foothills, Southern Rockies, Northern and Central Basin and Ranges, and the Arizona-New Mexico Mountains. The impact of wildfire on the snow phenology measures does not exhibit a clear dependence on burn severity but is sensitive to the change in LAI. In particular, larger reductions in LAI typically produced larger changes in the peak SWE and nSWE values. The effect of the wildfire depends on the dominant pre-wildfire tree genus. The smallest changes in the snow phenology measures typically occurred for spruce and pine forests, while the largest

changes usually occurred for the hemlock/other category. The effects of the wildfires on the snow phenology measures persist more than 10 years after the fires. The changes to the melt-out and peak SWE dates exhibit no clear dependence on the time since fire (for the periods of record available in this study), while changes to maximum SWE and nSWE were largest for times greater than 10 years. The effects of wildfires on the snow phenology measures are strongest at low elevations (below 1960 m). For higher elevations, the wildfire effects exhibit no clear dependence on elevation.

RF models were developed to quantify wildfire effects on snowpack across several ecoregions in the western U.S. Separate models were used to predict changes using two signal classifications (combined and fire) for four different snow measures. The data used to develop these signals is based on pre- and post-wildfire periods at 43 SNOTEL sites that have been impacted by wildfire (combined signal). Unburned comparison SNOTEL sites were identified for each of the 43 wildfire impacted locations. A total of 108 comparison sites, divided based on the same points in time as the associated burned sites, were used to remove climatic differences and isolate the effects of wildfire (fire signal). The snow measures modeled are consistent with those used in the empirical analysis presented in Chapter 2. The predictor variables consist of several sources of information including geographic (i.e., longitude, latitude); topographic (i.e., slope, northness, eastness, elevation, curvature); climatic information (i.e., temperature and precipitation); land surface energy fluxes (i.e., incoming shortwave radiation, HLI), and land cover (i.e., tree genera, total basal area). The RF model development used an exhaustive evaluation of predictor variable combinations within a k-fold cross validation training process to determine the final RF model for each snow measure. The RF models were used to predict areas of snow vulnerability in each ecoregion. There is substantial spatial variability for the combined

signal results but reduced variability for the fire signal results. Earlier peak SWE (up to 26 days) and melt-out (up to 22 days) dates for the combined signal can be expected for all ecoregions. The magnitude of earlier dates is smaller for the fire signal but the results still indicate earlier peak SWE and melt-out dates. The primary exception is fire signal melt-out dates in the Arizona-New Mexico Mountains, which may be up to 10 days later. Maximum SWE and nSWE are slightly reduced from wildfire effects across most ecoregions; however, when wildfire and climate are combined the decreases are more substantial (up to 30% median decrease). The most important variables for prediction of maximum SWE, peak SWE date, and melt-out date changes for wildfires alone are slope, incoming shortwave radiation and aridity, respectively. The most important variables for predicting changes to maximum SWE, peak date, and melt-out date changes using the combined signal data are mean days below freezing and mean winter temperature. Quantification of vulnerable areas for changes in SWE indicate that gently sloped terrain that is south-facing will likely be impacted most from wildfire. Areas with warmer winter temperatures (i.e., where snowfall occurs near the ice-water transition temperature) are also vulnerable to both climate and wildfire impacts. The snow water volume changes for areas burned from 2015-2020 resulted in SWE decreases for all ecoregions except the Northern Rockies and North Cascades. The maximum snow water decrease was 6% for areas burned between 2015-2020 in the Eastern Cascades Slopes and Foothills and the Arizona-New Mexico Mountains.

The need for general recommendations on snow model parameter adjustments following wildfire continues to increase each year as more and large wildfires occur. Again, this analysis used SNOTEL sites impacted by wildfire to evaluate the differences between pre- and post-wildfire melt-rates and Px temperatures (i.e., threshold temperature distinguishing rain and

snow). Using the differences of the mean values between each fire period, several GLMs were developed using a k-fold cross validation process. Models were developed for various planning horizons (i.e., ≤ 5 years, $5 \leq$ years, $10 \leq$ years, and all years). Included in the model development process was an exhaustive evaluation of predictor variables, which consist of several sources of information including geographic (i.e., longitude, latitude); topographic (i.e., slope, northness, eastness, elevation, curvature); climatic information (i.e., temperature and precipitation); land surface energy fluxes (i.e., incoming shortwave radiation, HLI), and land cover (i.e., tree genus, total basal area). The results of this analysis indicate that a melt-rate function structure with a single change point and two slopes provides the best overall functional form for melt-rates at the burned SNOTEL sites. Using this assumed function structure, melt-rate slopes indicate dependence on ecoregion, and slope magnitudes are generally positive (increased melt-rate) except in the most southern ecoregions. Differences in Px temperature direction and magnitude vary by SNOTEL site and ecoregion, which indicates these changes are localized and should not be considered uniform over larger areas. The melt-rate factors produced by the GLMs show predictive ability especially for planning horizons immediately after the wildfire extending to 10 years post-wildfire. Early ablation season melt-rates typically decrease while most later ablation season melt-rates increase post-wildfire due to the shifts in energy fluxes reaching the snow surface. The Px temperature adjustments produced by the GLMs show predictive ability, especially for planning horizons immediately after the wildfire extending to 10 years post-wildfire.

5.2 FUTURE RESEARCH

There are several areas of potential future research based on the work that is presented in this study. The three main focus areas are (1) collection of future snowpack data in burned areas,

(2) analysis of existing data that has been collected, and (3) translation of field measurements to generalized recommendations or tools for post-wildfire snow modeling.

The collection of future data in burned areas would benefit from some standardization in methods, type of variables measured, and instrumentation used to measure these variables. To date each research effort related to snowpack changes following wildfire has used different configurations of instrumentation and data sampling design. While site specific adjustments will still be required, there is enormous benefit to having comparable measurements from similar equipment across multiple regions. For example, snow depth measurements made once a month for non-established transects may be difficult to directly compare to automated SWE measurements collected at a single location. Investigation into the temporal and spatial resolution needed in burn areas to adequately quantify snowpack changes is another area of future work. Such a study would be enormously helpful in planning and budgeting the resources to assess changes in snowpack for a given domain.

In addition to more systematic ground-based data collection, there is an excellent opportunity to combine remote sensing products with this data. There is currently still no high spatial or high temporal SWE products available from remote sensing platforms. One of the most promising options in the near-term is snow LiDAR collection which provides high spatial resolution of snow depth (Broxton et al., 2019; Deems et al., 2013). The LiDAR collection is performed using unmanned, rotatory, or fixed-wing aircraft and only provides snapshots of snow depth during the winter. While many of the current post-wildfire research efforts are collecting snow LiDAR information, future research could include determining the minimum temporal resolution needed to fully capture the snowpack evolution from beginning of accumulation through ablation. Other remote sensing products, such as MODIS fractional snow cover, could

be better integrated with post-wildfire data collection and analysis. Additional research could include recommendations regarding commercially available remote sensing products that provide the most useful information related to snowpack changes post-wildfire.

Another area of research would be aggregation and analysis of all existing post-wildfire snowpack datasets. There have been many data collection efforts from previous fire events that could be combined into a single comprehensive dataset. While many of the issues related to sampling methods and design would need to be taken into account, combining this information along with the burned SNOTEL sites would allow for a more robust spatial analysis of snowpack changes. The aggregation of this data, and potential development of a clearinghouse for other researchers, would mark a substantial step forward in connecting research across multiple institutions.

Finally, one of the fundamental motivations for research is to ultimately provide solutions to societal issues or concerns. Therefore, a key path for future research should be development of guidance or tools for post-wildfire snow modeling. This path would include identification of other parameter adjustments for modeling snow in burned areas especially for temperature index snow models. Temperature index snow models continue to be widely used especially in rapid post-wildfire assessments performed by states and local communities. Therefore, research efforts should be made to help users of this type of snow model. Specifically, additional research related to P_x temperature differences post-wildfire will be helpful for modelers. Creation of a simple tool that could determine P_x temperature differences based on a few key input variables could be developed and included in the post-wildfire toolboxes currently being used in many states (e.g., California, Colorado).

5.3 REFERENCES

- Broxton, P. D., van Leeuwen, W. J. D., & Biederman, J. A. (2019). Improving Snow Water Equivalent Maps With Machine Learning of Snow Survey and Lidar Measurements. *Water Resources Research*, 55(5), 3739–3757. <https://doi.org/10.1029/2018WR024146>
- Deems, J. S., Painter, T. H., & Finnegan, D. C. (2013). Lidar measurement of snow depth: A review. *Journal of Glaciology*, 59(215), 467–479. <https://doi.org/10.3189/2013JoG12J154>

APPENDIX A

Table A1. Equations for melt-rate function adjustment following a wildfire.

Time Since Fire	≤5 years			5-10 years			10-20 years			All years		
Component	Change Point	Slope 1	Slope 2	Change Point	Slope 1	Slope 2	Change Point	Slope 1	Slope 2	Change Point	Slope 1	Slope 2
Input Variable Name												
Intercept	-7.019	-25.411	11.949	-2.008	-24.135	-5.226	1.038	0.573	1.060	-0.806	-23.697	2.493
Ecoregion: AZ-NM												
Ecoregion: C	-0.217	-0.542					-0.294				0.397	-0.367
Ecoregion: CBR			0.740	0.281								0.541
Ecoregion: CR		2.035	-0.835									
Ecoregion: ECSF			0.353							0.285		
Ecoregion: IB					-0.312						-0.529	
Ecoregion: MR		3.061	-0.966		0.544	0.503					1.359	
Ecoregion: NBR		-1.689	1.298			0.660					-1.934	1.141
Ecoregion: NC				0.428		-0.613				0.347		-0.304
Ecoregion: NR		1.108								0.407		
Ecoregion: SR												
Ecoregion: WUM												
Tree Genus: fir												
Tree Genus: hemlock/other		0.524	-0.468						-0.949		0.749	-0.455
Tree Genus: pine		-0.700	0.549	0.526							-0.279	0.407
Tree Genus: spruce		0.515	0.260	0.428	0.747						0.636	0.312
Total Basal Area									-0.010			
LAI 1-Year Pre-wildfire		-0.101									-0.844	
LAI 1-Year Post-wildfire	0.190	0.341	-0.138		0.214	0.130				0.110	1.098	-0.059
LAI Percent Change				0.549					-0.104		-1.435	0.282
Burn Severity Classification: high		0.732									0.705	
dNBR	0.000	0.001	0.001	0.001					0.000		0.002	0.001
Longitude		-0.332	0.117									
Latitude	-0.044	-0.259	0.141	-0.023	-0.119						-0.118	0.045
Elevation		0.002	-0.001								0.001	0.000
Slope												
Northness	-0.306			-0.532	-0.535				0.568	-0.183	-0.356	
Eastness	0.199					-0.352			-0.555	0.103	0.335	-0.141
Curvature		-0.559					-0.600	0.239			-0.689	
Mean Temperature		1.374	886.102			0.602				-310.549	0.927	864.354
Mean ATI	0.003		-4.175		0.007				0.005	1.464		-4.070
Mean AFDD	-0.002		-4.175							1.462		-4.070
Mean LTO		0.099			0.047	0.052					0.063	0.043
Mean Oct-Apr Precipitation			0.001	0.000								0.001
Aridity	-0.309											
Incoming Solar Radiation		-0.017	0.006		0.007							
HLI			0.633								2.613	

Table A2. Equations for Px Temperature adjustment following a wildfire.

Time Since Fire	≤5 years	5-10 years	10-20 years	All years
Input Variable Name				
Intercept	3.989	-8.788	0.582	-18.025
Ecoregion: AZ-NM				
Ecoregion: C	1.302			
Ecoregion: CBR	2.878			
Ecoregion: CR	-1.604	0.658		
Ecoregion: ECSF	0.773			
Ecoregion: IB	0.016			
Ecoregion: MR	-2.312			-0.486
Ecoregion: NBR	3.062			1.193
Ecoregion: NC	-0.244			
Ecoregion: NR	0.987			0.921
Ecoregion: SR				
Ecoregion: WUM				-0.427
Tree Genus: fir				
Tree Genus: hemlock/other	-2.069			-0.949
Tree Genus: pine				
Tree Genus: spruce	-0.252			
Total Basal Area		0.005		0.003
LAI 1-Year Pre-wildfire				
LAI 1-Year Post-wildfire			-0.582	
LAI Percent Change	-0.289			
Burn Severity Classification: high	-0.109			
dNBR			-0.002	0.000
Latitude		-0.320		
Longitude		-0.164		-0.120
Elevation	0.000			0.001
Slope			14.391	
Northness	0.659			
Eastness	0.306			
Curvature	0.753			
Mean Temperature				450.115
Mean ATI		0.005		-2.119
Mean AFDD	-0.006			-2.123
Mean LT0	-0.050	0.051	-0.004	
Mean Oct-Apr Precipitation		-0.002		
Aridity	-0.767	-0.882		
Incoming Solar Radiation		-0.009		
HLI	-1.501			